Ladle Shrouds as Flow Control Devices for Tundish Operations

by

Ken Morales-Higa

Department of Mining and Materials Engineering

McGill University, Montreal, Canada

March, 2011

A thesis submitted to McGill University in partial fulfillment of the requirements of the degree of Master in Engineering

ABSTRACT

The performance characteristics of a tundish, such as the flotation of inclusions and of slag entrainment, are largely influenced by the fluid flow phenomena. Physical and mathematical modeling in water is widely used to understand fluid flows in a tundish, and as a tool to improve, control and design procedures for high quality steel processing operations.

These approaches were used to study the performance of fluid flow for a new design of ladle shroud. The new “Dissipative Ladle Shroud” (DLS) was studied, using a one third scale, delta shaped, four-strand tundish. The results were compared with those achieved with the standard ladle shroud. The standard k-ε turbulence model, together with the continuity and momentum equations, were employed in order to analyze, and visualize, the velocity fields generated within the tundish operating at steady state.

Different cases have been analyzed, including a conventional ladle shroud (LS) with a bare tundish, and a tundish furnished with an impact pad. Similarly, the new design of the shroud (DLS) was studied under equivalent conditions. The physical experiments included the use of Particle Image Velocimetry (PIV) and conductivity tracer techniques. The PIV measured the instantaneous velocities at the outlet of the DLS and the LS at different flow rates, showing the detailed jetting characteristics of water leaving the two types of ladle shroud.

Residence Time Distribution (RTD) curves were also obtained for the different flow arrangements previously mentioned, and the dispersion of a colored dye tracer was observed at different intervals of time during tundish operation, and analyzed using the video visualization technique.

RÉSUMÉ

Les caractéristiques de performance d'un répartiteur telles la flottaison des inclusions et de la scorie sont largement influencées par les phénomènes d'écoulement des fluides. Les modèles physiques et mathématiques sont communément utilisés pour comprendre la dynamique des fluides dans un répartiteur et pour améliorer, contrôler et concevoir les procédés de traitement d'acier de haute qualité.

Cette approche a été utilisée pour étudier la performance de la dynamique des fluides avec un nouveau design de poche de couleé. La nouvelle "Dissipative Ladle Shroud" (DLS) a été étudiée en utilisant une échelle d'un tiers de répartiteur, en forme delta et possédant quatre drains de couleé. Les résultats ont été comparés avec ceux obtenues avec le poche de couleé normal. Le modèle de turbulence k-ε, avec les équations de conservation des masses et de quantité de mouvement, a été utilisé pour analyser et visualiser les champs de vitesse générés par l'opération du répartiteur en conditions stables.

Différents cas ont été analysés, incluant un "conventional ladle shroud" (CLS) avec un répartiteur vide, et un répartiteur muni d'un bloc d'impact. De même, le nouveau design de poche de couleé (DLS) a été étudié sous des conditions équivalentes. Les expériences physiques incluent l'utilisation du "Particle Image Velocimetry" (PIV) et de techniques de traceur de conductivité. Le PIV mesure la vitesse instantanée à l'issue du DLS et du CLS à différents taux de flux, en montrant les caractéristiques détaillées du jet d'eau quittant les deux types de poche de couleé.

Des courbes de Distribution des Temps de Résidence (RTD) ont également été obtenues pour les différents arrangements de flux précédemment mentionnés, et la dispersion d'un traceur de teinture colorée a été observée et analysé à différent intervalles de temps pendant l'opération du répartiteur en utilisant une vidéo de visualisation technique.

ACKNOWLEDGEMENTS

I owe my deepest gratitude to my supervisor Professor R.I.L. Guthrie and co-supervisor Dr. Mihaiela Isac for their constant effort in providing the guidance, support and academic advice from the beginning to the end of my studies.

I would like to convey my gratitude to Dr. Luis Calzado for his enthusiasm in providing help and technical knowledge for the water-model experiments, and also for his assistance in translating the abstract to French.

Special thanks go to my colleagues and friends, including K. Chattopadhyay, Jaspreet Gill, Patrick Lemieux and Dr. Donghui Li for their support and friendship.

I would like to acknowledge the contribution of the McGill Metals Processing Centre (MMPC) for the provision of exceptional experimental facilities, stimulating research environment and financial support.

I would like to thank the Natural Sciences and Engineering Research Council of Canada (NSERC) for their financial support from the beginning to the end of my studies.

I am grateful to the National Council of Science and Technology in Mexico (CONACyT) for their financial support in order to complete my studies.

I would also like to thank National Institute Polytechnique in Mexico (IPN) for the support given during the physical experiments.

Lastly, I wish to thank my family. I am in deep gratitude to my mother Naoko for her moral and emotional support and to my sister Erika for her encouragement. I would like to express my sincere gratitude to my father, Rodolfo, for his patience and unconditional support; it is to him that I dedicate this thesis.

NOMENCLATURE

ρ : Density, $\mathrm{kg/m^3}$

g : Gravitational acceleration, $\frac{m}{s^2}$

μ : Molecular viscosity, kg/m*s

v : Kinematic viscosity, $\frac{m^2}{s}$

u : Instantaneous Velocity, $\frac{m}{s}$

P : Pressure, $\frac{N}{m^2}$

μ_{eff} : Effective viscosity, kg/m*s

μ_l : Laminar viscosity, kg/m*s

G : Generation term, $\frac{m^2}{s^2}$

μ_t : Turbulent viscosity, kg/m*s

k : Turbulent kinetic energy, $\frac{m^2}{s^2}$

ε : Energy dissipation rate, $\frac{m^2}{s^3}$

$\bar{t}$: Theoretical residence time, s

V : Volume of the water in the tundish, L

Q : Volumetric flow rate, $\frac{L}{min}$

θ : Dimensionless time

θ_c : Dimensionless mean residence time

t_m : Mean residence time, s

V_d : Dead volume fraction, L

Q_a : Volumetric flow rate through active region, $\frac{L}{min}$

C_i : Instantaneous dimensionless concentration

V_{dpv} : Dispersed plug flow, L

θ_i : ith dimensionless time

θ_{min} : Dimensionless time corresponding to the first appearance of tracer

θ_{peak} : Dimensionless time corresponding to the maximum tracer concentration

V_m : Mixed volume, L

t_{min} : Time corresponding to the first appearance of the tracer, s

t_{peak} : Time corresponding to the maximum concentration, s

ς : Vorticity vector, s^{-1}

a : Fluid acceleration, $\frac{m}{s^2}$

τ_{ij}^{l} : Laminar viscous stresses, $\frac{N}{m^2}$

τ_{ij}^{t} : Reynolds stresses, $\frac{N}{m^2}$

F : Vorticity force, $\frac{N}{kg}$

τ_{xz} , τ_{yz} , τ_{xy} : Reynolds Shear stresses acting in the XZ, YZ, XY planes, $\frac{m^2}{s^2}$

τ_{xx} , τ_{yy}, τ_{zz} : Normal Reynolds stresses acting in the X, Y, Z axes, $\frac{m^2}{s^2}$

TABLE OF CONTENTS

CHAPTER 1

INTRODUCTION

1.1 INTRODUCTION

During the steelmaking process, the displacement of the steel melt from the ladle to the continuous casting moulds is executed through a vessel named a tundish. This vessel is divided into two sections: an inlet section, where steel melt is fed from the ladle and an outlet segment, from which the melt is supplied to the moulds. The tundish also functions as a reactor in which the main purposes are the following: the formation and removal of macro inclusions as they rise to the melt surface (while the melt travels through the tundish into the molds), the minimization of heat losses, the formation of macro inclusions and the delivery of the melt in a balanced way into the molds in order to achieve even temperatures and steel qualities when casting. Sequential casting is possible, thanks to the presence of the tundish. This is mainly because the steel melt must be supplied to the molds continuously from the tundish by partial draining, when the ladle changes take place, causing the incoming melt to the vessel to be stopped momentarily. [1]

1.2 THE CONTINUOUS CASTING PROCESS

During the last decades, the steel industry has been evolving rapidly mainly because of the continuous casting process. The continuous casting reduces additional processes involved in the ingot casting. Therefore, several advantages are attained, such as a reduced number of operations, equipment, energy consumption, labor and time requirements.

Previous to the continuous casting step, the molten metal is tapped from the furnace into the teeming ladle for secondary steelmaking operations. After degassing, alloying, and fixing the casting temperature, the ladle is positioned at the top of the continuous casting machine. The de-oxidized liquid steel is next

transferred from the ladle through a ladle shroud into the tundish. The refractory shroud is used to protect the incoming steel from being in contact with air as it is sealed to the outlet of the ladle. The steel flow rate is controlled by a ladle shroud with a slide gate valve, or equivalent, while the bottom of the shroud is submerged in the steel bath within the tundish. The vessel, feeds liquid steel into the moulds of the casting machines through a series of Submerged Entry Nozzles (SEN´s). The casting moulds are made of copper, are cooled with water and oscillate so as to prevent the freezing steel shells from sticking to the walls when solidification has begun. The surface of the strand between the support rolls is cooled down by water or air sprays until the steel core is solidified completely.

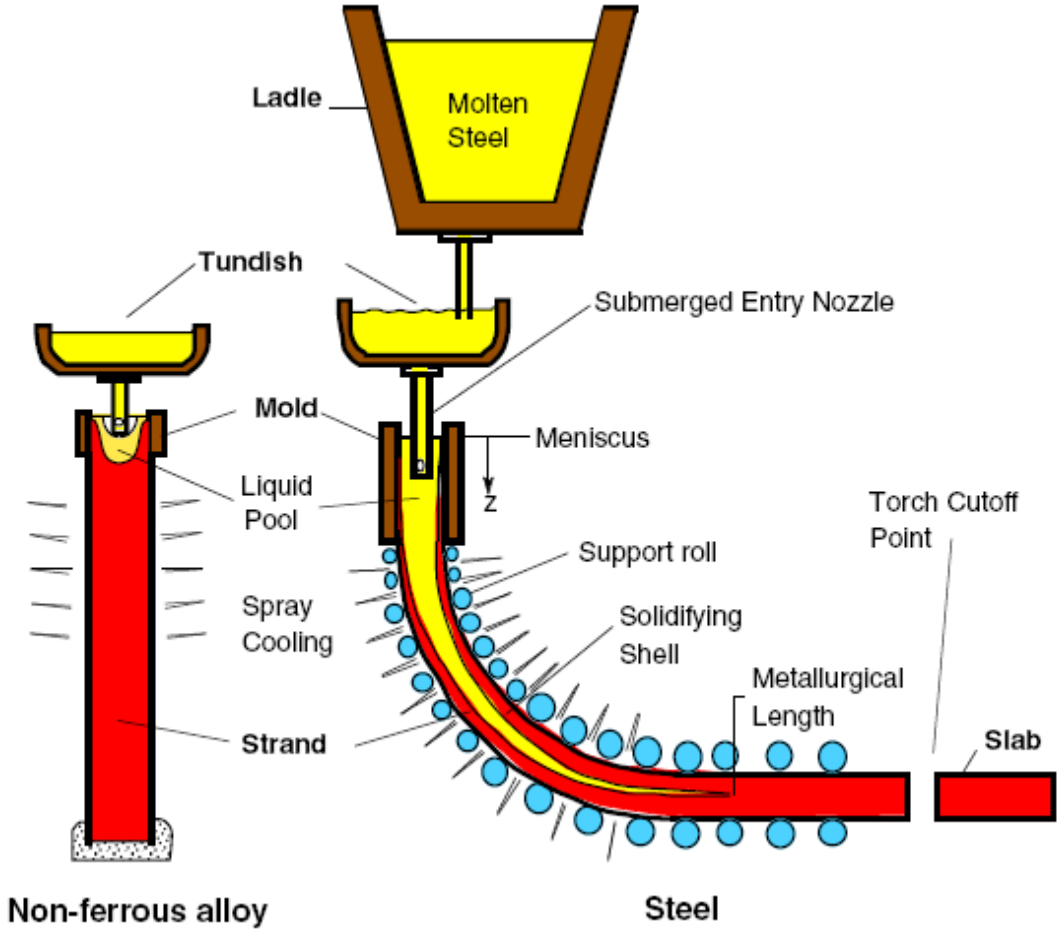

Figure 1.1 Schematic diagram of the elements and processes in the continuous casting machine[51].

1.3 MOTIVATION FOR THE PRESENT WORK

The efficiency and optimization of the performance of the tundish requires detailed control of the flow of steel. If the molten fluid is not controlled adequately, the quality of the steel can drop during its transfer from the ladle to the moulds; therefore many efforts have been made in the research of fluid flows in tundishes, in order to achieve longer residence times and to eliminate all dead zones. Special attention has been taken to the design, equipment and arrangement of different flow control devices in order to modify the fluid flow inside the tundish. Less consideration has been given to the flow patterns that can be obtained when the molten steel is transferred through different ladle shroud designs. By the manipulation of the geometry of the ladle shroud, the fluid flow can be drastically modified prior to being discharged. For instance, one can decrease the momentum of the incoming jet, and as a consequence change the fluid flow patterns throughout the volume of the vessel. The present work is addressed towards the study of a new design of ladle shroud which can perform as a flow modifier. The possible advantages that this might bring, if working alone, include less preparation time, lower operating costs and higher availabilities at the caster. If used in conjunction with another flow modifier, longer residence times, less slag entrainment and decrease the erosion of the walls, could be anticipated.

1.4 OBJECTIVES

The main objectives of this study was 1) to compare the performance of the proposed ladle design, the dissipative ladle shroud (DLS), with that of a conventional ladle shroud (LS), with and without additional flow control devices (FCD), using a one third scale model of a delta shaped four strand tundish. 2) To analyze the feasibility of substituting complex tundish furniture with a unique ladle shroud design, and 3) to analyze and understand the role of the DLS as a flow

control device. For these purposes, physical and mathematical simulations have been performed.

CHAPTER 2

LITERATURE REVIEW

2.1 INTRODUCTION

To produce an upward velocity component over a large portion of the steel within the tundish is very important to the designs of melt flows, since it is the essential mechanism that enhances and has a large influence on the removal of macro inclusions.[1]

It has been shown that the optimum design of a tundish can eliminate dead zones and enhances fluid flow control. HE Youduo and Y. Sahai[2] investigated the effect of different parameters such as inclination of tundish walls, the geometrical size of tundishes and the double wall inclination tundish on fluid flow. The most important parameter is the longitude/height ratio. It was found that it has to be larger than 3.5 in order to diminish the amount of fluid flow unable to ascend towards the surface and to proceed with the removal of the macro inclusions. A wall inclination of 10 to 15 degrees to the vertical improves the fluid flow, eliminating stagnant zones inside the tundish, while the double inclined wall greatly dissipates the fluid motions, decreasing the intensity of the recirculations and has an effect in making the fluid less turbulent in the downstream half of the tundish.[2] A. V. Kuklev et al.[35] discussed the advantages of increasing the volume of the tundish. They proposed that the longer the residence times the larger were the numbers of inclusions removed.

A.Tripathi and S. K. Ajmani[16], compared the fluid flow performance inside a six strand billet caster tundish in which one side is curved, against a conventional delta shaped, using a three-dimensional mathematical model. The curved area, along the pouring chamber of the tundish, improved inclusion flotation. It also

increased the plug flow as well as residence time distribution and the dead volume was decreased.

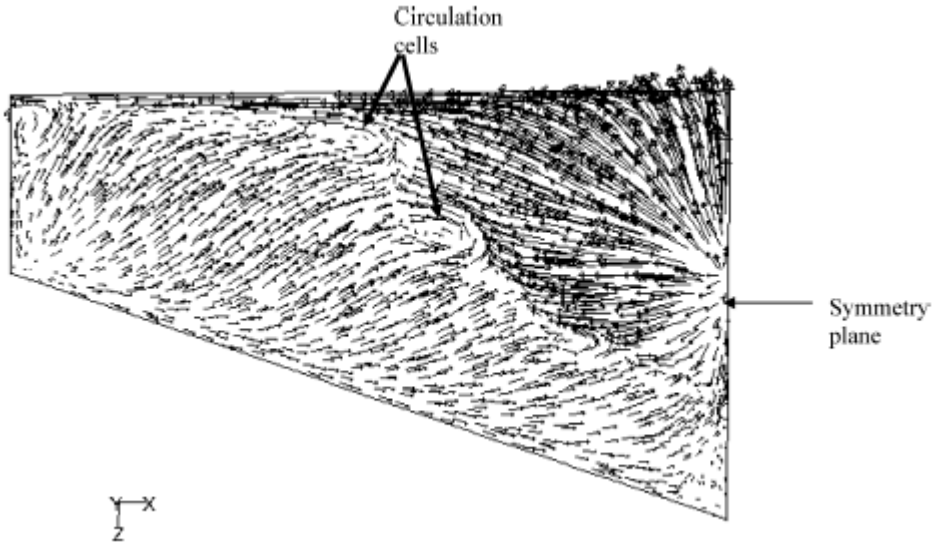

Figure 2.1 Velocity field on the horizontal plane for a regular delta shape tundish

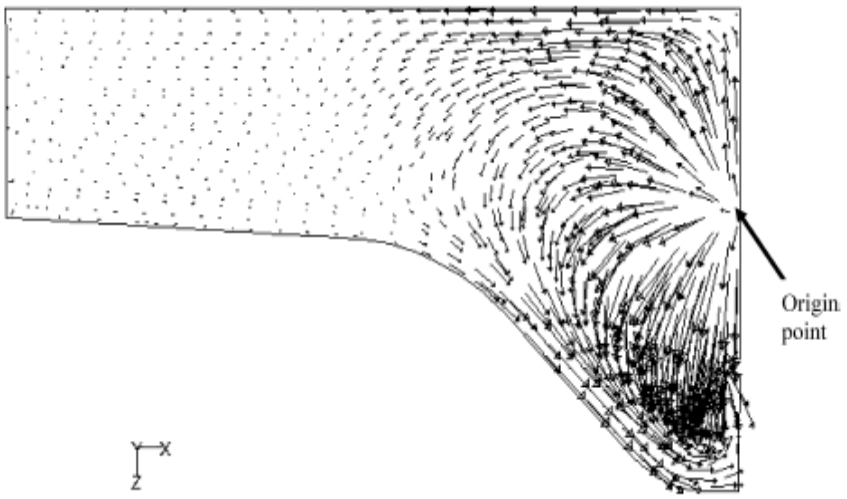

Figure 2.2 Velocity fields on the horizontal plane for a delta curved shaped tundish

The contour shape along the pouring chamber may be useful in diminishing the recirculation of the melt fluid, rather than using sharp edges.

In recent years, efforts have been oriented into the internal design of the vessel. Different designs of flow modifiers within the tundish have been studied by mathematical and water modeling, with the main objective of having better fluid flow characteristics. These flow control devices (FCD) can be pour pads, weirs, dams, baffles with holes and turbulence inhibitors. [1]

The turbulence inhibitor controls the degree of splashing of liquid steel during ladle changes or at the beginning of the casting sequences. It is also useful in increasing the plug flow, the residence time and decreasing the dead volume. Finally, the turbulence inhibitor reorients the impingement jet from the ladle shroud upwards. This is useful for inclusion flotation purposes and in the prevention of high liquid steel velocities in the flowing liquid, which can cause lining wear of the walls. Weirs are used to control the incoming flow that disturbs the surface and are placed in the higher part of the tundish. The dams are placed on the floor and doesn´t cover completely the transversal area of the tundish. The baffles cover completely the bath surface height, and are structured with internal angled holes, to distribute the inclusions towards the bath surface. These FCD are used alone or with different combinations.[17]

R.I.L. Guthrie[3], demonstrated that the arrangement and the design of the flow control devices is very important in order to obtain suitable flow characteristics. This was obtained by replacing a 45 degrees from the horizontal impact pad, with a new FCD. The FCD acted so as to change the direction of the flow towards the back of the tundish and buffering the wavy movement of the surface, thereby eliminating dead zones and the entrainment slag droplets.

The designs of the internal furniture in a tundish vary, depending on the size, height, the internal design and operating conditions. Any flow control device has

to be designed according to those parameters. Therefore, the designs as well as the location of them have to change in parallel as the mentioned criteria [4].

The previous work done in this area is essential for the present and future development of “tundish metallurgy”. In the following text, a review of flow control devices used in general and their effects on the melt fluid, the improvements obtained from them and the current trends are going to be presented.

During the last twenty years, various techniques, including physical and mathematical simulations, have been used in order to study the transport processes in tundishes. These include tracer dispersion, agglomeration and float out of inclusions and the transport of momentum and energy. The physical phenomena, in nature, are convective and turbulent diffusion processes. As such, the correct prediction and analysis of the turbulent flow fields is fundamental in understanding and analyzing the other important variables. Special emphasis in this area is given to the prediction, reliability and visualization of the velocity fields within the steel in the tundish. Some of the physical techniques that have been used for these studies, are Particle Image Velocimetry (PIV) and Laser Doppler velocimetry(LDV) to visualize the velocity fields. The tracer addition technique is used to predict the Residence Time Distribution (RTD). This has been used extensively by different researchers rather than the PIV techniques, and is mainly applied to validate mathematical models by comparing the similarity in the two RTD curves obtained, i.e. by physical experiments and mathematical simulations [29]. Anil Kumar et al. describe the procedures and important features for analyzing RTD curves in multi-strand tundishes. Here, a description for obtaining measurements of various flow volumes fractions such as dead, plug, well mixed, etc. is reviewed. A thorough description of this pulse tracer techniques has been discussed by Levenspiel.[30]

For the mathematical simulations, commercial software packages are more commonly used nowadays mainly because of the powerful framework that they have for coupling different phenomena, the variety of options available to treat different turbulence models and the reliability when comparing with physical

experimentation and the visualization tools for the data post-processing. For the tundish fluid flow analysis, different software and turbulence models are used. These have been extensively reviewed in the literature.[18] [19] [20] Anil Kumar et al.[31] mentioned the different variables that are taken into account when analyzing tundish systems, such as boundary conditions, inlet turbulence parameters, turbulence models, and nodal configurations, in order to assess the basics of mathematical modeling and to obtain good agreement with physical simulations. They mention that the well known k-ε turbulence model can predict, with accuracy the fluid flow patterns inside a tundish during steady state practices. The k-ε turbulence model is widely used by the researchers and engineers rather than other models. The Reynolds Stress Model (RSM) is more powerful for predicting transient tundish operations. A thorough description of the turbulence models are discussed elsewhere [32][33][34]. As can see from those articles, there is a tendency for researchers around the world to select the Standard k-ε model for steady-state conditions, for analyzing fluid flows, and to do the validation of mathematical models with physical simulations by comparison of predicted and experimental RTD curves.

As mentioned in the previous section, with the proper design and placement of the FCD´s, steel melts can be distributed in a uniform pattern according to the dimensions of a tundish. Therefore, the single or twin strand tundish caster is employed to make sure the fluid is being transported in an even fashion to one, or both, of the strands, respectively.[5]

2.2 FLOW CONTROL DEVICES (FCD) AND THEIR EFFECTS

One of the first approaches in characterizing the fluid flow by combining mathematical and physical modeling of a full-scale water model tundish was executed by S. Joo and R.I.L. Guthrie [8] [9] and S. Joo, J.W. Han, and R.I.L. Guthrie[10]. An in-house code, METFLO-3D, was developed to model transport phenomena, together with the development of an inclusion sensor for the in-situ, continuous detection, of particles suspended in aqueous systems. These

approaches were very useful in improving the operating conditions and arrangements of flow modifiers inside a full scale water model of the Lake Erie Works tundish of Stelco. In this three part paper, they were able to model isothermal and non-isothermal flows physically, and with J.W. Han, to use mathematical models to study the important role of natural convection currents, back in 1988.

K.J. Craig et al.[6], in 2001, characterized steel flow by a design optimization study performed on the steady state for a Columbus Stainless steel single-strand tundish, operating under steady-state, using a water model and mathematical simulations. Three cases were considered: water in the first two cases and the last case was steel, with the main purpose of analyzing the effects of the buoyancy forces and temperature gradients in the fluid flow, and in optimizing its design. Two arrangements within the tundish were studied: the first with one dam and one weir, while the second was based on a baffle with angled holes and an impact pad. An improvement of 34 % was reported in the minimum residence, using water as the working fluid. Positive results have been also obtained when considering steel as the working fluid, leading to a 26% improvement in the minimum residence time versus the first design. These results were obtained with a zero angled baffle.

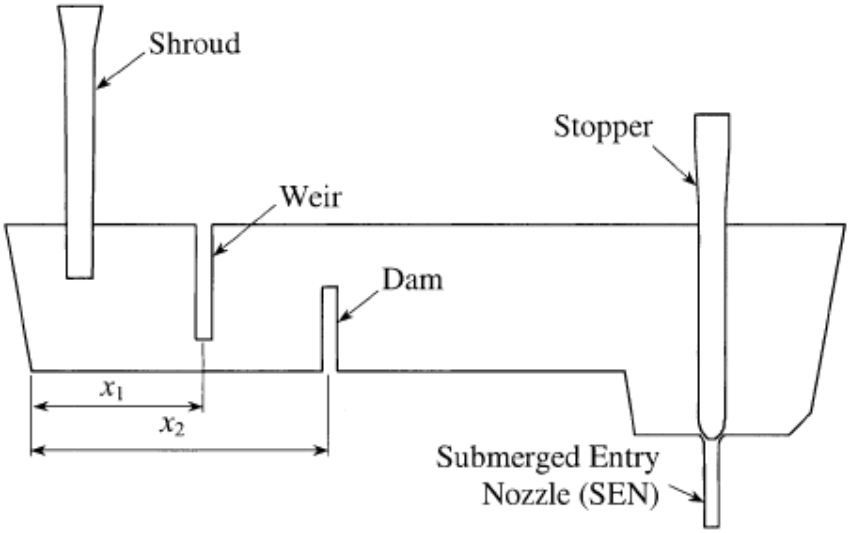

Figure 2.3 Arrangement of the Columbus Stainless single-strand tundish

C.M. Fan et al.[7] studied the different phenomena involved in the fluid flow inside a single strand stainless steel tundish, such as mass and momentum transfer, as well as inclusion removal, using physical and mathematical modeling approaches, and the k-ε two equation turbulent model. Different FCD´s were used, the arrangements were mainly settled as follows: a stopper rod located above the outlet which was the former one (Fig.2.4), the second involved a square plane pad (Fig. 2.4a) the third included a weir and a dam with a hole at the bottom(Fig. 2.4b), the fourth included a reversed L assembled with the pouring pad(Fig.2.4c) and the last arrangement used a pouring pad as shown in Fig. 2.4d.

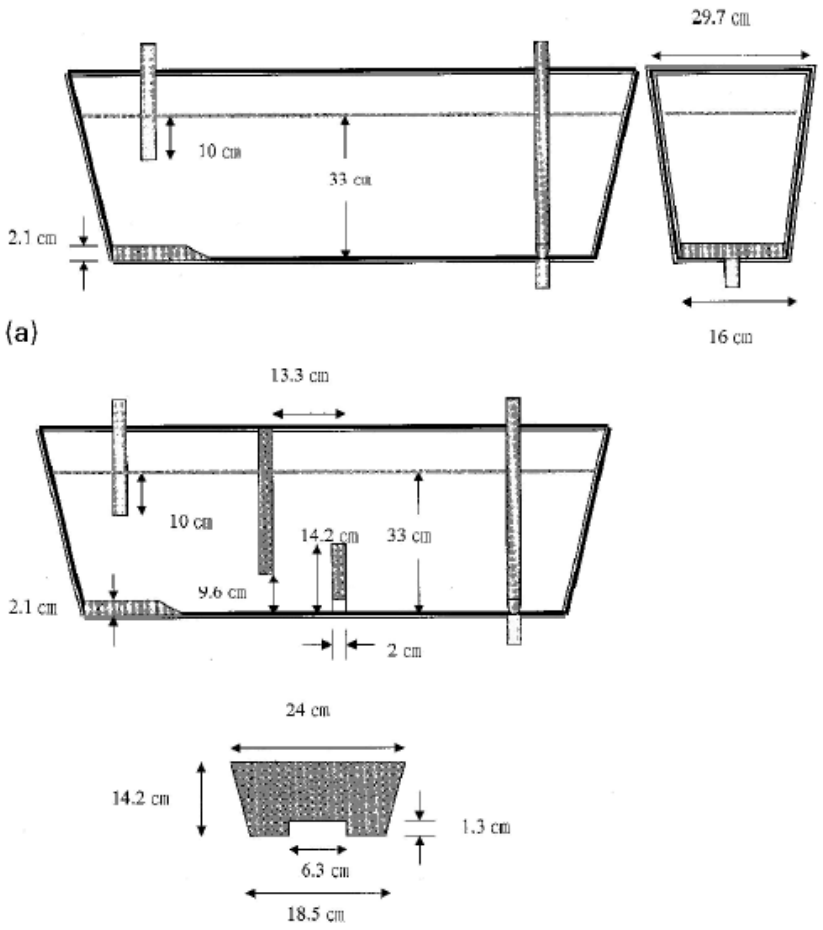
29.7 cm
10 cm
33 cm
2.1 cm
16 cm
(a)
13.3 cm
10 cm
14.2 cm
33 cm
9.6 cm
2.1 cm
2 cm
24 cm
14.2 cm
1.3 cm
6.3 cm
18.5 cm

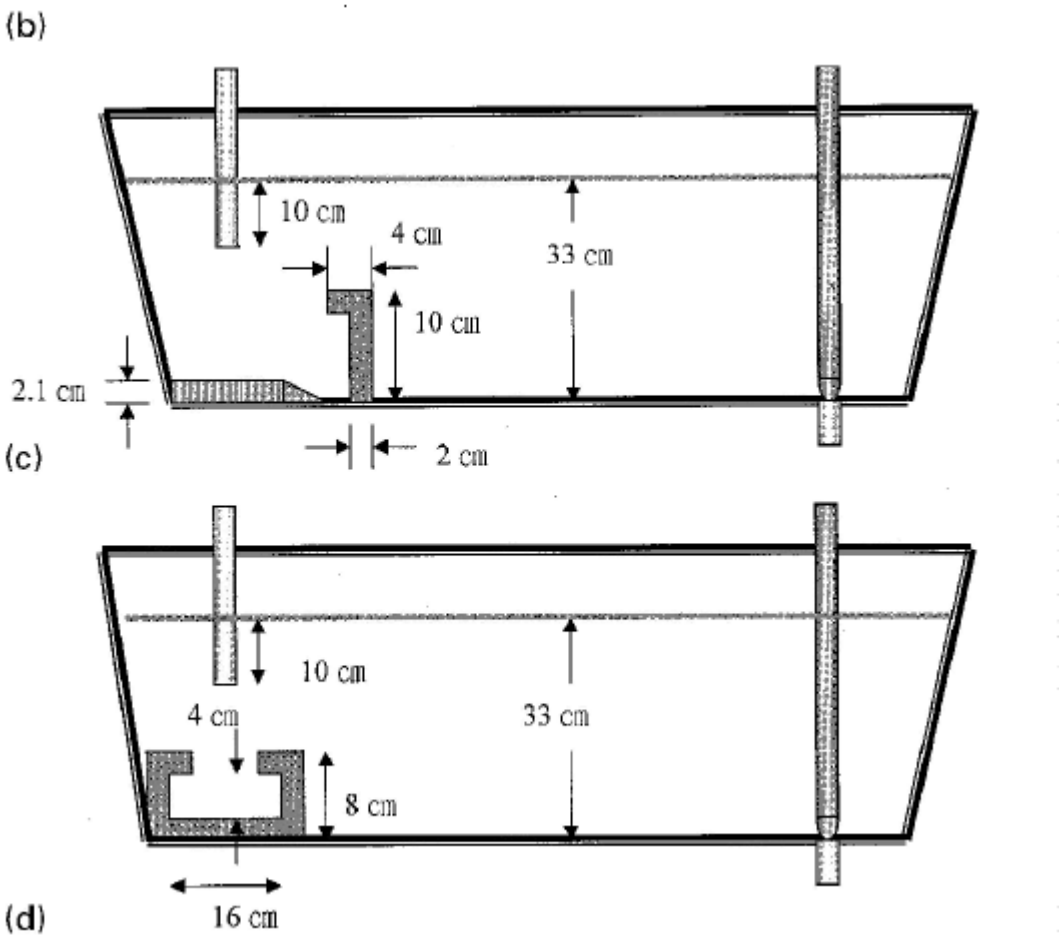

Figure 2.4 a) plain tundish, b) tundish with weir-dam, c) tundish with dam of reversed L shape(RL) d)tundish with pouring pad(PP)

It was found that the arrangement with the pouring pad decreased the dead zone more than others. With their mathematical model, they verified that the pouring pad arrangement was able to remove a greater number of inclusions, attaining the highest removal rate of inclusions(RRI). It was also discovered that the size of inclusions, rather than the composition, has a deep effect on the flow behavior of the inclusion.

Another useful approach to enhance inclusion flotation is to add argon through the ladle shroud as mentioned by different authors [54][55][56]. Along with the different FCD´s, argon bubbling helps to remove inclusions whose sizes are less than 50 μm [54]. The mechanism of inclusion removal consists in the stirring of

the entry jet from the ladle shroud by small bubbles, enhancing the adhesion and flotation of particles towards the bath surface. WANG Jun et al.[61] investigated the fluid flow in tundish with a weir in order to explain the effects of the gas flow rate, the placement of a porous cross beam, and the combination of the flow control devices on the slag-metal interface. It was found that the position of the argon blowing in the tundish is very important when assembled with FCD´s. If the distance of the porous cross beam from the weir is too large, deep recirculations within the tundish are created. Oppositely, if the porous beam and the weir are closer, a better control of inclusions flotation is attained. Conversely to what was previously mentioned regarding to the advantages of using gas bubbling, the detrimental effects of a high gas flow rate in entraining an upper slag phase has also been studied [47][22].

Ramos-Banderas et al.[12] studied fluid flow in a one strand tundish furnished with a turbulent inhibitor(TI), using a mathematical model, together with physical simulations in a water model fitted with a gas bubbling system.

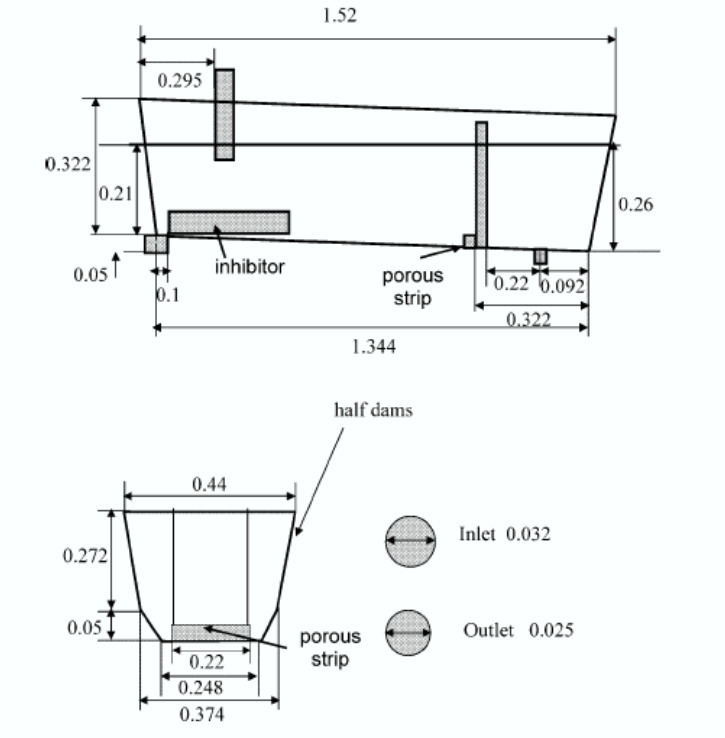

Figure 2.5 One strand tundish furnished with a Turbulence Inhibitor(TI)

A two phase model was simulated using a Eulerian-Eulerian model, where water was considered as the primary phase and air as the secondary phase. The mathematical models included three different arrangements: the tundish had a transverse gas bubbling curtain which increases the mixing processes as the gas bubbling flow rate rises, causing complex recirculations in the volume of the tundish and a decrease in plug flow fractions. By comparing different arrangements inside the tundish, the combination of the TI and gas bubbling, lead to good inclusions removal, measured by the mathematical model, as long as the gas flow rate is controlled. Conversely, the bare tundish lead to chaotic fluid flow patterns. It has been seen that bubbling gas as well as a good arrangement of the FCD has to be controlled, in parallel, in order to avoid slag entrainment and high recirculation rates within the melt flow. However, bubbles in water can be significantly smaller than the typical bubbles generated in liquid steel-refractory systems, so these data need to be verified in steel tundishes.

A.VARGAS-ZAMORA et al.[13] analyzed the effects of buoyancy and inertial forces on fluid flows subjected to gas bubbling and thermal stratification conditions, in a one-strand tundish, using a 2/5 scale water model. Physical experimentation by PIV and mathematical simulations were carried out. Under isothermal conditions, the fluid flow was shown to have a plug flow pattern, contrary to the non-isothermal experiments. When adding hot step inputs, it was found that the gas bubbling, instead of decreasing the thermal gradients along the length of the tundish volume, divides the thermal fields into two, one on each side of the bubble curtain. In addition to this, the velocity fields were shown to be high at the bath surface, as an effect of inert gas buoyancy forces. The combination of using a turbulence inhibitor and low flow rates of gas injection, through a gas curtain, were more effective in the improvement of the fluid flow and yielding higher plug fractions. Conversely, higher flow rates created recirculations on both sides of the gas bubble curtain.

Buoyancy effects on the melt flow of steel have also been reported by authors such as R.D. Morales et al. [14] and S. Lopez Ramirez et al. [58] using

mathematical simulation approaches for a two-strand slab caster. The thermal gradients, as well as the velocity profiles caused by step-input temperatures by the different flow rate variations were predicted. The ratio of the buoyancy to inertial forces can be characterized by: Gr/Re^2. From this approximation, it can be said that the buoyancy forces are significant if the ratio is larger than one and they can have an important influence over the flow patterns. Positive buoyancy forces increase the residence time of the fluid, providing more time for non-metallic inclusions to be floated out. This phenomenon takes place when the steel melt is near the slag layer. It has been shown that a TI and baffle arrangement was more useful to float out the inclusions than the other arrangements incorporating a pair of baffles and a pair of weirs. A TI redirects the flow towards the surface, enhancing the residence time of the fluid near the slag layer. On the other hand, a TI is also useful to decrease the steep thermal changes. When low molten steel flow rates are achieved, along with large differences between the ladle stream and output tundish temperatures, the conditions for strong flotation forces are appropriate. Conversely, the buoyancy forces are less significant if a high input of flow rate is used, since the inertial forces reduce the buoyancy number. By these studies, it was shown that a Turbulence Inhibitor is very useful in controlling the turbulence, as well as promoting the flotation of inclusions.

Fluid flow characteristics in terms of momentum transport and heat transfer were studied by R.D. Morales et al. [15] in a two strand slab caster tundish, using water modeling and numerical techniques, considering three types of arrangements: a bare tundish, a tundish equipped with a pair of weirs and a pair baffles(W&B) and a tundish inhibitor with a pair of baffles(TI&B). Under isothermal conditions, an intense by-pass flow was the main characteristic of the bare tundish and W&B arrangements. The TI&B showed better control of the fluid flow, giving longer minimum residence times and higher plug flow fractions, as well as less dead volume along the tundish. When the fluid is transported from the ladle to the tundish with step-inputs of hot steel, the buoyancy forces cause the incoming steel to float towards the surface. In comparison, with step-inputs of

cold steel, a by- pass flow along the length of the tundish is created, that are especially visible for the bare tundish and the W&B arrangements. In the case of the TI&B arrangement, stratifications of thermal energy are developed, but in a more balanced way. During cold steel additions, the TI attained a better control of the thermal changes, attaining a decrease in the rate of steel output temperature. The TI&B was more effective in controlling the movement along the surface than was the W&B arrangement. The TI is more effective in controlling turbulence than is the W&B. This is mainly because the energy is dissipated inside the volume of the TI, and recirculations are formed before the fluid gets closer to the slag layer, thereby enhancing the residence time of the flow near the bath surface and enhancing the flotation of inclusions. When the entering velocity flow and associated kinetic energy are conserved in the upwelling fluid on its way towards the bath surface, slag rentrainment and overall asymmetric flow along the volume of the vessel can occur, together with the formation of an eye around the ladle shroud. The exposed steel can be re-oxidized and large inclusions are formed [15].

Steel flow in a two strand tundish with off-centered ladle shrouds was also studied (A. Aguilar-Corona et al.[57]) in terms of thermal stratification, using two flow control arrangements, using a non-isothermal water model. The first arrangement consisted of a pair of baffles(PB) and the other one, a Turbulence Inhibitor and a pair of dams(TI-D).

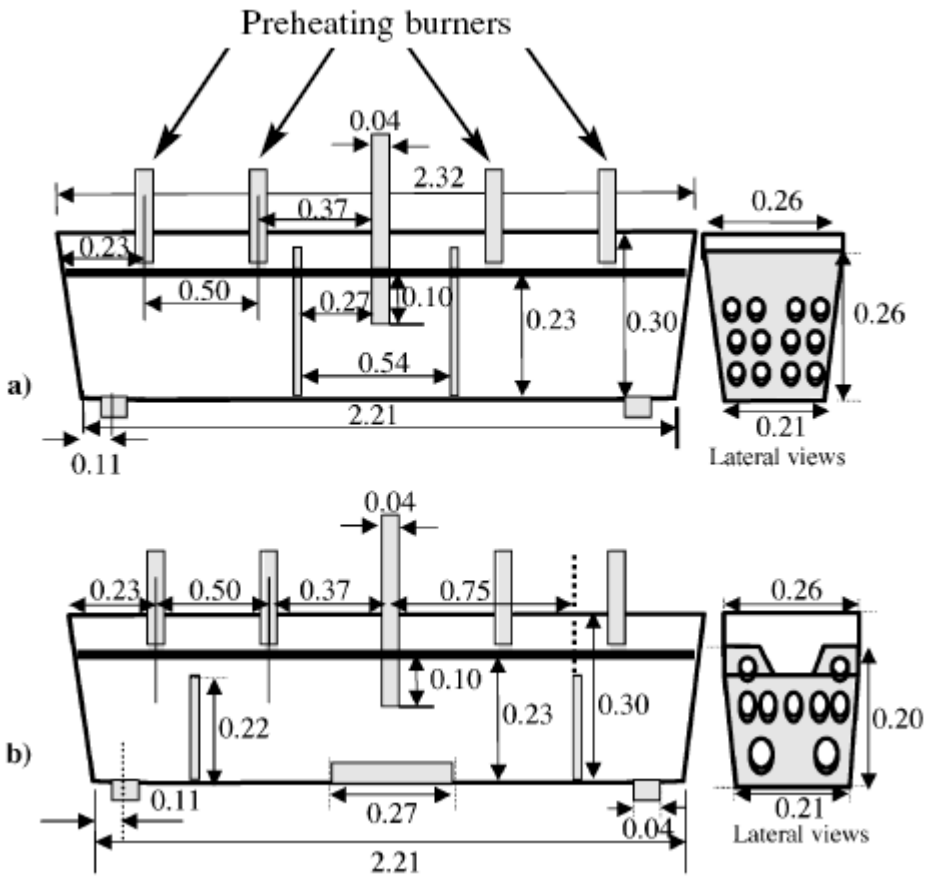

Figure 2.6 a) arrangement with the two baffles(PB), b) TI-D arrangement with a turbulence inhibitor and two multi-pot dams

Thermal experiments, adding higher entry water temperature, and with the ladle shroud placed at the center, off centered 1 ladle shroud diameter(1D) and off-centered two ladle shroud diameters(2D), were investigated. Physical experiments were done by PIV for visualization of the velocity fields. It was found that for any position of the ladle shroud and the rate of casting, the TI-D arrangement performed better by decreasing the thermal gradients along the length of the tundish, prolonging the buoyancy forces and increasing the fraction of plug flow, independent of the ladle shroud position. It was also discovered by measuring the thermal responses at the outlet, that the buoyancy forces were also enhanced in that area, and therefore promoted the flotation of inclusions.

The positive effects of using a Turbulence Inhibitor, alone or in combination with other flow modifiers, during tundish operations, has been investigated and proved. A TI is useful to avoid tundish slag entrapment, pick up of oxygen and nitrogen from the surrounding atmosphere, a decrease of downgraded steel during a grade and/or ladle change, etc., when casting in two or single strand tundishes. When casting in multistrand tundishes, the efforts of maintaining homogeneous chemical and temperature properties become more intense. A good furniture arrangement inside the tundish is important for improving the fluid flow characteristics. Jorge Madias et al.[24] characterized the fluid flow with mathematical and physical modeling in a six-strand tundish by placing a pouring box at the outlet of the ladle stream and comparing those results with an arrangement involving a flat impact pad and baffles. The pouring box improved the minimum and median residence times for all the strands as well as the plug flow fraction. It also decreased slag emulsification and dead volume.

R.D. Morales et al.[21] investigated by mathematical simulations and physical experiments the effects of using a TI in a four-strand bloom caster tundish. Three different cases were selected for the study: a bare tundish (BT), a tundish with two pairs of baffles and a waved impact pad (BWIP), a tundish with turbulence inhibitor and a pair of dams(TI&D). A coupled mass transfer model with the k-ε turbulence model has been used to predict the tracer displacement along the length of the vessel and it showed good agreement with the chemical mixing of the tracer in the water model experiments.

It was found that the TI&D performed better than the other arrangements and as a result, the injected tracer was shown to have a better distribution along the length of the tundish, with lower values of axial and transverse mixing and higher values of plug flow. Similarly, it reported a larger minimum residence time. Similar residence time distribution(RTD) curves were achieved in the inner and outer outlets, from which it can be assumed that the homogenous temperatures in the outlets as well as steel cleanliness are attained.

H.B. Kim et al.[23][50] studied transport phenomena in a full scale four strand delta- shaped tundish, using mathematical and physical simulations. These approaches were useful in suggesting better operating conditions, higher productivity and steel quality. Shamik Ray et al.[48][11], also working on the same tundish, compared the performance of fluid flow using a shallow Impact Pad, developed by previous researchers of the same group, with the newer Turbostop. They found that the previously developed shallow Impact Pad, was superior in attaining longer averaged residence times of fluid inside the tundish, with less slag entrainment during ladle changes. These workers have been the only ones to study inclusion removal using physical models and an electric sensing home sensor for detecting the sizes, and frequency, of inclusions exiting the strands. They were able to show that RRI´s were largely independent of the ratios of mixed and plug flow volumes in a tundish.

Pradeep K. JHA et al. [59] investigated the effects of the height and position of the dams in the tundish and the size of the particles, on the percentage of inclusions removed. A discrete random walk model was applied during inclusion trajectory calculations. It was found that with the increase in the height of the dams, the removal of the inclusions improved, but when the height was decreased and placed nearer the outlets, the inclusions removal was diminished mainly because when the dams were close to the outlets, some recirculatory flow patterns were created.

Another approach of studies involving fluid flow in multi-strand tundishes was Liangcai ZHONG et al.[60] using physical experiments and mathematical modeling. They analyzed the fluid flow inside a four-strand tundish by doing a comparison between two arrangements of FCD, the first one with baffles and the second with baffles and a TI. The analysis was done by performing physical experiments, injecting a tracer, and by mathematical modeling. With the first configuration, the jet, after impacting the bottom of the tundish, was creating large recirculations directed towards the surface. This was causing tundish slag entrapment and lining corrosion. Asymmetric fluid flows were formed along the

tundish, causing shorter minimum residence times at the inner outlets. The results obtained showed that the second arrangement improved different variables such as minimum residence time and dead volume fractions, leading to a similar RTD curves for the inner and outer strands. The movement of the surface as well as the turbulent motion of the molten liquid has been damped achieving a more symmetrical flow on both sides of the tundish.

Anil Kumar et al. [25] carried out mathematical and physical simulations in a four strand tundish in order to compare the fluid flows obtained. The physical experiments included the injection of a tracer, as well as PIV techniques, in a scaled water model. Three arrangements were selected: a bare tundish (BT), in the presence of a dam (D&T) and a third arrangement with a Turbulent Inhibitor and a dam(TI&D).

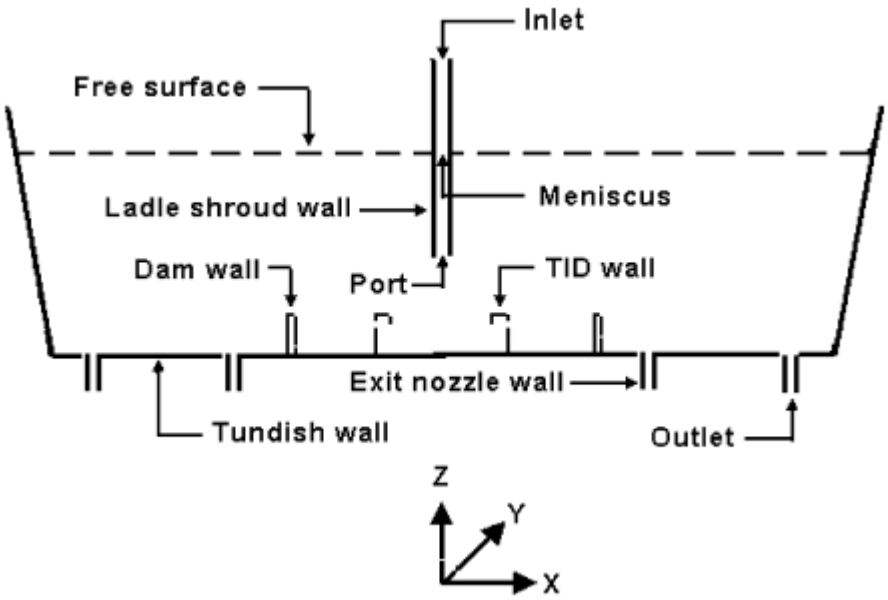

Figure 2.7 Schematic of the model with different physical boundaries

The results have shown that the bare tundish leads to short-circuiting and large dead volumes. The dams showed good results in controlling the incoming jet and in redirecting the flow towards the surface, but the TI&D arrangement yielded more similar velocity fields within the volume of the tundish concerning distribution to the inner and outer strands. This arrangement had larger fractions

of plug flow and minimum residence times as well as a lower fraction of dead volume.

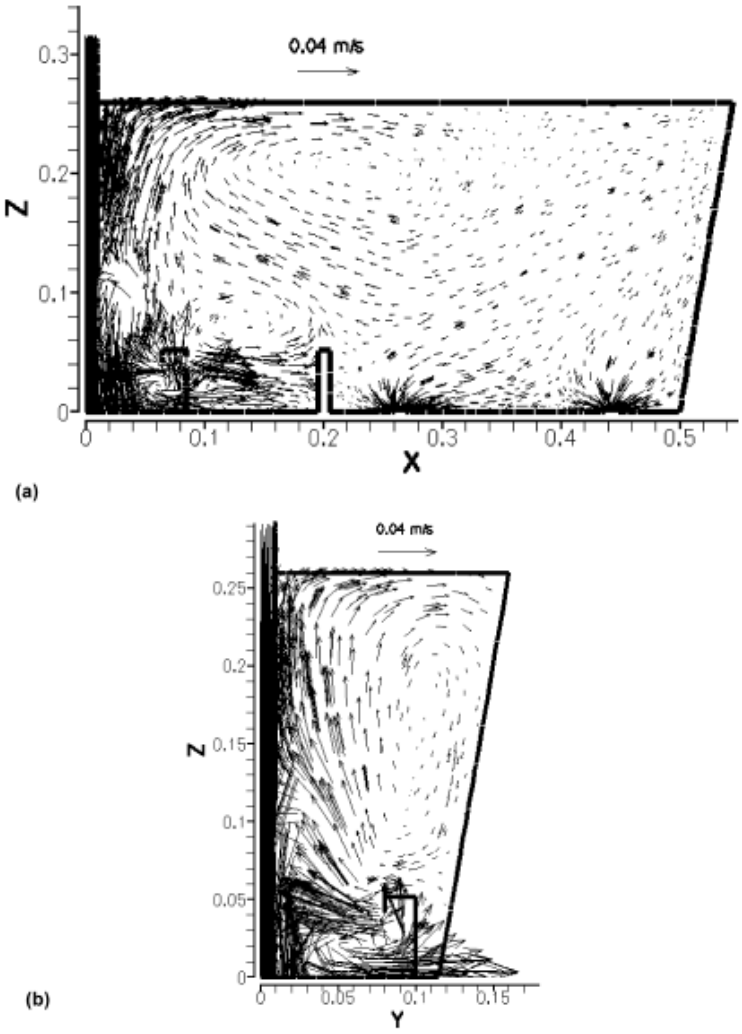

Figure 2.8 Predicted velocity fields by the mathematical simulations with the TI+dam arrangement

P.K. Jha et al.[36] studied mixing phenomena in a six strand billet caster tundish in parallel with the species concentration equation, in order to compute different

variables such as mixed, plug and dead volumes. The validation has been done by comparing the results that had been obtained before in a single strand bare tundish. An advanced pouring box (APB) was placed so as to surround the incoming inlet jet. The analysis has been taken by varying the height of the ABP. It was observed that an optimum height and immersion of the shroud exist, in which the fraction of mixing is larger than that of the dead volume, for a particular position at the outlets. The optimum height for the ABP was found to be 21 cms. After attaining the optimum height for the ABP, it was found that the optimum depth for the shroud was 30 cms., where the mixing/dead volume was the highest and a higher mean residence time was achieved.

Numerical modeling was performed by T. Merder et al. [37] for the study of the fluid flow phenomena in a continuous casting six-strand tundish, using the commercial software FLUENT. Two arrangements were selected for the study, one with an impact pad and the other with the impact pad and a dam. It was found that the dams and pad arrangement decrease the dead volume and increase the plug volume.

Guanghua Wen et al. [38] studied fluid flow in a six-strand bloom caster tundish by physical and mathematical models. The particles´ removal was modeled by mathematical simulations with thermal gradients. It was established that inside the tundish exists a strong buoyancy effect that affects the fluid flow. When equipped with a FCD, the buoyancy forces act in a more uniform pattern.

A Espino-Zarate et al. [39] characterized tundish fluid flow, using different turbulence inhibitors, and tracer dispersion experiments. Mathematical simulations were also executed. It was found that the key parameter for attaining plug flow patterns by the use of inhibitors, is the rate of dissipation of kinetic energy. The turbulence inhibitors that produce abrupt dissipation gradients are less efficient than those with a gradual decrease of energy. Two arrangements were compared for two different designs of TI with baffle arrangements. The second arrangement was found to be more efficient in decreasing the dead volume and increasing the plug flow fractions.

2.3 NEW ALTERNATIVES OF FLOW CONTROL DEVICES AND CURRENT TRENDS

Recently, some researchers have been dedicating their efforts towards maintaining the fluid for longer periods of time inside the tundish and improving the performance of the commonly used FCD such as weirs, dams, baffles, etc. Some approaches have been oriented towards giving a rotational motion to the fluid using different FCD during the stay of liquid steel inside the tundish. G. Solorio-Diaz et al.[26] proposed a new design of a ladle shroud named the "Swirling Ladle Shroud(SLS)". This consisted of a pipe plus three intermediate chambers of larger diameter that worked as buffers to the fluid velocity. At the top, the shroud was equipped with a blade whose function was to initiate the swirling motion.

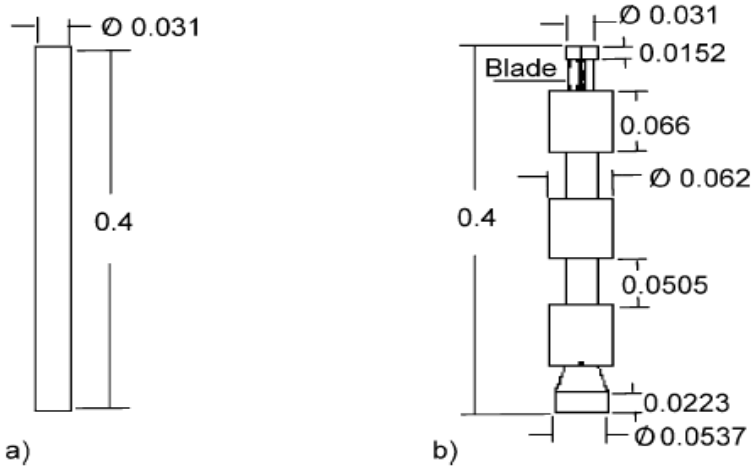

Figure 2.10 a) Conventional ladle shroud b) swirling ladle shroud(SLS)

The SLS controls the jet entering inside the tundish, decreasing the impact velocity to a third at the bottom of the tundish, as compared to that of the conventional ladle shroud. Different physical and mathematical simulations, including the PIV techniques and a variety of turbulence models, such as the k-ε and RSM have been used. They recommended using the RSM in the tundish when dealing with swirling motions, since the predicted velocity fields were in

good agreement with the results obtained by the physical experimentation executed by PIV. Other experiments have been carried out in the SLS involving non-isothermal conditions and the role of this FCD for the removal of inclusions. Under thermal gradients, flows intensify the formation of vortices close to the outlets. This is harmful because when inclusions are entrained by those vortices, they are directed towards the outlets. As the SLS decreases the turbulence at the entry of the jet into the tundish, the entrainment of slag is decreased if compared with the conventional ladle shroud.[27][17]

Qinfu HOU et al.[28][41][43] have proposed a Swirling Flow Tundish (SFT), whose main objective is to give the entry jet a swirling motion through a cylindrical swirling chamber(SC). To analyze the fluid motion inside the SFT, physical and mathematical simulations have been executed. The trials were done using an asymmetrical one-strand 1:25 and a symmetrical two-strand 1:3 scale model. The inclusion´s trajectory has been studied using the discrete phase model (DPM) with the commercial package FLUENT. It was shown that the SFT was more efficient in the removal of small inclusions with sizes in the range of 20 µm than a tundish fitted with a Turbulence Inhibitor. This can be important for a high quality product in the steel industry. One important characteristic was that the Swirling Chamber is in an asymmetric position, leading to asymmetrical flows along the length of the tundish with the possibility of vortexing flows and entrainment of upper slag phase.

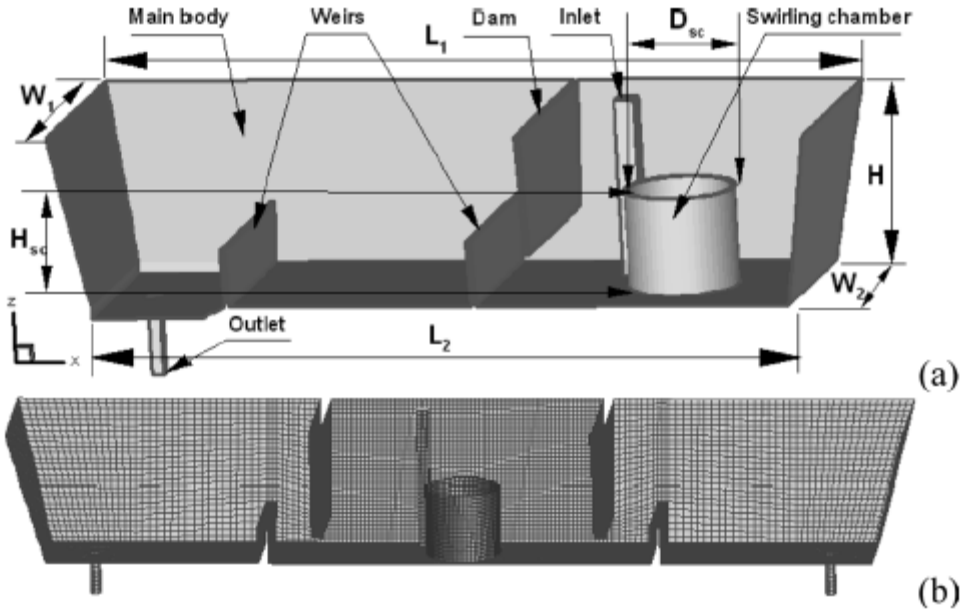

Figure 2.11 a) Single strand tundish with the swirling chamber(SC) arrangement, b) Two strand tundish fitted with the swirling chamber(SC)

Another novel proposal, also following along the lines of creating a centrifugal velocity inside the a single-strand tundish has been developed by Yun Wang et al.[40], using physical tracer experiments and mathematical simulations. Here, the effects of the dam spacing and rotation speed of the fluid flow were analyzed. The mechanism of inclusions flotation is based on the rotation of the fluid in the centrifugal chamber induced by electromagnetic forces. This procedure has been demonstrated to have good results during plant trials. After the results obtained by the mathematical simulation using steel as a fluid, it was concluded that the rotational motion induced by the magnetic field in the centrifugal chamber reduces the dead volume related to the position of a dam. By reducing the space in the dam, the evolution of the rotational flow increases the flow path, resulting in a larger fraction of plug flow. The highest ratios of plug to dead volumes are reached when the dam spacing cause a stronger transverse circulation. A balanced magnetic field was recommended to maintain a balanced rotational motion. Fang Wang et al.[42] simulated mathematically a centrifugal flow tundish by the Large Eddy Simulation (LES) technique. This model (LES) offers a deeper

insight into transport phenomena regarding to the fluid flow taking place under transient conditions. Three cases were studied: Electromagnetic force with the Direct Nozzle(EDN), Bending Nozzle (BN) with height potential energy of molten steel, and a combination of electromagnetic force and bending nozzle(EBN).

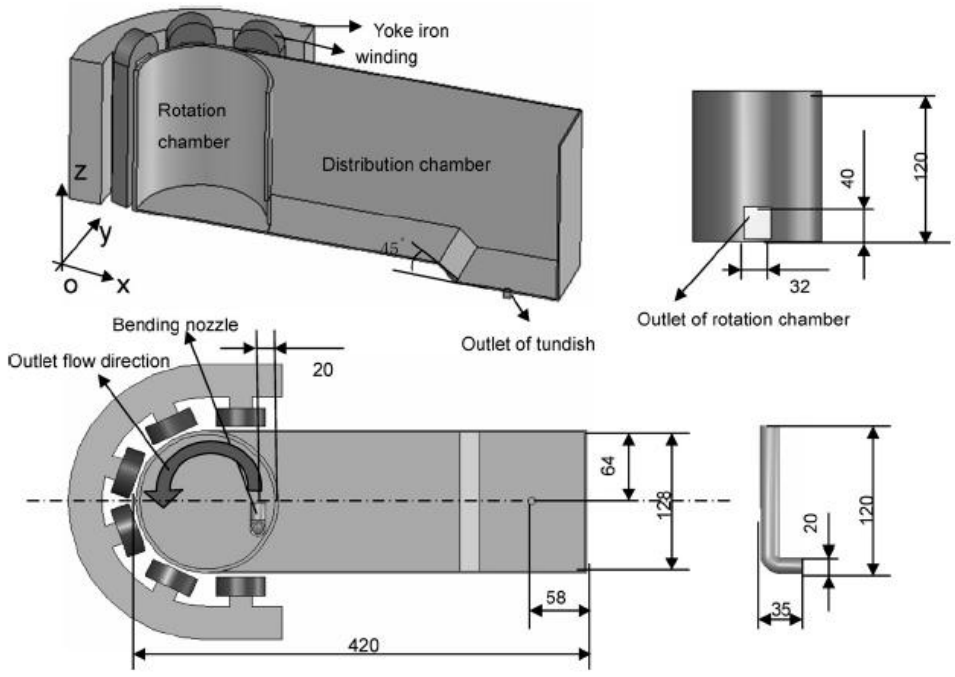

Figure 2.12 Schematic of the physical model

It was found that when the EDN arrangement is applied, inside the rotation chamber, two strong recirculations are generated. In the case of BN, the horizontal swirling gets stronger than the vertical segment. In the last case, EBN, the evolution of the swirling flow is highly enhanced. They found the BN increases the velocity in a comparable range with that of the EDN case, which makes the BN a simple and alternative option for centrifugal tundish operations.

The LES technique has been used less than other turbulence models. In fact there are not many researchers addressing its usage in the literature, largely because it is very computationally consuming. Pradeep K. Jha et al.[44] made a comparison of different turbulence models, including the LES, in order to

compare different predictions. The LES predicts, very well, the steep gradients in the transport processes, and thus it can be a useful and detailed tool to describe the physical phenomena taking place inside the tundish. Nouri Alkishriwi et al. [45] have simulated the LES for a tundish equipped with a stopper rod, during unsteady state operations. To achieve a reliable solution, the computational domain was divided into 12 million grid points, from which 5 million were at the entry jet, in order to get a detailed description of the turbulence parameters in that region. The memory requirement was in the order of 15 GB and the time elapsed was close to 250 hours. Additionally, 150 hours were required to gather statistical data. Detailed structures of the entry jet can be obtained which cannot be predicted with accuracy by the Reynolds Average Navier-Stokes methods.

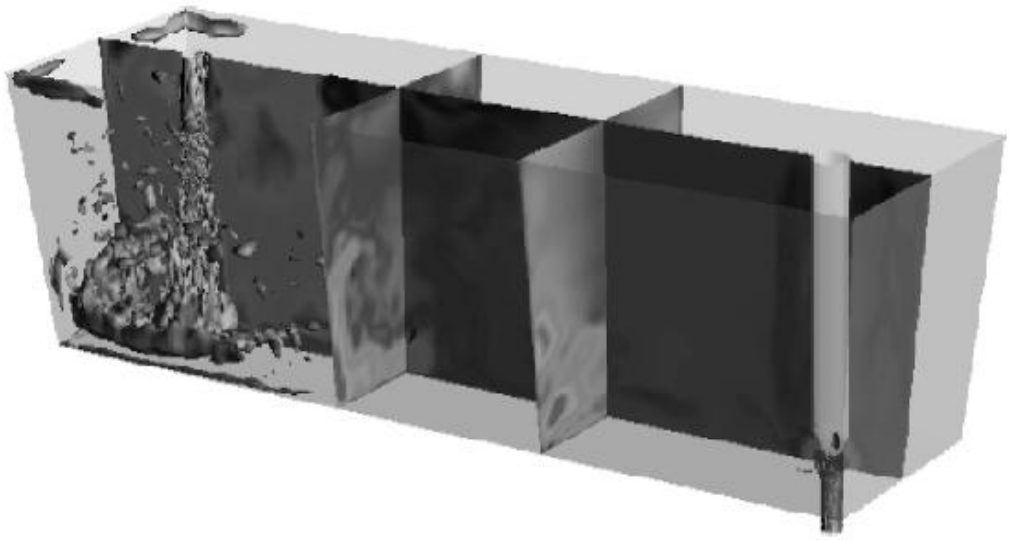

Figure 2.13 Schematic of the LES of a velocity field in the tundish

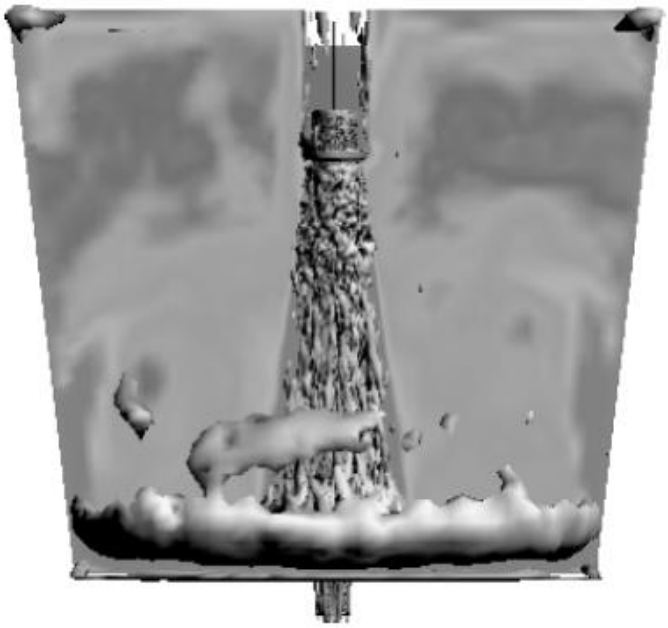

Figure 2.14 Contours of velocity of the entry jet

Another important factor that is nowadays taken into account by the researchers is the coupling of different phases and phenomena in order to get a more realistic view of the actual transport processes occurring. Carlos A. Llanos et. al [46] simulated a multiphase steel/slag/argon mathematical model for ladle operations.

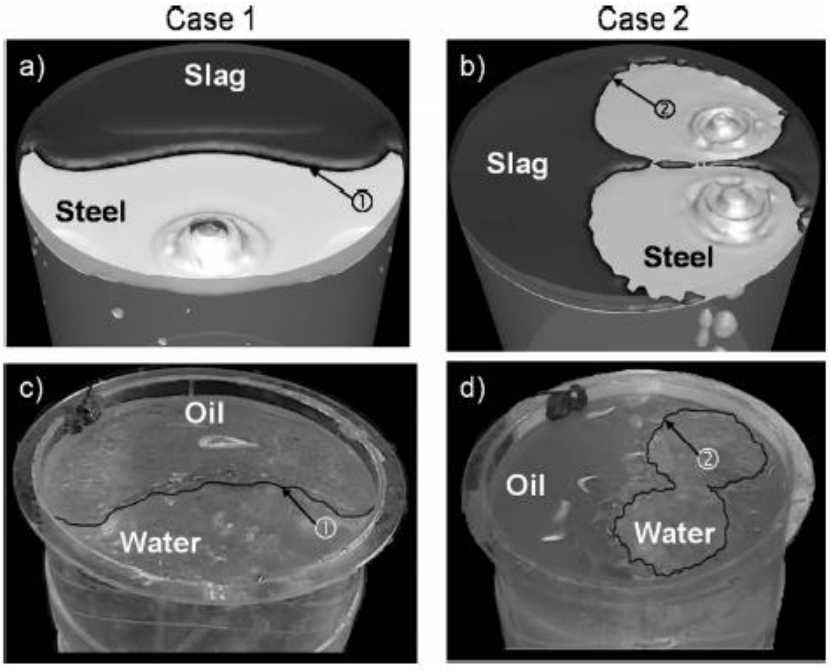

Figure 2.15 Slag opening view for: a) mathematical simulation, b) physical experiments.

The volume of fluid (VOF) has been considered to simulate the interaction between the phases, taking into account surface tension. Using different positions and conditions of argon injection inlets, they were able to predict a decrease of the slag layer opening, thus making the multiphase modeling an important approach to increase the resemblance to the actual processes.

As we can see, the current trends are to reduce as much as possible the usage of FCD inside the tundish, and to improve the mathematical models by coupling several phenomena involving different phases. Large computational investments into parallel processing are required. In some parts of the world, the tundish has been increased in its length, and depth. Similarly, it is treated by plasma reheating in order to maintain isothermal conditions during casting. This can reduce the use of Flow Control Devices consumption.[18] The efforts of researchers and engineers are now more oriented towards the development and optimization of mathematical models compared to physical experiments, leading to a high computational investment.

2.4 FINAL REMARKS

It has been shown that Flow Cotrol Devices(FCD) are useful tools for controlling the fluid flow through a tundish. In general, the Turbulence Inhibitor(TI) is the most efficient, alone or together with other FCD´s. A reliable prediction of the turbulent flow fields is fundamental to the understanding and analysis of the passage of liquid steel through the tundish. Consequently, techniques such as Particle Image Velocimetry (PIV) and Residence Time Distributions (RTD) are used extensively in this area. Overall, the RTD technique is more widely used rather than lasers when analyzing fluid flow in tundish, mainly because of its simplicity, economic advantages, and the useful information obtained from them, such as, plug volume, dead volume, etc. However, if an in-depth observation of the fluid flow is desired, the laser techniques are more detailed and superior. Consequently, higher expenses are involved as well as the time consumed in experimental analysis.

Nowadays, a combination of RTD techniques with mathematical modeling is more common for analyzing fluid flows in tundishes by engineers and researchers. Increasing reliance is being made of fluid flow visualization through mathematical simulations, carried out using commercial packages, such as FLUENT-ANSYS, COMSOL, etc.

On the other hand, as mentioned before, we can see that the current trends are to reduce the usage of FCD´s. Larger tundish designs, combined with external heating, can be useful towards attaining larger averaged residence times along the length of the tundish, as well as an efficient temperature distribution. The use of electromagnetic forces in the tundish is an interesting approach which can be useful in increasing the flotation of micro inclusions. However, these techniques haven´t been fully implemented yet. Therefore, the control of the fluid flow through the ladle shroud, as seen in the Swirling Ladle Shroud, can be a simple solution and a reliable option to attain higher steel qualities. However, potential difficulties such as clogging by entrained inclusions need to be tested.

CHAPTER 3

SIMULATION PROCEDURES

3.1 EXPERIMENTAL TECHNIQUES AND PROCEDURES

3.1.1 INTRODUCTION

The physical modeling experiments were carried out in a one-third scale model of a four strand delta shaped tundish of a billet caster. Figures 3.1a, 3.1b and 3.1c show the geometry of the tundish for top, front and side views, respectively.

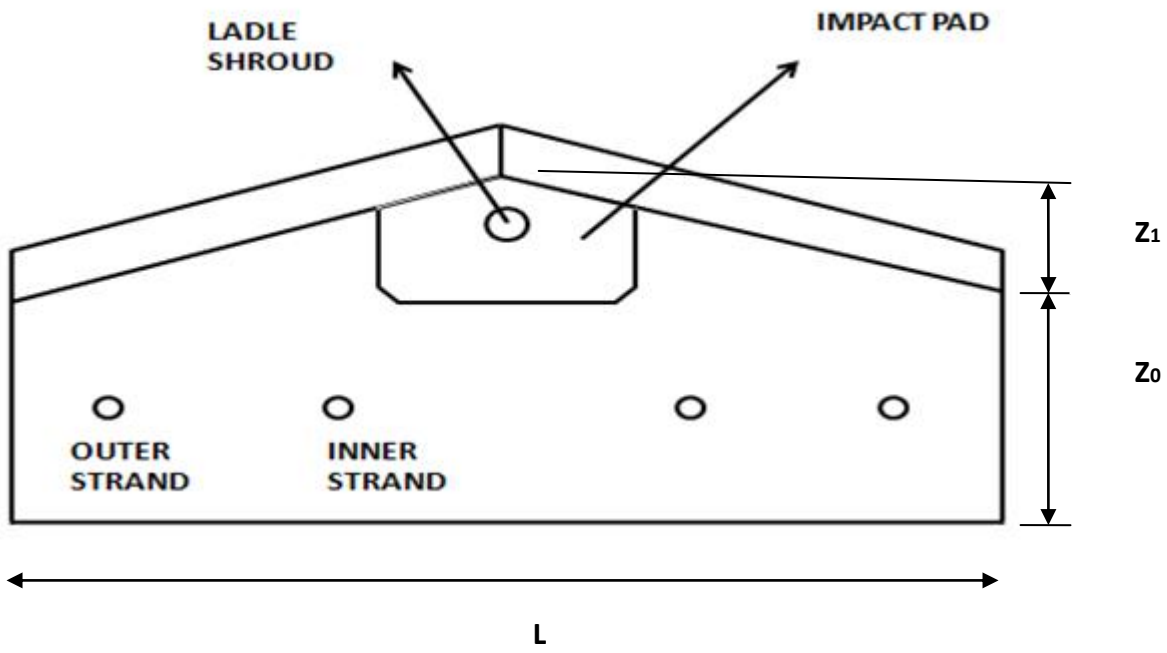

Figure 3.1a Top view of the one-third scale model of the four strand delta-shaped tundish

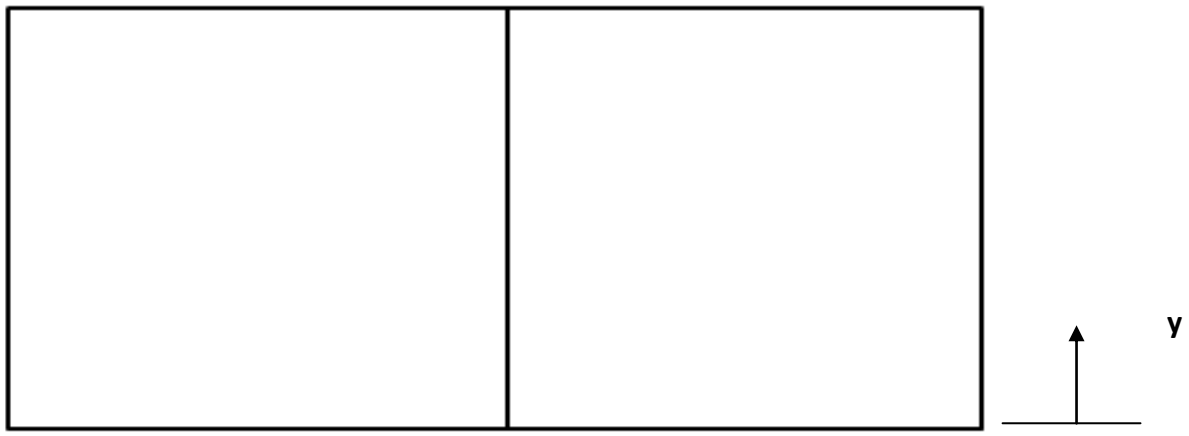

Figure 3.1b Front view of the four strand delta-shaped tundish

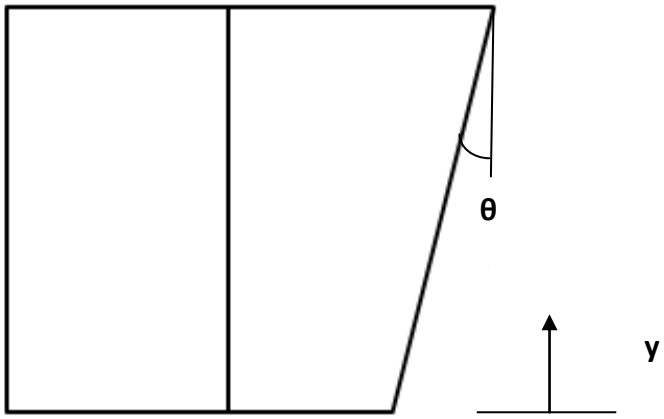

Figure 3.1c. Side view of the four strand delta-shaped tundish

To obtain the liquid volume of the delta shaped tundish model, the following relation can be applied:[49]

$$V = L * (z_o + \frac{z_1}{2}) * y + L * \tan\theta * y^2$$

Where, L = length of the tundish bottom

z_1 = width difference between middle and the side at tundish bottom.

z_o = side width at tundish bottom.

Θ = side wall inclination

y = level of the liquid

The water supply is obtained by a large and wide hose connected directly to the laboratory pump, in which large flow rates can be attained. After that, the water runs through a connector, a reducing pipe, the flow meter which measures the desired flow rate and finally the selected ladle shroud that feeds the plexi glass tundish model. The experiments were based in four different cases, including:

1) The conventional ladle shroud arranged with the bare tundish (LS-bare).
2) The conventional ladle shroud with the Impact Pad (LS-IP).
3) The Dissipative Ladle Shroud with the bare tundish (DLS-bare).
4) The Dissipative Ladle Shroud with the Impact Pad (DLS-IP).

The geometry of the conventional (LS) shroud is shown in Figure 3.2a, along with the final design of the dissipative ladle shroud (DLS). Figure 3.2b shows the Impact Pad used in the experiments.

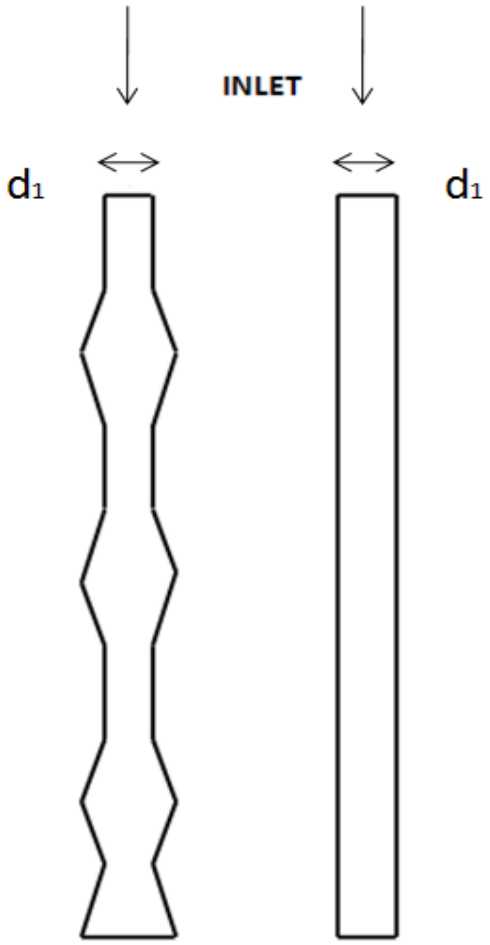

Figure 3.2a Scheme showing the shape of the DLS and LS

Figure 3.2b Scheme showing the shape of the Impact Pad

The flow rate was maintained at 11 L/min, corresponding to the steady state operations, obtained by following the Froude similarity criteria. The height of the water was maintained at 17 cms. The shroud was positioned at a height of 15 cms from the bottom of the tundish, therefore submerged 2 cms inside the water. The volume of water in the tundish is calculated to be 65.2 L.

Table 3.I summarizes the properties of water at 20°C and steel at 1600 ° C as well as the experimental conditions. The kinematic viscosity is very similar at this temperature for both fluids, therefore water modeling is a reasonable approach in tundish operations.

Properties and conditions	**Model** **Water (20°C)**	**Prototype** **Steel (1600°C)**
Molecular viscosity (μ), kg/m*s	0.001	0.0064
Density (ρ), $\mathrm{kg/m^3}$	1000	7014
Kinematic viscosity (ν= μ/ρ), $\frac{m^2}{s}$	1.0 x 10^{-6}	0.91 x 10^{-6}
Flow rate at steady state (L/min)	11	170
Scale of tundishes	1:3	1:1

Table 3.1 Properties of the water and experimental conditions

3.1.2 DYE AND TRACER INJECTION

Equipment for the tracer experiments consisted of the model tundish with its flow arrangement inside, a flowmeter ahead of the inlet to quantify water throughputs,

and a syringe located in the upper part of the LS or DLS, in order to inject the tracer solution. At each one of the two outlets on either side of the tundish, electric conductivity probes were fixed to measure changes of water conductivity with time after injecting (through a 50 ml syringe of a NaCl water solution with a concentration of 200 g/L), at an instant assigned as time zero. The analog signals of both conductivity probes were digitized by a Data Acquisition Software (DAS) in a PC to be able to measure conductivity in a real time basis. Monitoring two of the outlets or strands in one side of the strand assumes implicitly that the flow is symmetric and therefore, all changes of conductivity with time in the inner and outer strands of the other side must behave similarly to the ones which were monitored. The pulse injection of the tracer was used to obtain the corresponding curves of Residence Time Distribution (RTD) curves to analyze fluid flow characteristics. To visualize flow patterns inside the tundish a red dye tracer was injected and the mixing process with flowing water was recorded by a conventional video for each experimental case. Figure 3.3 shows a schematic of this setup.

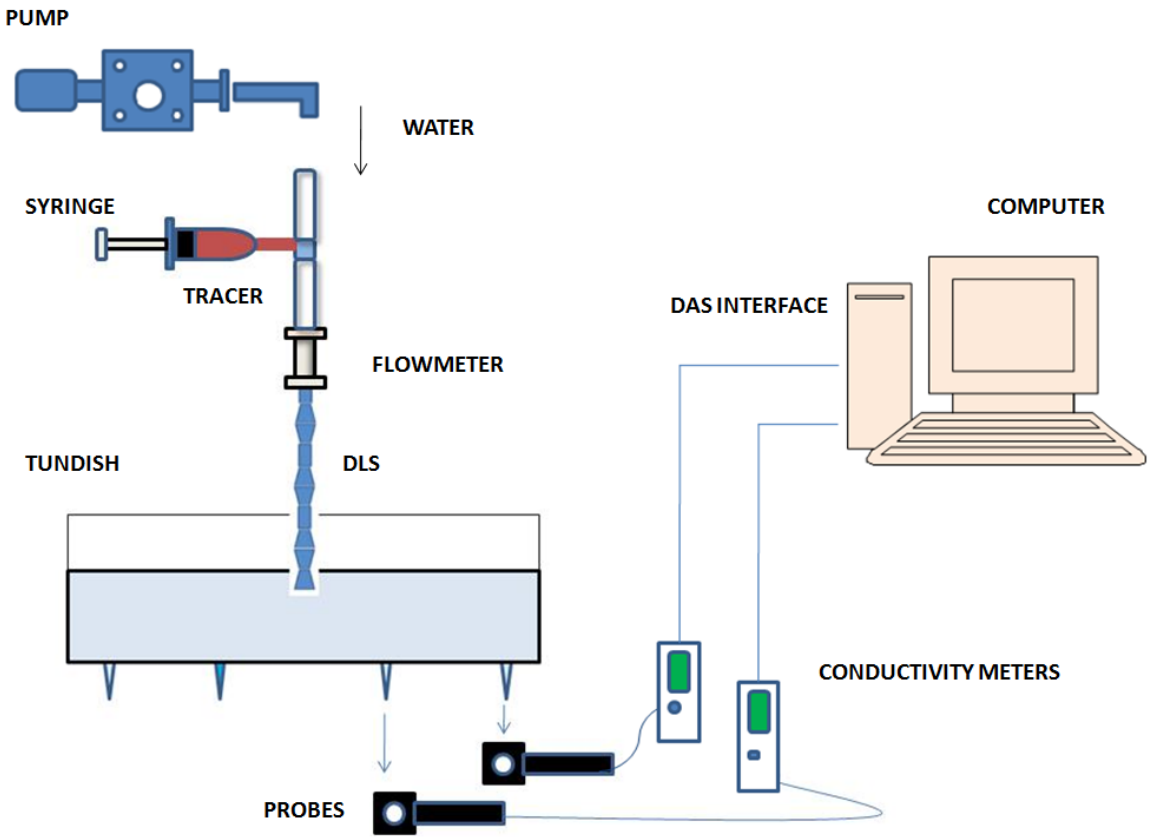

Figure 3.3 Schematic diagram for tracer experiments setup

3.1.3 PARTICLE IMAGE VELOCIMETER (PIV)

The second setup focused on the dynamic behavior of the entry jet when using both the conventional LS and the DLS. For that purpose, a Particle Image Velocimeter (PIV) from DANTEC® was employed, consisting of a laser gun with a power of 20 mJ, a Coupled Charged Device (CCD) to record the motion of seeding particles in the flow, and software to perform Fast Fourier Transform analysis of the velocity signals transferred to a computer. The interrogation area involved the shroud discharge region, in order to monitor the turbulence of the entry jet. A mirror with an angle of about 30^0 with respect the horizontal plane was placed below the tundish bottom and the laser gun was located in its front. The laser light sheet from the gun is reflected on the mirror forming another longitudinal-vertical laser sheet that coincides exactly with the central axis of the LS or DLS tip (see Figure 3.4). At some given time, a slurry of seeding particles (polyamide particles with a size of 20 microns and density of 1.04 g/cm^3) was injected into the entry water flow, with the syringe, and the recording time starts to follow the flow dynamics. Figure 3.5 shows a schematic of the second experimental setup.

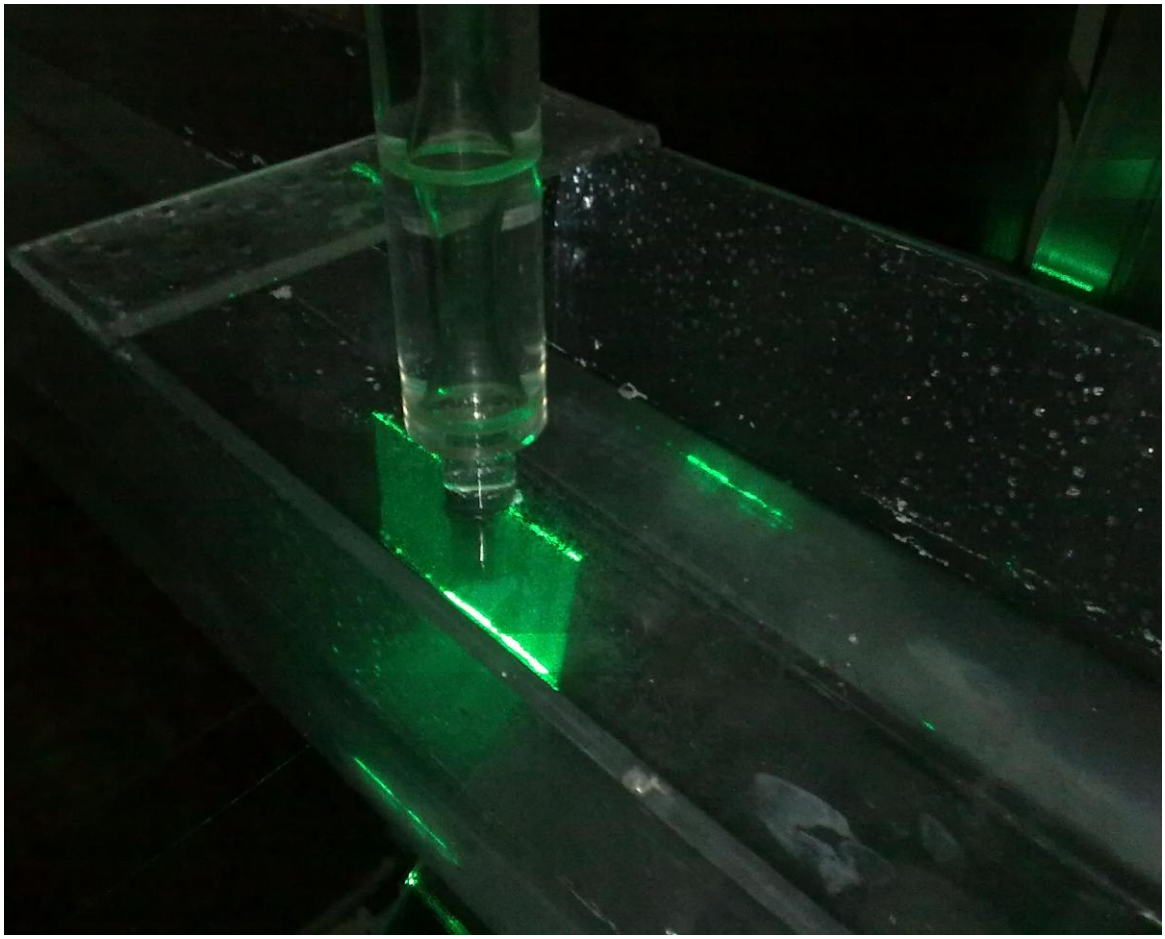

Figure 3.4 A reflected PIV sheet intersecting the central axis of the shroud, set in a longitudinal-vertical plane of the tundish

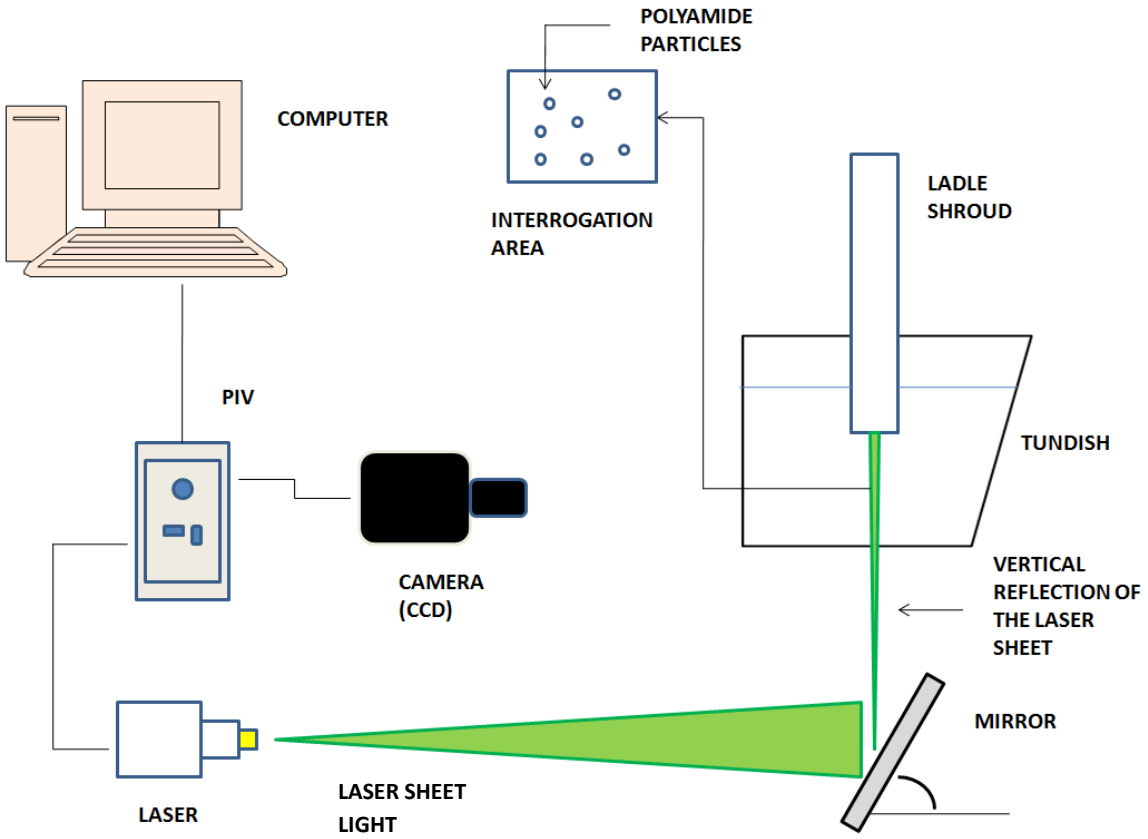

Figure 3.5 Schematic diagram for the PIV experiments setup

3.2 MATHEMATICAL MODELLING

The fluid used is water, under isothermal conditions and maintained at a temperature of 20 ° C. The fluid flowing through the tundish is maintained at the steady state. Therefore, the phenomena involved during filling and emptying the tundish was neglected. The free surface of the water is assumed to be flat and the slag depth to be thin enough to be neglected. Based on these assumptions, the flow field was obtained by the solution of the continuity and momentum conservation equations in the three-dimensional domain. The k-ε turbulence model [32][33] was adopted for solving the k and ε equations of turbulence. In here, k is the turbulent kinetic energy and ε the dissipation rate of the turbulent kinetic energy.

3.2.1 EQUATIONS FOR CONTINUITY, MOMENTUM AND TURBULENCE

The governing equations are the following:

Continuity:

$$\frac{\partial \rho}{\partial t} + \frac{\partial}{\partial x_j}\left(\rho u_j\right) = 0 \qquad (1)$$

Momentum:

$$\frac{\partial}{\partial t}(\rho u_i) + \frac{\partial}{\partial x_j}\left(\rho u_i u_j\right) = -\frac{\partial P}{\partial x_i} + \frac{\partial}{\partial x_j}\left[\mu_{eff}\left(\frac{\partial u_i}{\partial x_j} + \frac{\partial u_j}{\partial x_i}\right)\right] + \rho g \qquad (2)$$

Transport of kinetic energy of turbulence:

$$\frac{\partial}{\partial t}(\rho k) + \frac{\partial}{\partial x_i}\left(\rho u_i k - \frac{\mu_{eff}}{\sigma_k}\frac{\partial k}{\partial x_i}\right) = G - \rho\varepsilon \qquad (3)$$

Rate of dissipation of the kinetic energy of turbulence:

$$\frac{\partial}{\partial t}(\rho\varepsilon) + \frac{\partial}{\partial x_i}\left(\rho u_i \varepsilon - \frac{\mu_{eff}}{\sigma_\varepsilon}\frac{\partial k}{\partial x_i}\right) = \frac{\varepsilon}{k}(C_1 G - C_2\rho\varepsilon) \qquad (4)$$

Where:

$$G = \mu_t \frac{\partial u_i}{\partial x_i}\left(\frac{\partial u_i}{\partial x_i} + \frac{\partial u_i}{\partial x_j}\right) \qquad (5)$$

The effective viscosity is the sum of laminar viscosity and turbulent viscosities:

$$\mu_{eff} = \mu_l + \mu_t \qquad (6)$$

The turbulent viscosity is related to the turbulent energy and dissipation rate of turbulent energy by:

$$\mu_t = \frac{C_D \rho k^2}{\varepsilon} \qquad (7)$$

Here, $C_1 = 1.43, C_2 = 1.92, C_D = 0.09, \sigma_k = 1.00,\ \sigma_\varepsilon = 1.30$ are the empirical constants of the $k - \varepsilon$ model.

The set of partial differential equations were discretized using the Finite Volume Method in the commercial software ANSYS-FLUENT. The second order upwind scheme was used for the k, momentum and ε equations. The SIMPLE (Semi-Implicit Method for the Pressure-Linked Equations) algorithm[52] was used to solve the pressure–velocity coupling in the momentum equation.

Chapter 4.

RESULTS AND DISCUSSIONS

4.1 RESIDENCE TIME DISTRIBUTION (RTD)

The residence time distribution curves were obtained for the arrangements mentioned in the previous chapter.

The theoretical or nominal residence time was obtained by:

$\bar{t} = \frac{V}{Q}$ where V = volume of liquid in tundish (8)

$Q =$ volumetric flow rate of liquid into the tundish

The tundish was operated in steady state with a throughput of 11 L/min.

Therefore, the nominal time becomes:

$\bar{t} = \frac{0.065 \times 1000}{11}$ x 60 = 355.5 s

The non-dimensional and mean residence times up-to two times $\bar{t}$, were obtained by the following relations:

Mean residence time up-to θ = 2, $\theta_c = \frac{\sum_{\theta=0}^{2} C_i \theta_i}{\sum_{\theta=0}^{2} C_i}$ (9)

The mean residence time was also obtained as: $t_m = \theta_c \times \bar{t}$ second. (10)

The fractions of dead volume, the plug flow volume and the mixed volume were obtained from the experimental C curves using the following relations:

The dead volume fraction, $\frac{V_d}{V} = 1 - \frac{Q_a}{Q}\theta_c = 1 - \left(\sum_{\theta=0}^{2} C_i \Delta\theta\right) \cdot \frac{\sum_{\theta=0}^{2} C_i \theta_i}{\sum_{\theta=0}^{2} C_i}$ (11)

The dispersed plug volume fraction, $V_{dpv} = \left(\frac{\theta_{min} + \theta_{peak}}{2}\right)$ (12) , where

θ_{min} refers to the first appearance of the tracer in the outlet and θ_{peak} to the dimensionless time elapsed to reach the maximum concentration.

Finally, the mixed volume is obtained by: $V_m = 1 - V_{dpv} - V_d$ (13)

In all the cases, short-circuiting was observed, meaning that the tracer first reached the inner nozzle, and later, the outer nozzle. Hence, the changes in concentration were first registered for the inner nozzles. Figures 4.1, 4.2, 4.3 and 4.4 show the RTD curves for each of the cases. The t_{min} to the first appearance of the tracer is very similar in the LS-bare and DLS-bare cases, being larger in the LS-IP, while the DLS-IP case had the longest minimum residence time. The $t_{peak}$for the LS-bare has been detected to be the minimum, while the DLS-IP, the maximum. The DLS-bare and LS-IP had very similar values times of maximum concentration for both strands. Whenever the tundish is not equipped with the Impact pad, two tracer peaks in the inner strand are observed, the first one with a higher concentration, for both cases. In these cases, the second peak is observed after the highest peak of the outer strand was detected.

The patterns of the fluid flow inside the tundish have been described by H. Kim et al. [49] as follows: A portion of fluid elements with high tracer concentrations head towards the inner strand, where the first discharge peak is recorded. Similar packets of fluid elements is also recirculating near the discharge space, the largest portion of which is headed towards the outer strand, attaining a high peak. After that, the remaining packet leaves the tundish through the inner strand causing the second peak to appear at the inner SEN. This effect is more visible in the LS-bare, for which the largest portion of packets of fluid elements leave through the inner strand, causing the first concentration peak. The fluid discharged by the LS hits the bottom of the tundish with high momentum. As a consequence, it heads towards the exit nozzle over the inner strand, carried by recirculations that enhance the short-circuiting.

The DLS-bare retains more the fluid before the first and the second packets of fluid are leaving through the inner strand. By discharging the fluid at a lower velocity, over a wider area, the DLS distributes its downward momentum more broadly, thereby diminishing momentum energy directed towards the bottom of the tundish, damping the recirculatory motions and reaching the inner nozzle with less velocity. When the tundish was equipped with the flow control devices, the second peak was not observed and the short-circuiting flow was delayed. This is because the Impact Pad generates an upward velocity towards the surface and decreases the recirculations near the inner strand.

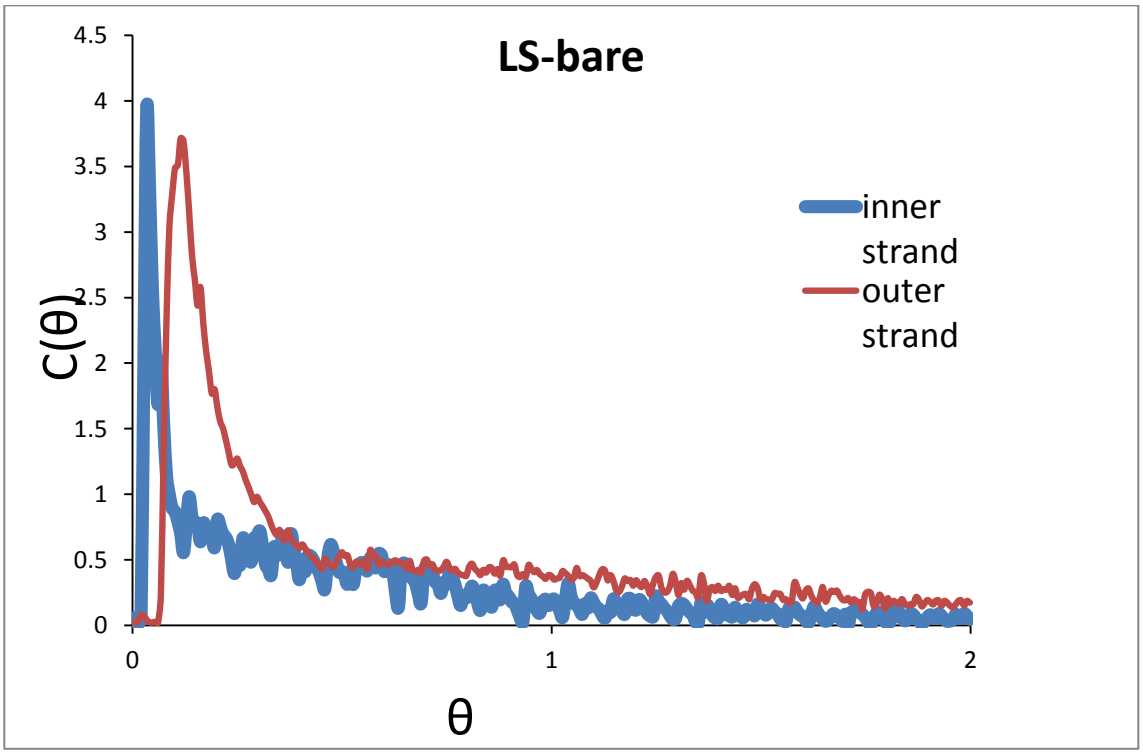

Figure 4.1 RTD curves corresponding to LS-bare case for the inner and outer strands

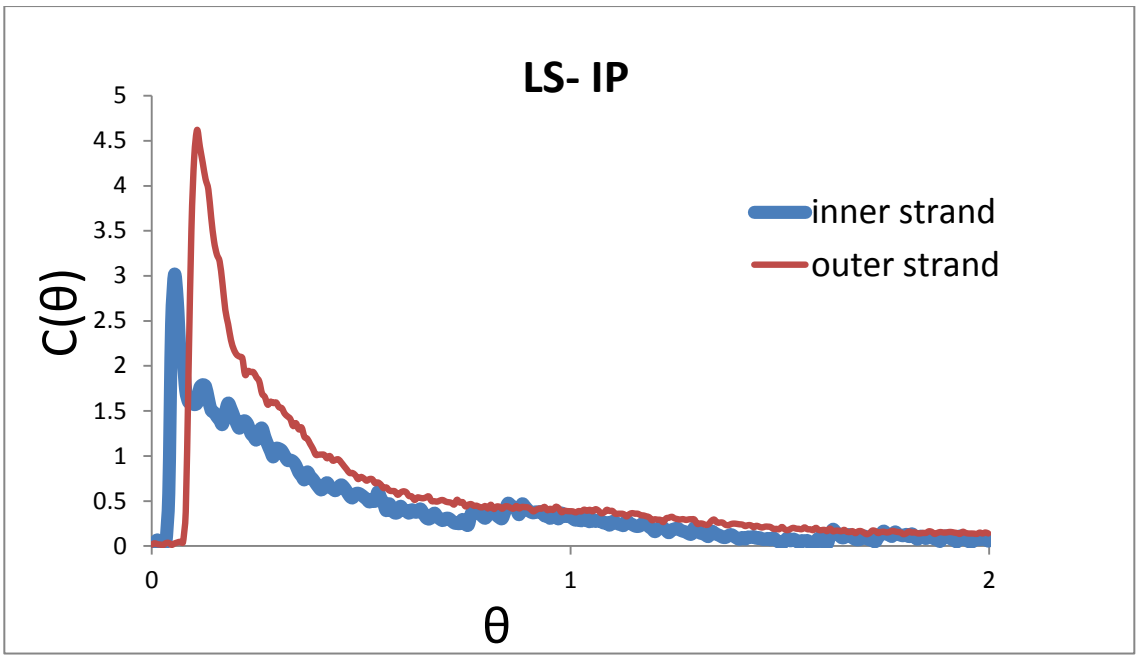

Figure 4.2 RTD curves corresponding to the LS-IP case for the inner and outer strands

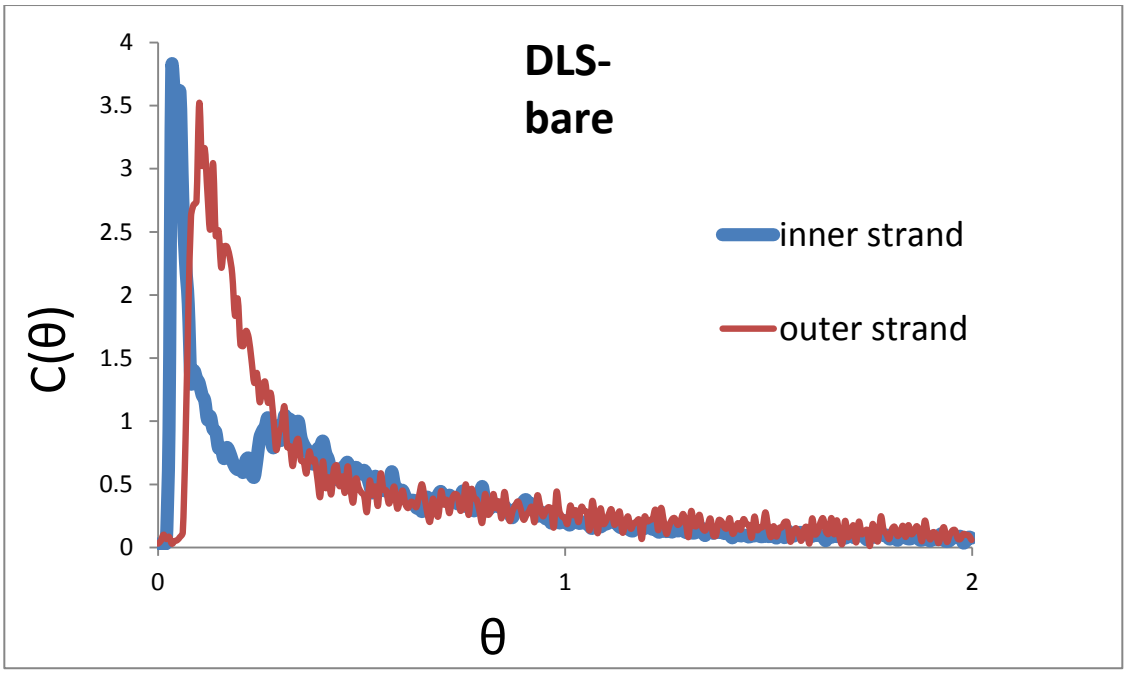

Figure 4.3 RTD curves corresponding to the DLS-bare case for the inner and outer strands

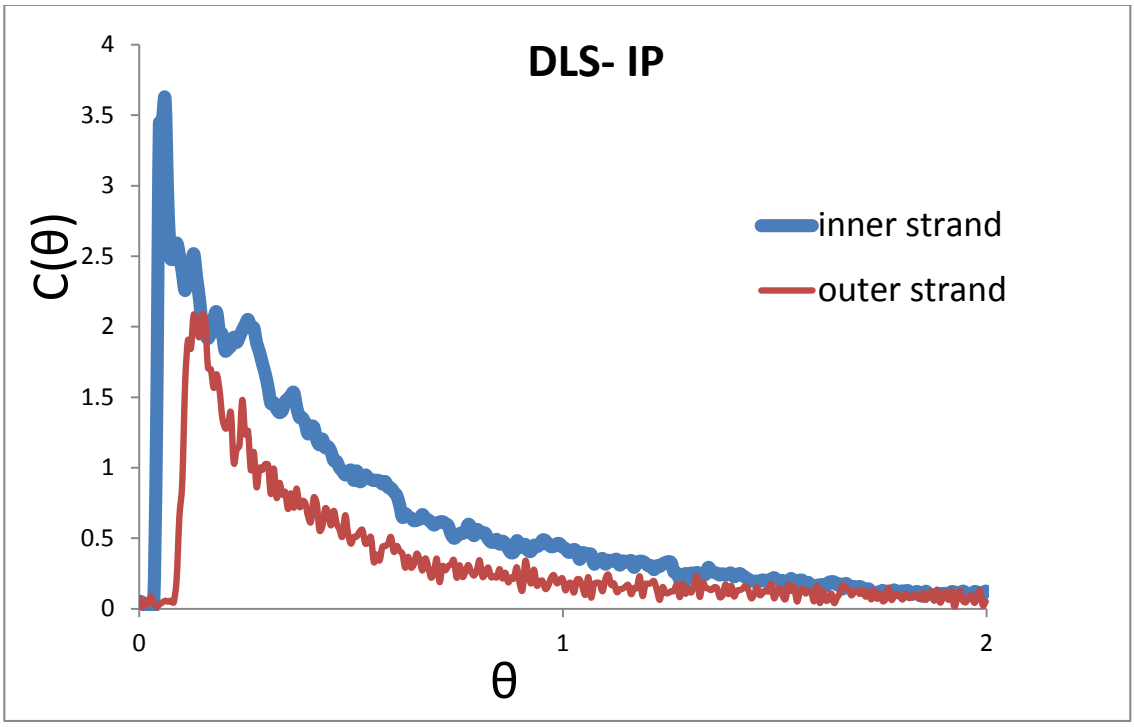

Figure 4.4 RTD curves corresponding to the DLS-IP case for the inner and outer strands

In all the cases, the mean residence times were larger for fluid exiting the outer nozzle, except for the DLS-IP case, for which θ_c was larger for the inner nozzle. The least difference in residence times between the outer and inner nozzles was identified for the DLS-IP. The DLS-bare came second. The largest difference between fluid residence times exiting the inner and outer nozzles was obtained for the LS-bare. We can conclude that a more uniform pattern of fluid flow is obtained with the DLS-IP and the DLS-bare. Figures 4.5 and 4.6 show that the LS-IP had the longest residence times for the outer strand, and the DLS-IP had the longest for the inner strand.

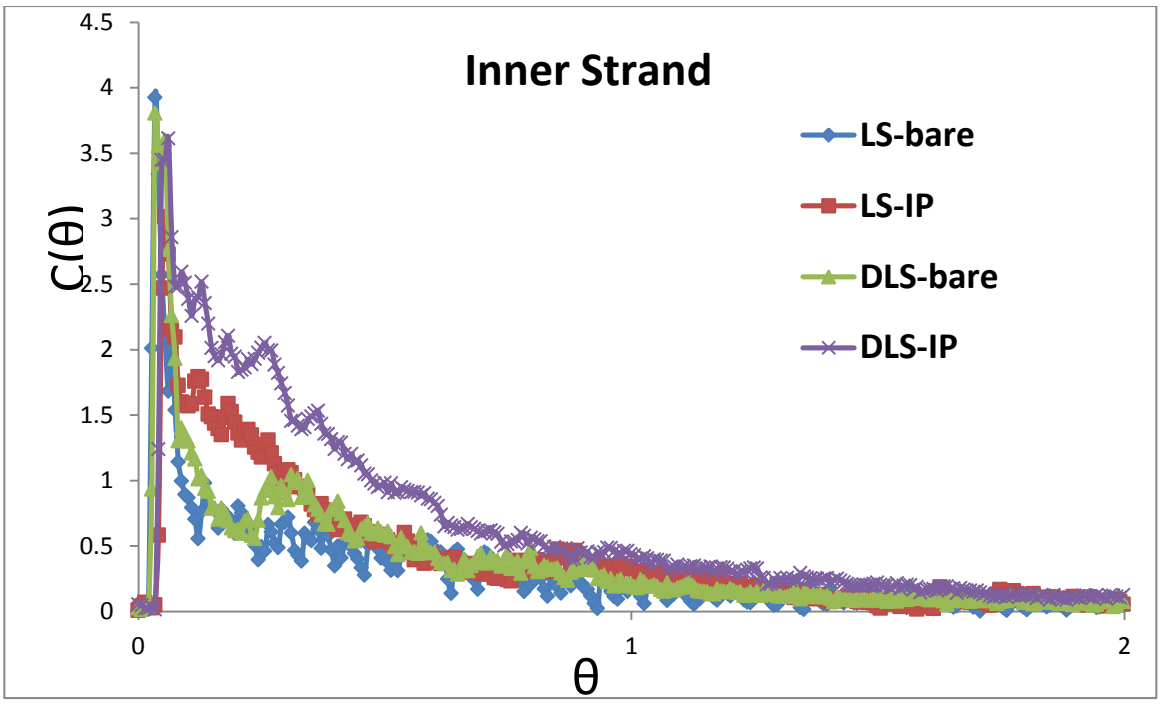

Figure 4.5 RTD curves corresponding to the inner strand for all the cases studied

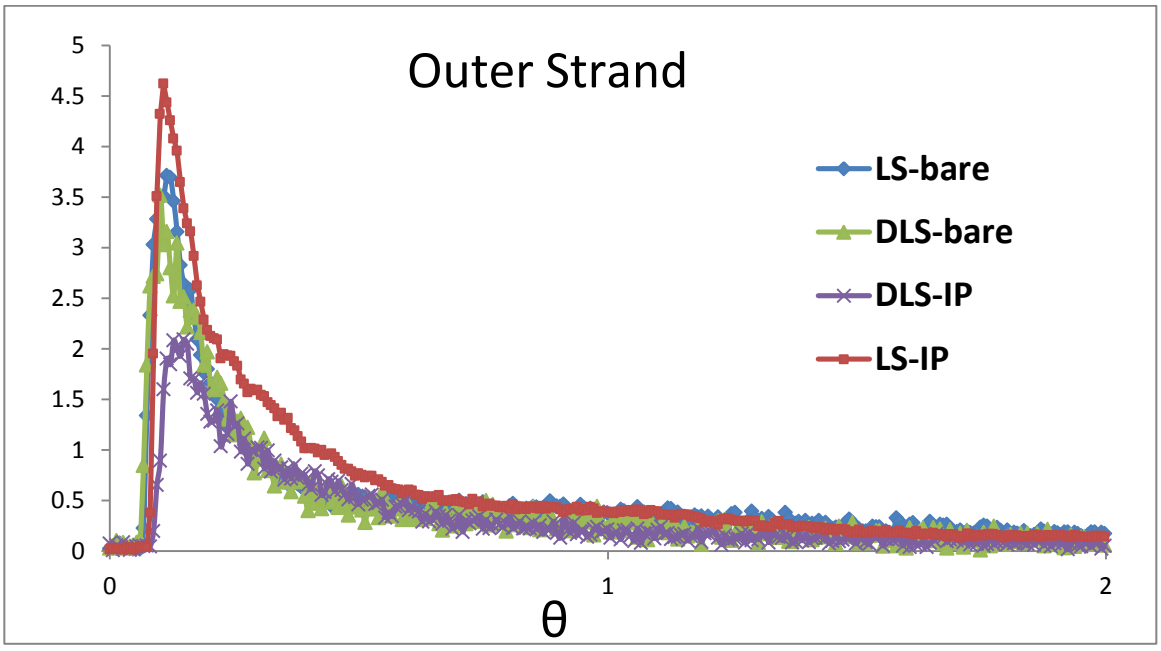

Figure 4.6 RTD curves corresponding to the inner strand for all the cases studied

The quantification of volume fractions expressed as well mixed, plug and stagnant components, together with their corresponding dimensionless times, are

shown in Figures 4.7a and 4.7b for the LS-bare and DLS-bare cases respectively. Figures 4.8a and 4.8b show equivalent cases for the LS-IP and DLS-IP, respectively. Table 4.1 summarizes the different parameters calculated.

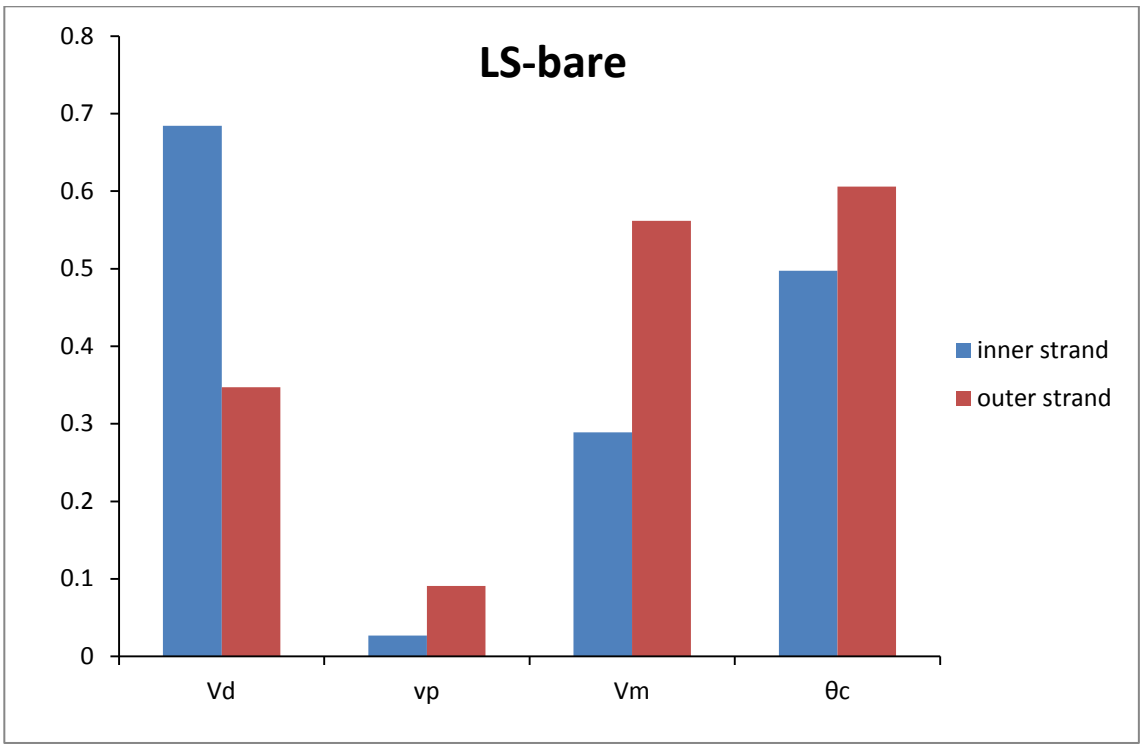

Figure 4.7a Volume fractions of the inner and outer strands for the LS-bare case

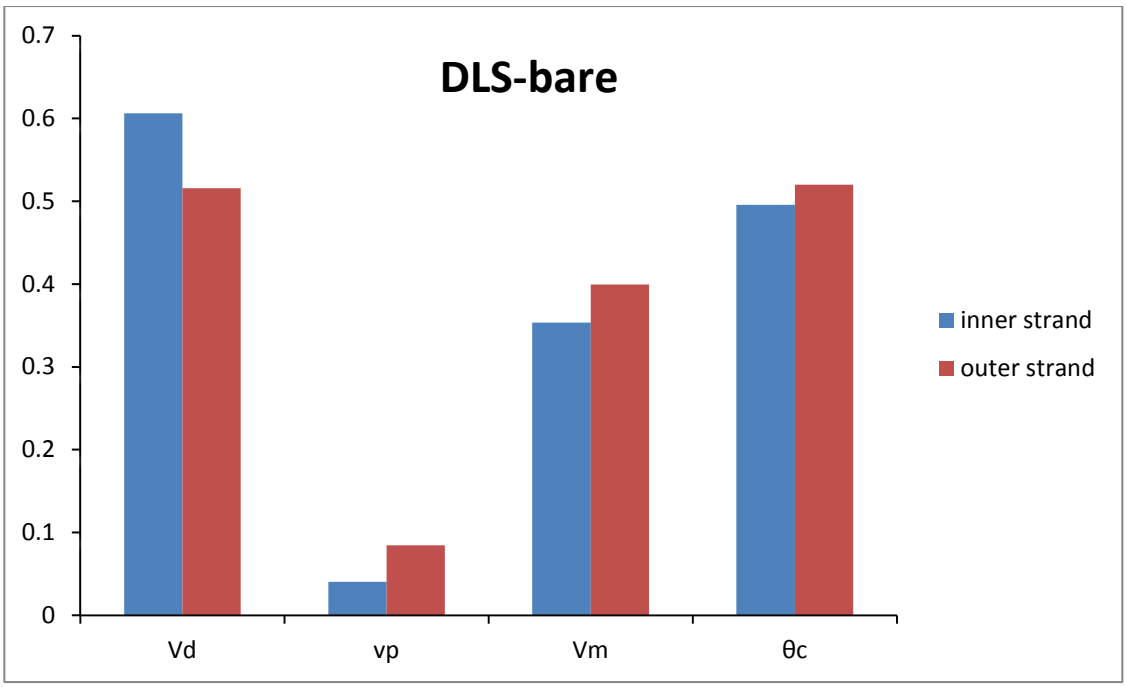

Figure 4.7b Volume fractions of the inner and outer strands for the DLS-bare case

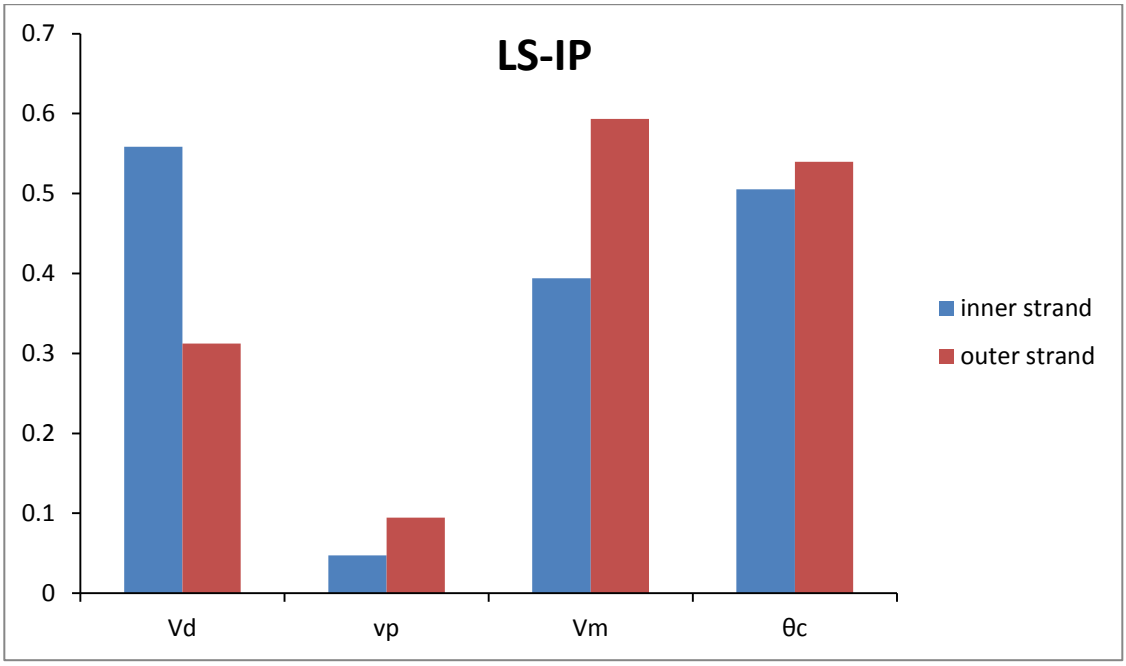

Figure 4.8a Volume fractions of the inner and outer strands for the LS-IP case

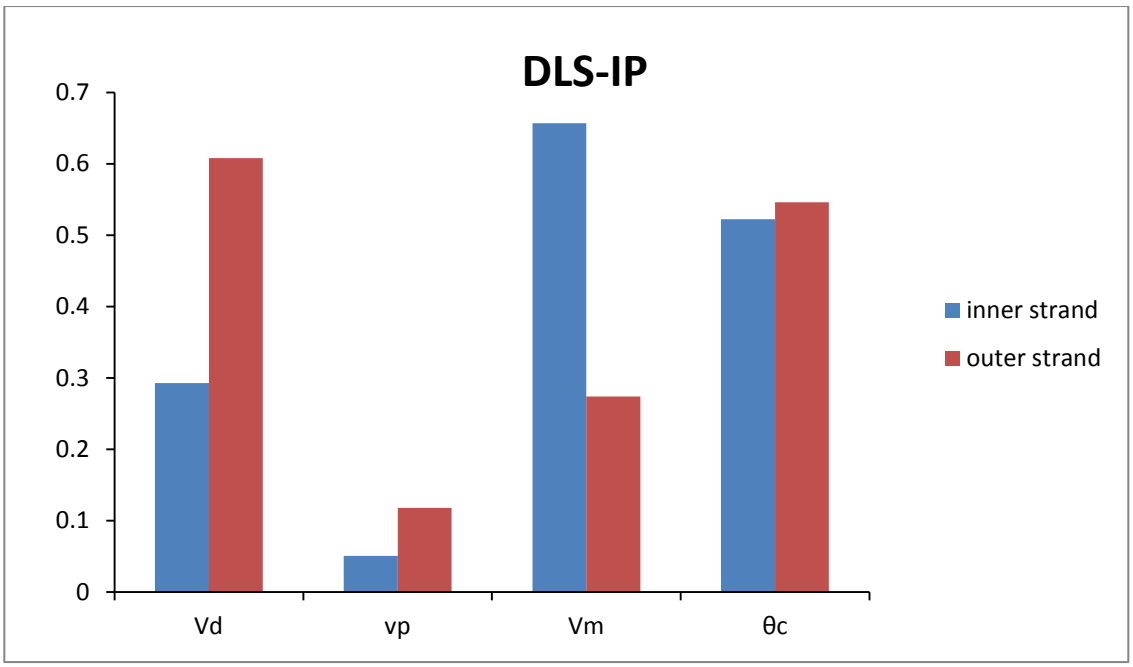

Figure 4.8b Volume fractions of the inner and outer strands for the DLS-IP case

Cases	Strand	tmin(s)	tpeak(s)	tm(s)	θc	vp	Vd	Vm
Case I	inner	9.60	12.00	176.86	0.50	0.03	0.68	0.29
	outer	24.00	40.80	215.39	0.61	0.09	0.35	0.56
Case II	inner	9.60	19.20	176.32	0.50	0.04	0.61	0.35
	outer	24.00	36.00	184.86	0.52	0.08	0.52	0.40
Case III	inner	14.40	19.20	179.64	0.51	0.05	0.56	0.39
	outer	28.80	38.40	191.82	0.54	0.09	0.31	0.59
Case IV	inner	14.40	21.60	185.76	0.52	0.05	0.29	0.66
	outer	31.20	52.80	194.22	0.55	0.12	0.61	0.27

Table 4.1 Calculated parameters from the RTD curves

The largest fractions of plug flow volumes were obtained for the DLS-IP case, followed by the LS-IP, the DLS-bare and, lastly, the LS-bare. Even though the DLS-IP was shown to have the largest fractions of plug flow and a more balanced set of residence times between the inner and outer strands, the DLS-bare succeeded in registering the most even fractions of dead, plug and mixed volumes, showing fewer differences between both strands. The results of the fractions suggest that a more even distribution of liquid steel fractions to the inner and outer strands is possible with the DLS-bare, followed by the LS-IP, the DLS-IP and lastly, the LS-bare, which exhibited the largest differences. In the DLS-IP arrangement, the mixing volume fractions for the inner strand are the largest among all cases. These mixing patterns in the fluid flow may help to increase the agglomeration of micro-inclusions. This case would enhance flotation of macro-inclusions, due to the larger and balanced mean residence times among the inner and outer strands.

4.2 NUMERICAL PREDICTIONS OF FLUID FLOW

4.2.1 FLUID FLOW PATTERNS INSIDE THE LADLE SHROUDS

A reference line was created at the center of the ladle shroud in FLUENT-ANSYS in order to compute the variation in the velocity magnitude along the axial direction, which in this case is the Z axis as shown in Figure 4.9a.

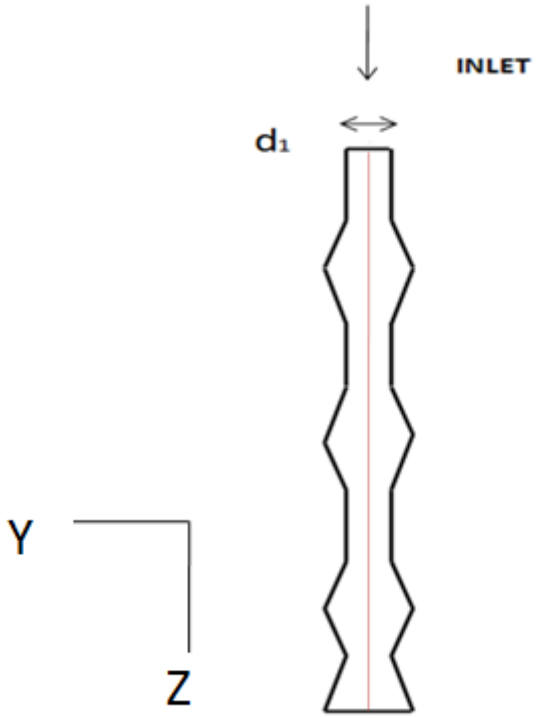

Figure 4.9a Schematic of the reference line positioned at the center of the ladle shroud

G. Solorio-Diaz et al. [17][26][27] simulated mathematically the fluid flow inside the DLS with the Reynolds Stress Model (RSM) in order to obtain the variation of the Reynolds stresses, which are the fluctuating component in the Reynolds Averaged Navier-Stokes equations (RANS) and the main factors in charge of inducing and propagating the turbulent kinetic energy.

When operating with the Conventional Ladle Shroud (LS), the Reynolds stresses in the normal directions X, Y and Z ($\tau_{xx} = -\rho\overline{v'_x v'_x}$, $\tau_{yy} = -\rho\overline{v'_y v'_y}$, $\tau_{zz} = -\overline{v'_z v'_z}$) slightly decrease as the fluid flows through the ladle shroud into the tundish. By contrast, the shear stresses acting in the planes XY, YZ and XZ remain relatively constant. As the fluid flows through the conical sections of the Dissipative Ladle Shroud (DLS), the shear stresses ($\tau_{xy} = -\rho\overline{v'_x v'_y}$, $\tau_{xz} = -\rho\overline{v'_x v'_z}$, $\tau_{yz} = -\overline{v'_y v'_z}$) fluctuate significantly, strongly affecting the normal stresses and the magnitudes of velocities, during jet deformation in the X and Y directions [17]. In the first cylindrical section of the DLS(Figure 4.9b), the velocity along the Y direction is much less, therefore the Reynolds shear stresses acting in the YZ plane ($\tau_{yz} = -\rho\overline{v'_y v'_z}$) remain relatively constant. In the second section, the velocity increases in the Y direction as the fluid expands through the conical section, decreasing the velocity along the axial direction of the shroud. In the third section the velocity in the axial direction, increases again, as the conical section is contracted. The Reynolds shear stresses acting on the fluid deform the jet from positive to negative as the DLS expands and contracts. As the Reynolds stresses act in opposite direction, when the fluid is flowing through the DLS, the magnitude is decreased. As a consequence, the normal stresses and the magnitude of the velocity are decreased. In the fourth section, the velocity first decreases and then increases. Similarly, the velocity fluctuates in the X direction (see Appendix 1 to consult the velocities and Reynolds Shear Stresses inside the ladle shrouds). When comparing the last segment of each analogue section, the velocity has decreased significantly as we can see in the last part of the first cylindrical section compared to the last one of the fourth and seventh sections in Figure 4.9b and 4.9c. Similarly, the following sections have the same tendency. Therefore, the velocity magnitude of the fluid entering into the tundish is decreased. By the constant deformation of the jet inside the DLS, the micro-inclusions carried from the ladle, may have a higher interaction with each other.

The collision between clusters of particles can make them agglomerate, prior the liquid steel being discharged into the tundish.

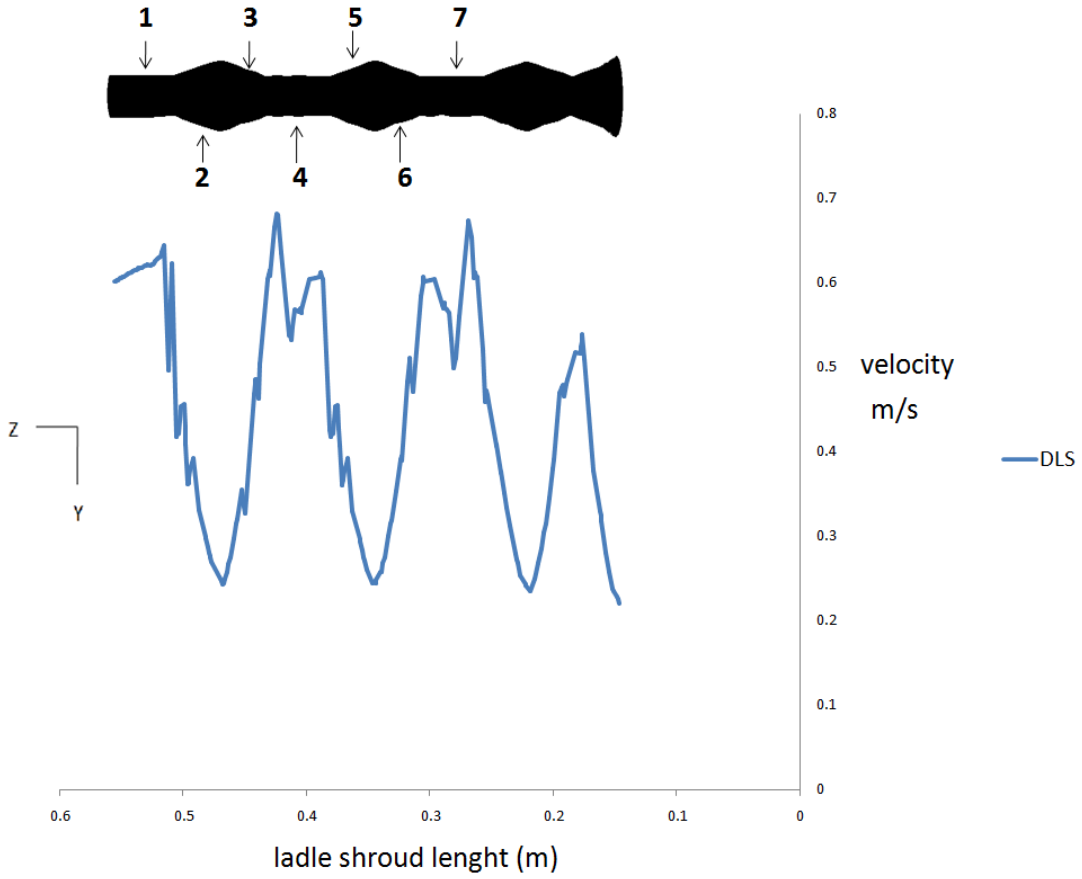

Figure 4.9b Velocity magnitude at the axis of the DLS obtained from ANSYS-FLUENT (the sections 1, 4 and 7 are cylindrical and 2,3,5,6 conical)

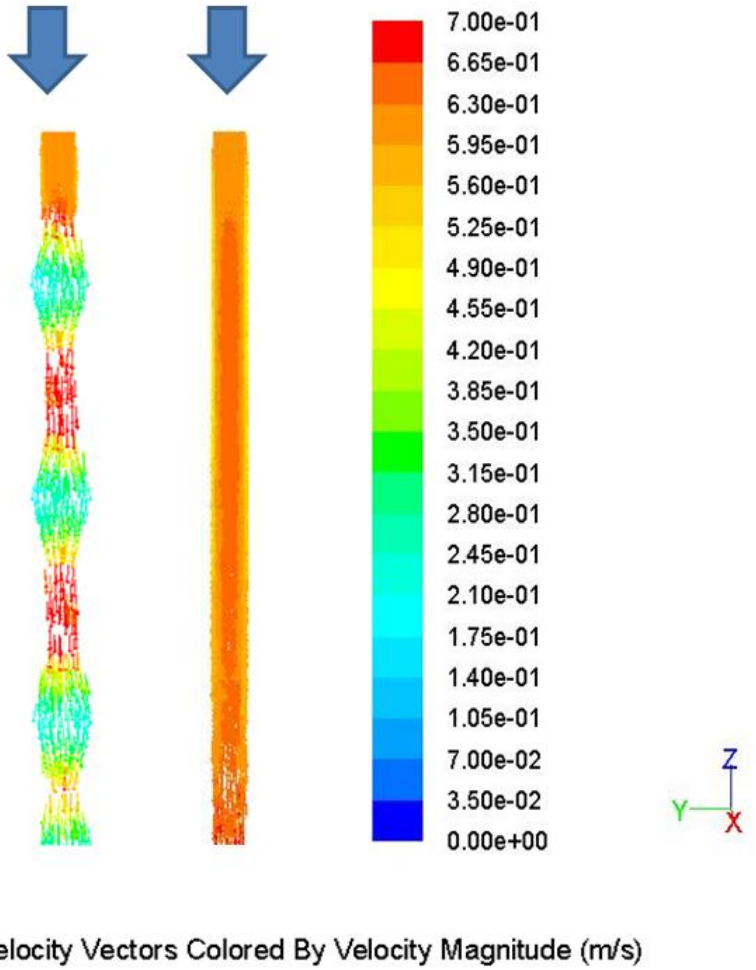

Figure 4.9c Velocity vectors at the conventional and dissipative shrouds obtained from ANSYS-FLUENT

4.2.2 FLUID FLOW PATTERNS INSIDE THE TUNDISH

The flow patterns for the isothermal, steady state, three dimensional velocity fields inside the tundish were compared for the arrangements mentioned in the previous sections at different planes, including: a longitudinal plane located at the outflows, a longitudinal plane on the axis of the shroud, a transverse plane on the axis of the shroud and transverse planes on the inner and outer strands. Figure 4.10a and 4.10b show the geometries created in ANSYS-FLUENT and post-processed in TECPLOT for the LS-IP and DLS-IP. The geometries for the bare

tundish cases were created in a similar fashion. Figures 4.11a and 4.11b show the planes used for the analysis.

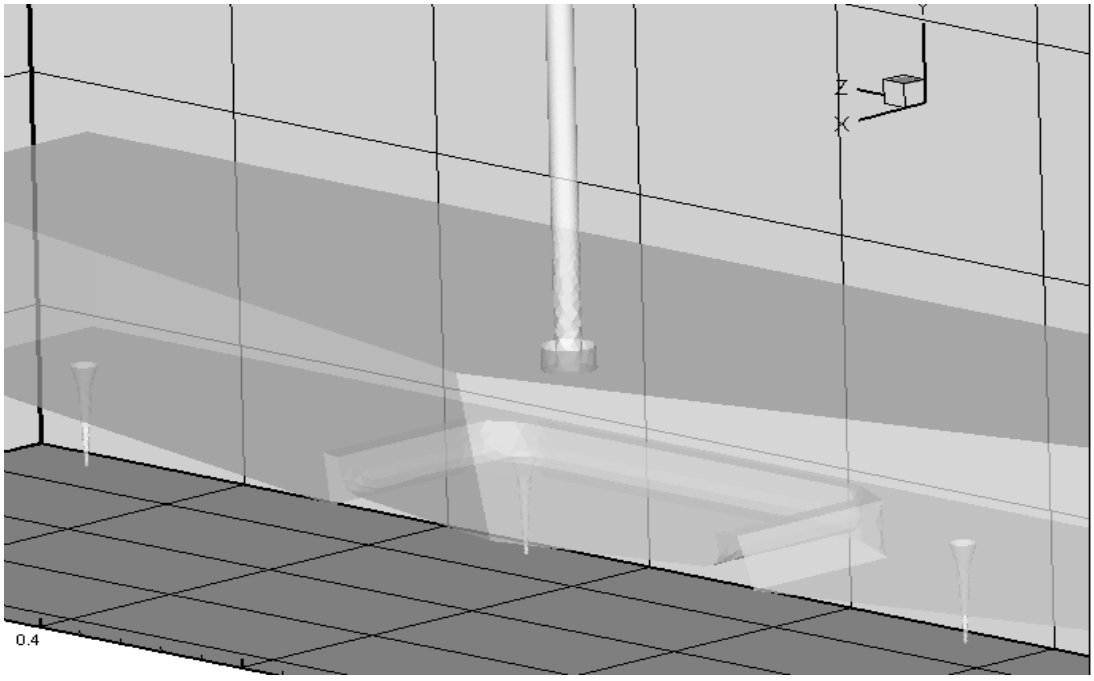

Figure 4.10a. Tundish incorporating the Conventional Ladle Shroud and an Impact Pad(LS-IP)

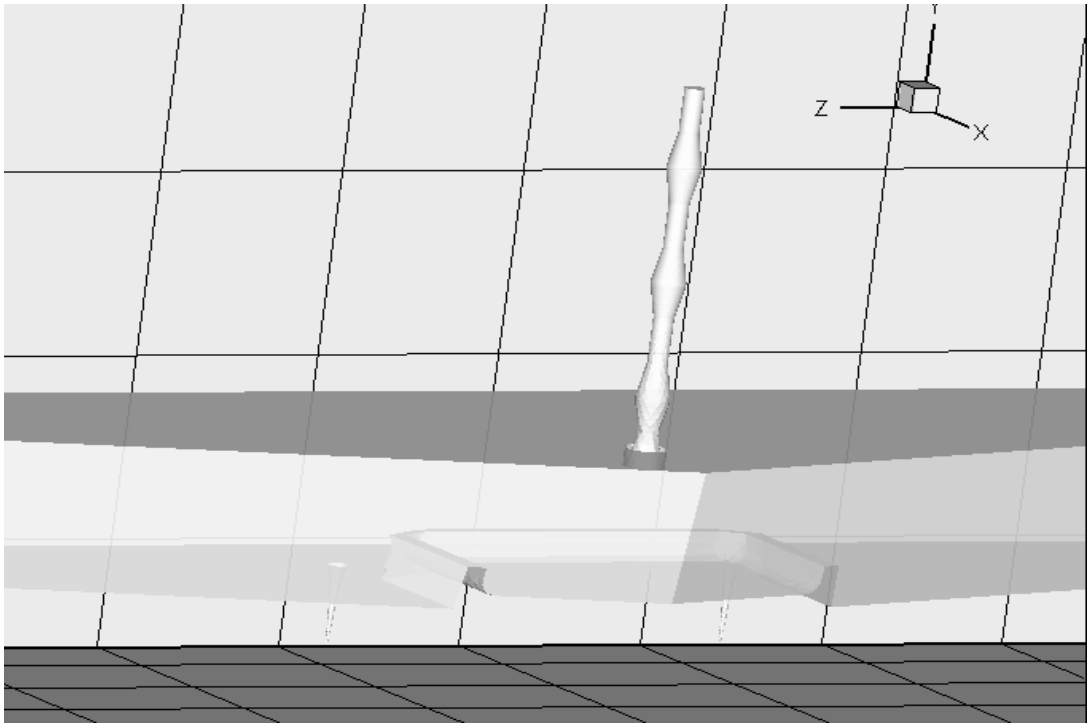

Figure 4.10b. Tundish incorporating the Dissipative Ladle Shroud and an Impact Pad(DLS-IP)

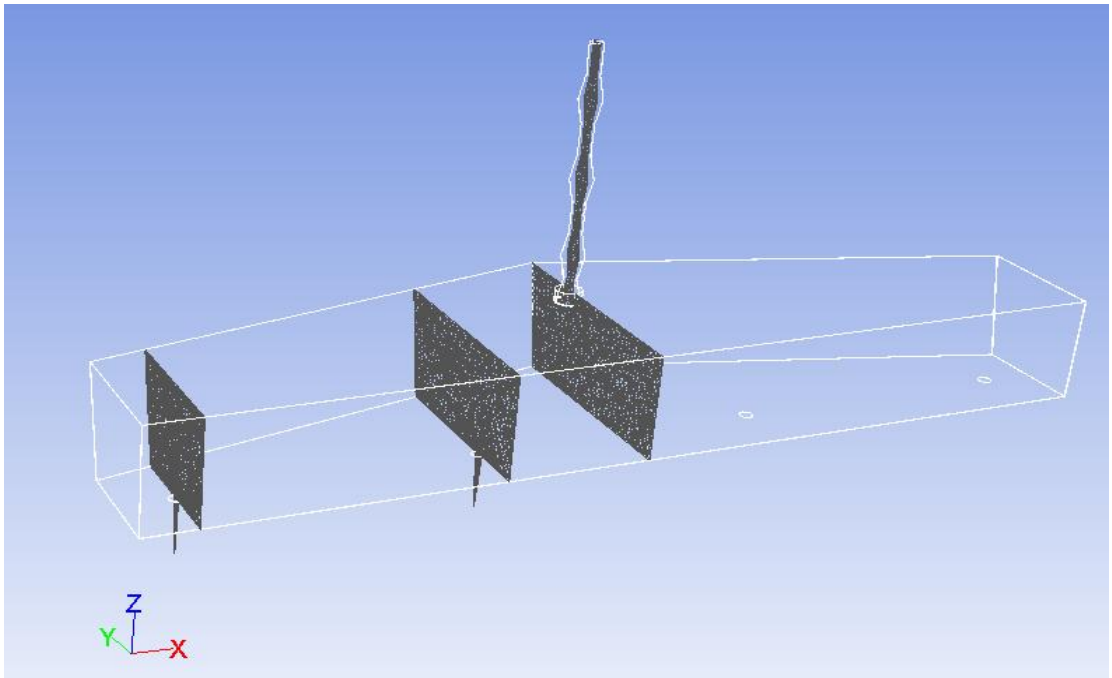

Figure 4.11a. Transverse planes selected inside the tundish to compute the velocity fields with ANSYS-FLUENT

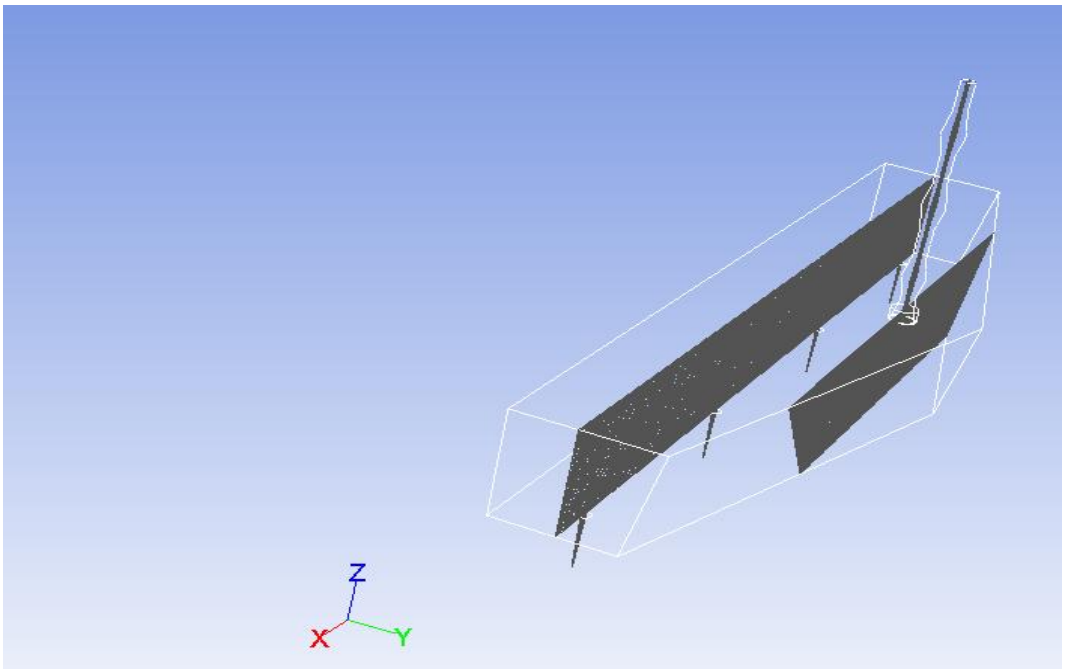

Figure 4.11b. Transverse planes selected inside the tundish to compute the velocity fields with ANSYS-FLUENT

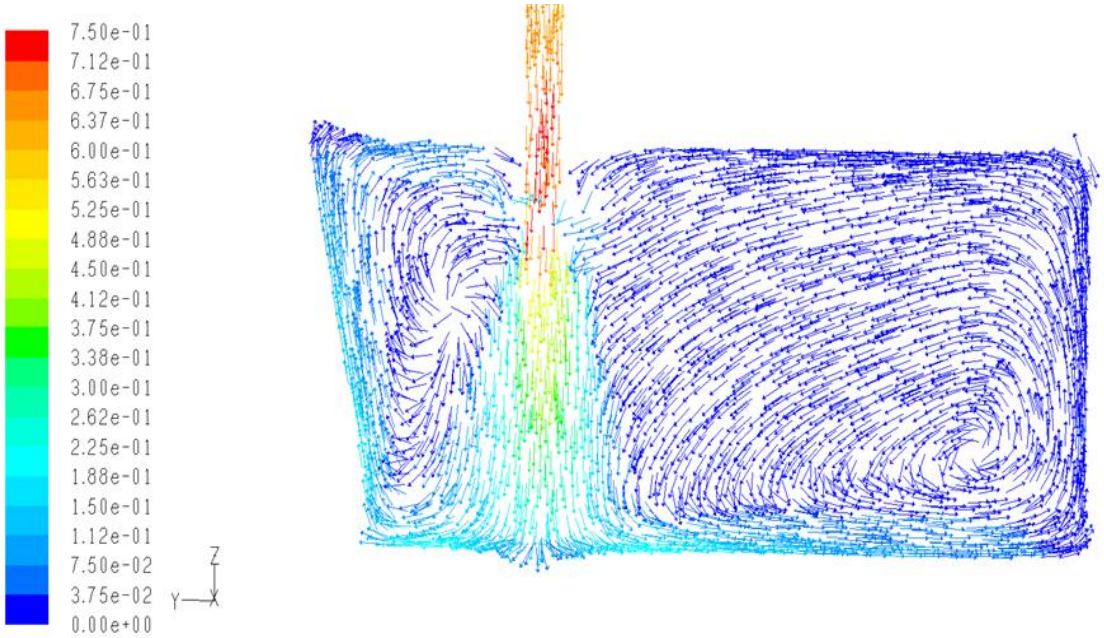

Figure 4.12a. Transverse plane interscting the axis of the shroud, showing computed velocity fields for the LS-bare in m/s

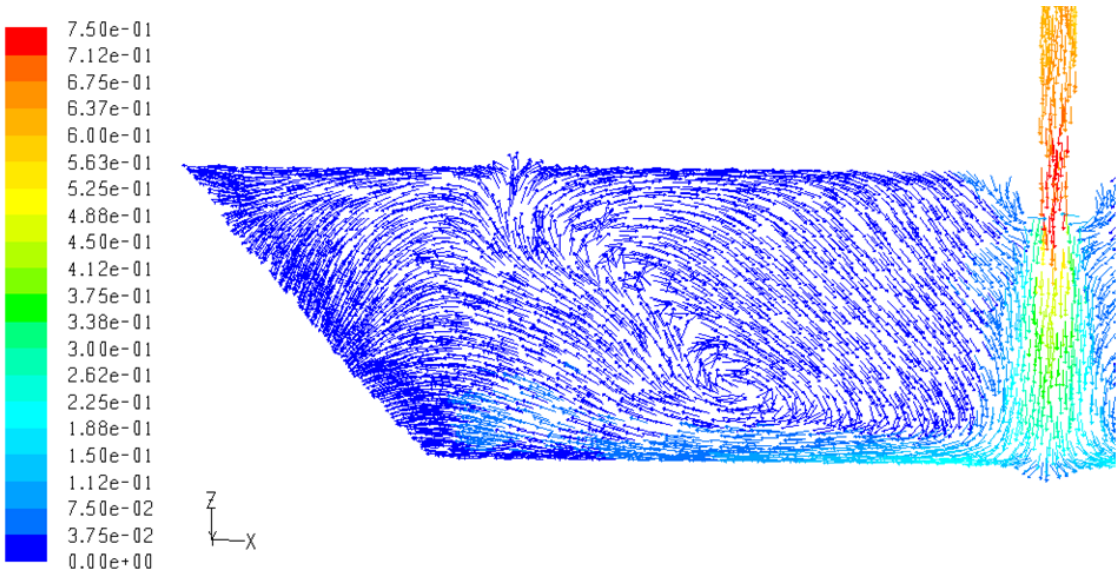

Figure 4.12b. Longitudinal plane along the axis of the ladle shroud, showing the velocity fields for the LS-bare in m/s

The jet enters the tundish with high turbulent kinetic energy. As explained in the previous section, the stream of fluid, transported by the recirculations, are directed towards the longitudinal and transverse directions of the tundish. Two main recirculation zones can be seen for the LS-bare arrangement in Fig. 4.12a. The recirculation on the left impacts the delta-shaped walls and reaches the bath surface with higher velocity due to the proximity of the shroud. After reaching the walls, the fluid divides into two main parts, one of them directed towards the free surface of the tundish while the other reenters the recirculatory flow. The same fluid patterns can be seen at the longitudinal plane, in which the fluid is directed towards the bath surface after reaching the lateral walls Fig. 4.12b.

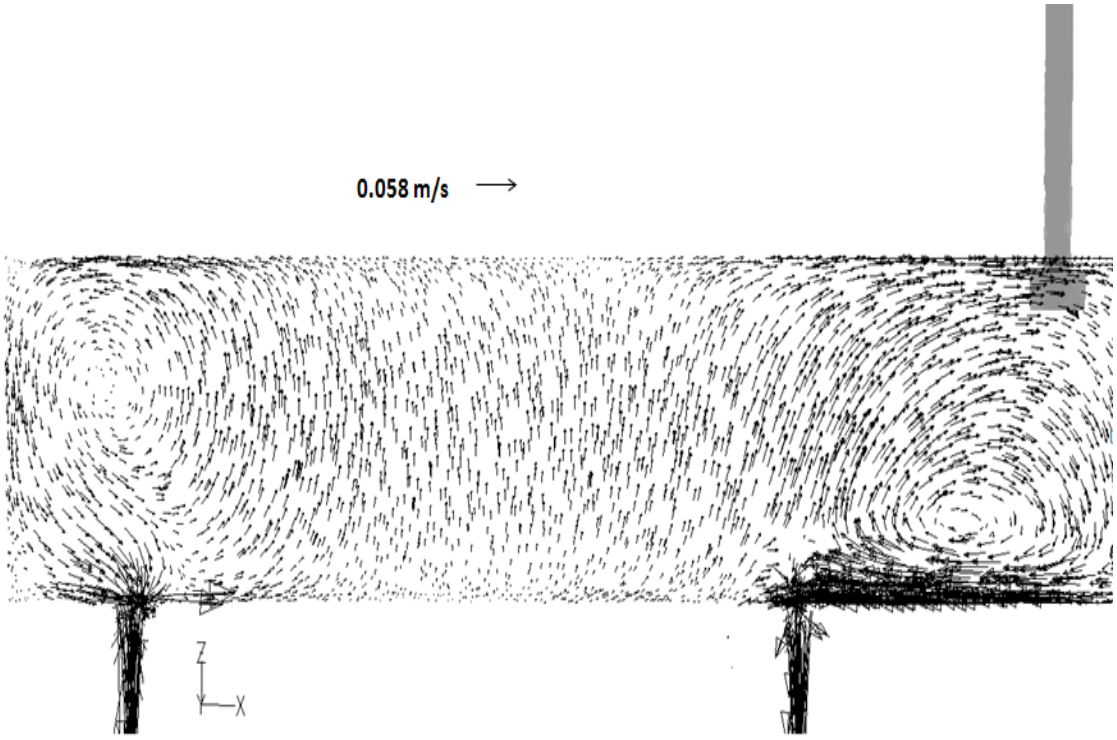

Figure 4.12c. Longitudinal plane over the outlets, showing the velocity fields for the LS-bare in m/s

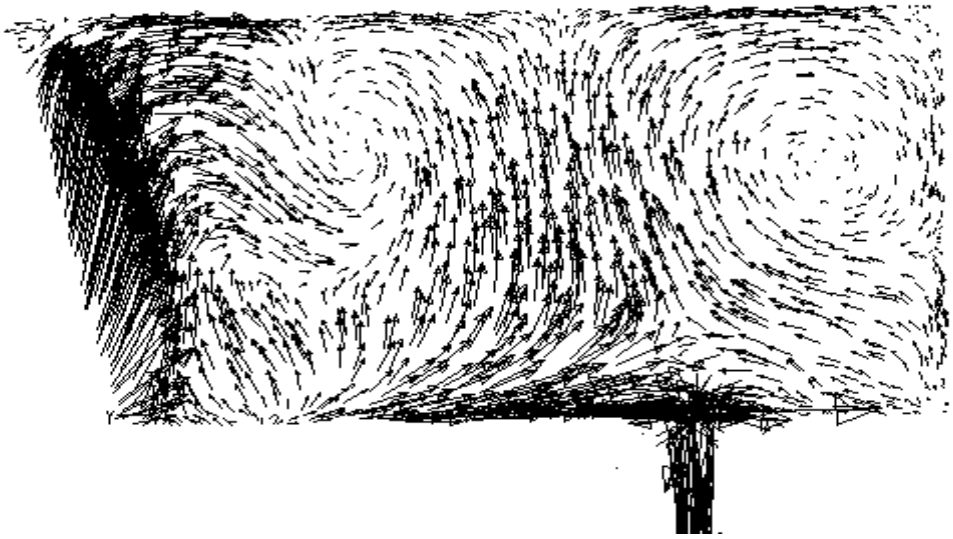

Figure 4.12d. Transverse plane along the inner strand, showing the velocity fields for the LS-bare in m/s

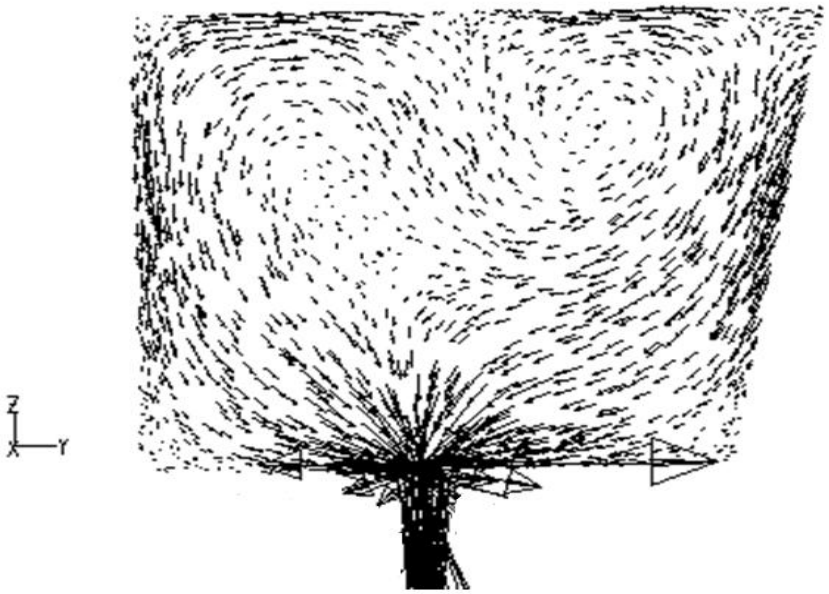

Figure 4.12e. Transverse plane along the outer strand, showing the velocity fields for the LS-bare in m/s

A strong recirculatory flow can be observed near the inner strand area in Fig. 4.12c and Fig. 4.12d. The velocity vectors are directed towards the bath surface and the inner outlet with a high magnitude, which can also explain the short-circuiting and the two peaks discussed in the previous sections. The fluid flowing towards the outer strand has an upward motion reaching first the wall and then leaving the tundish as observed in Fig. 4.12c. and Fig. 4.12e. The fluid pattern in the outer strand also explains the longest averaged residence time obtained among all the cases. Shamik R. et. al[48] also obtained similar results when modeling the fluid flow in the same model of a full scale tundish. During the slag entrainment experiments, the number of beads collected was larger for the inner than the outer strand, to which far fewer of beads reported. The explanation is that the beads trapped in the recirculatory zones are more likely to be leaving through the inner strand.

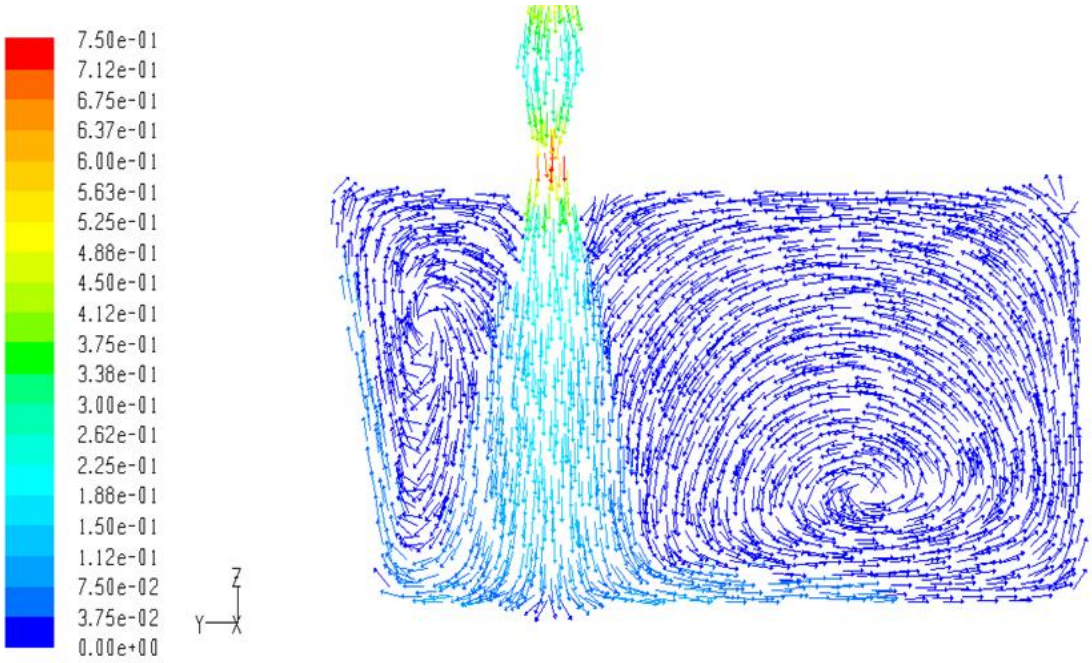

Figure 4.13a. Transverse plane along the axis shroud, showing the velocity fields for the DLS-bare in m/s

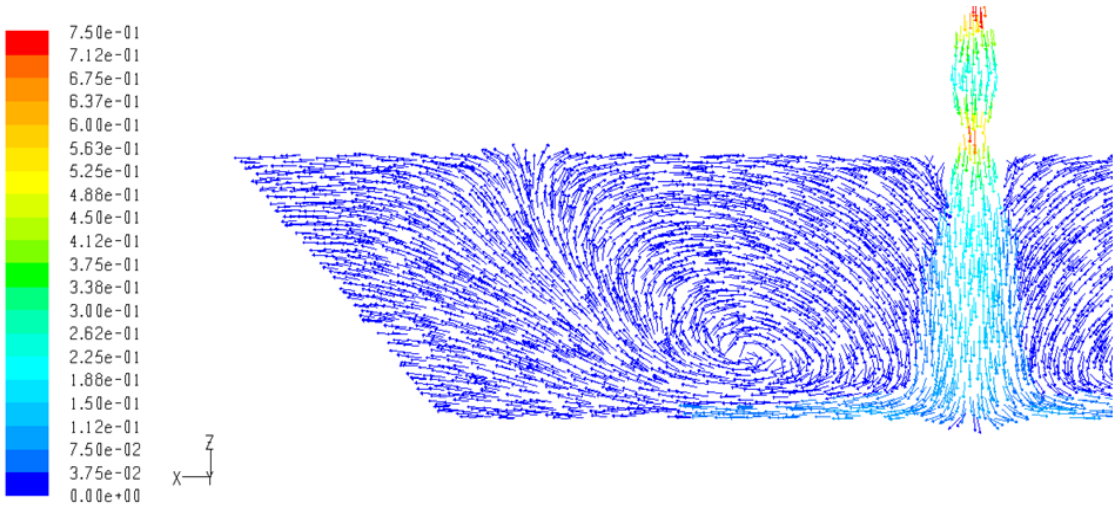

Figure 4.13b. Longitudinal plane along the axis shroud, showing the velocity fields for the DLS-bare in m/s

As explained before, when the tundish is assembled with the DLS, a decrease in the discharge velocity is obtained as the fluid enters the vessel (Figs. 4.9, 4.13a, 4.13b). It is also observed that the field of discharge widens into the tundish. Adding the effect of the DLS to the entry of the inlet stream, the expansion of the jet also damps the impact velocity on the bottom of the tundish, decreasing the intensity of the recirculatory motion. When the fluid flows upwards after returning from the walls, it reaches the bath surface with lower velocity magnitudes compared with the conventional ladle shroud arrangement.

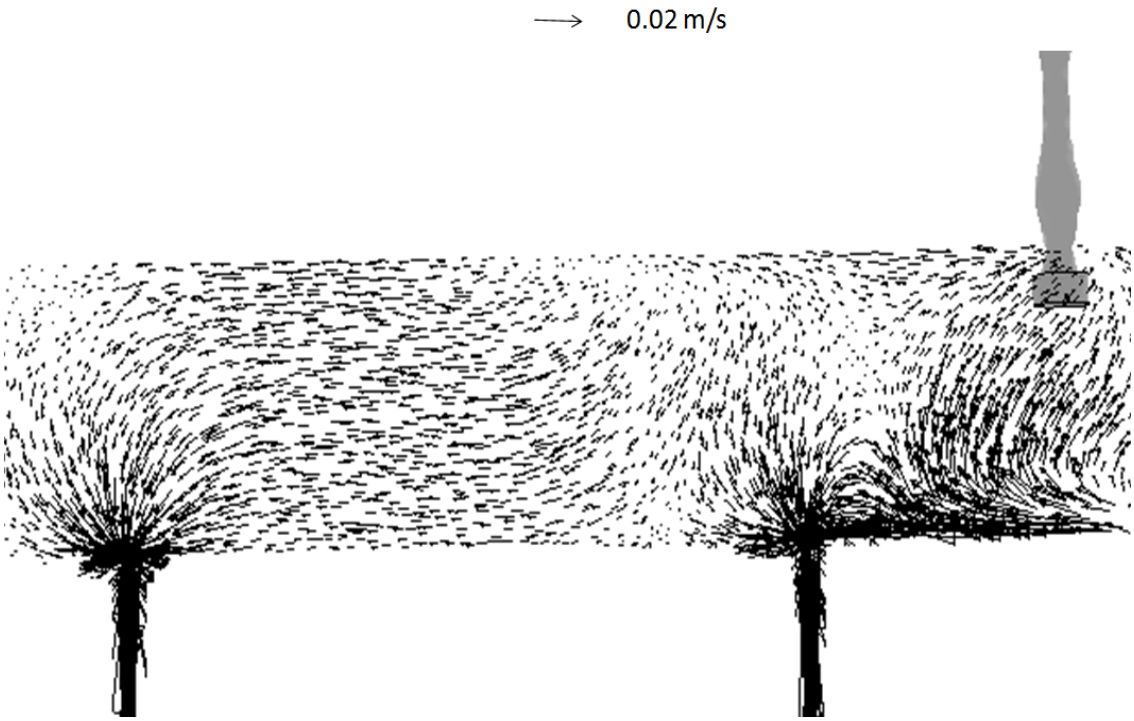

Figure 4.13c. Longitudinal plane over the outlets, showing the velocity fields for the DLS-bare in m/s

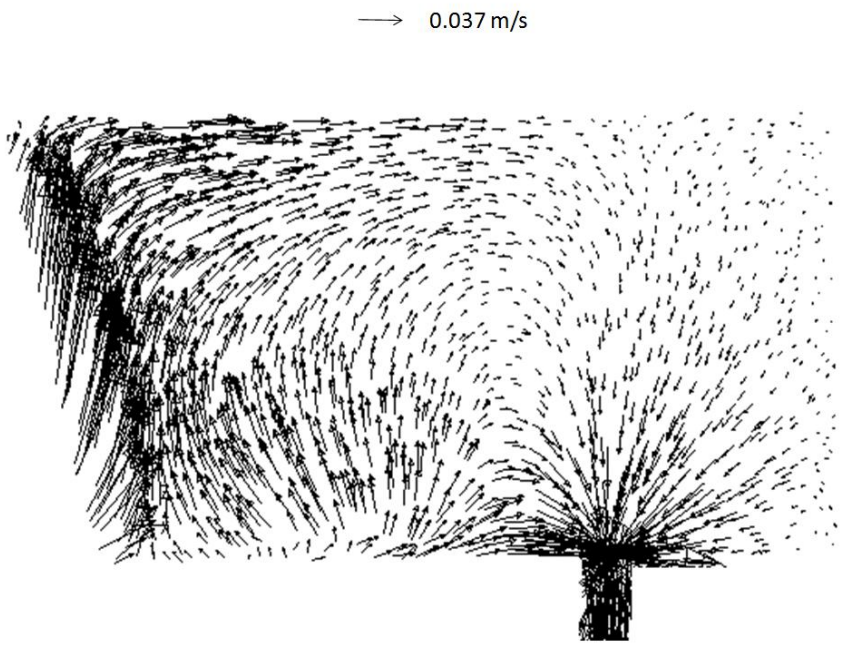

Figure 4.13d. Transverse plane along the inner strand, showing the velocity fields for the DLS-bare in m/s

.

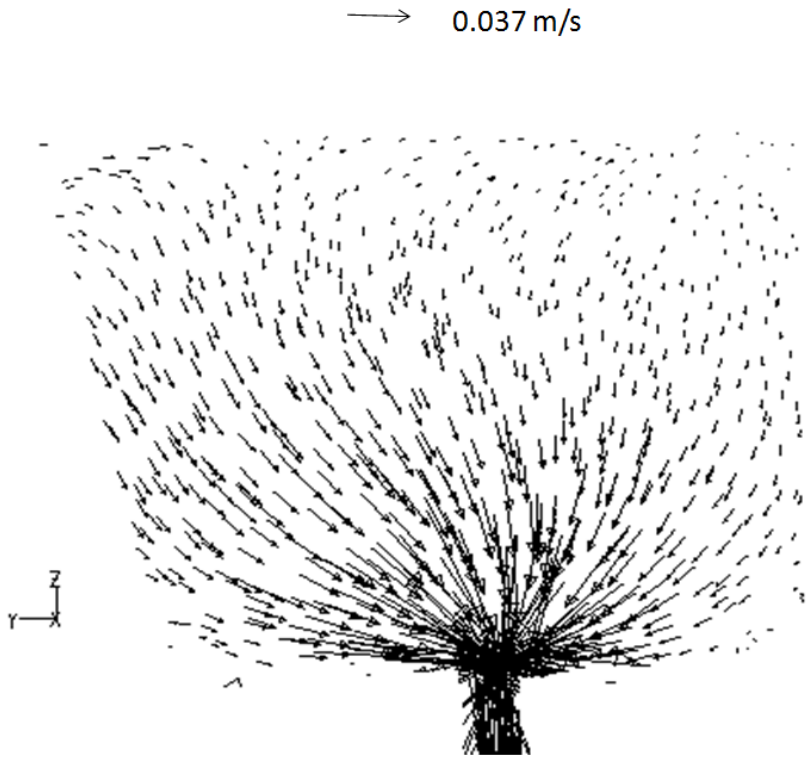

Figure 4.13e. Transverse plane along the outer strand, showing the velocity fields for the DLS-bare, m/s

The strong recirculatory flow predicted near the inner strand area in the LS-bare arrangement (Fig. 4.12c and Fig. 4.12d) is not observed with the DLS-bare arrangement (Fig. 4.13c and 4.13d). Rather, the fluid is distributed more evenly within the tundish before passing through the inner and outer strands. The fluid stream is directed partly towards the bath surface. The other part moves towards the inner strand at a high velocity magnitude, which explains the short-circuiting flow. For the outer strand, the fluid flows uniformly along the longitudinal plane, reaching the outlet in a more ordered fashion (Fig. 4.13c and 4.13e).The fluid flow patterns mentioned, explain the similar values of volume fractions and residence times obtained for the inner and outer strands in the RTD experiments.

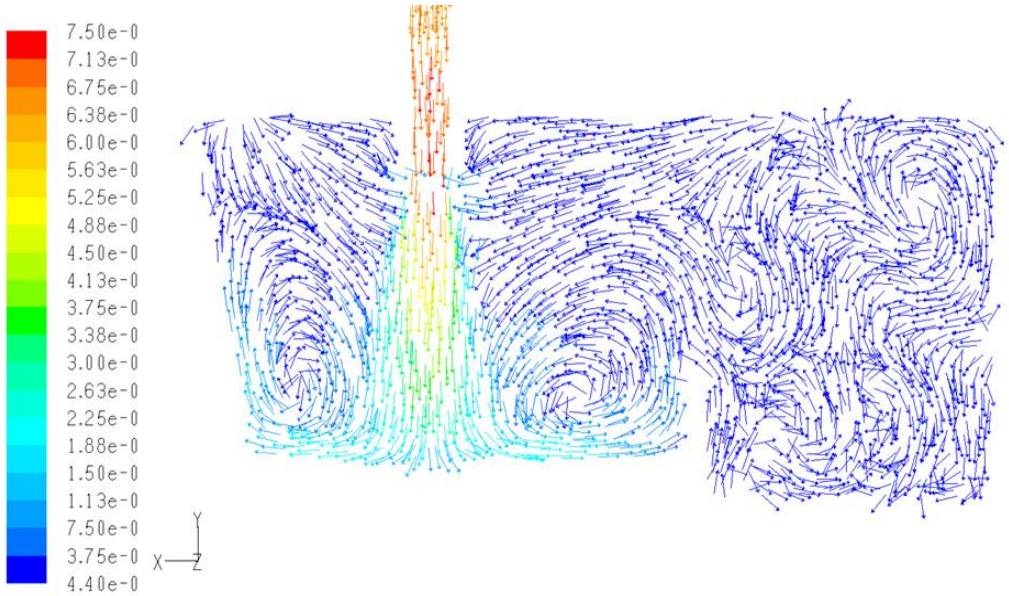

Figure 4.14a. Transverse plane along the axis shroud, showing the velocity fields for the LS-IP in m/s.

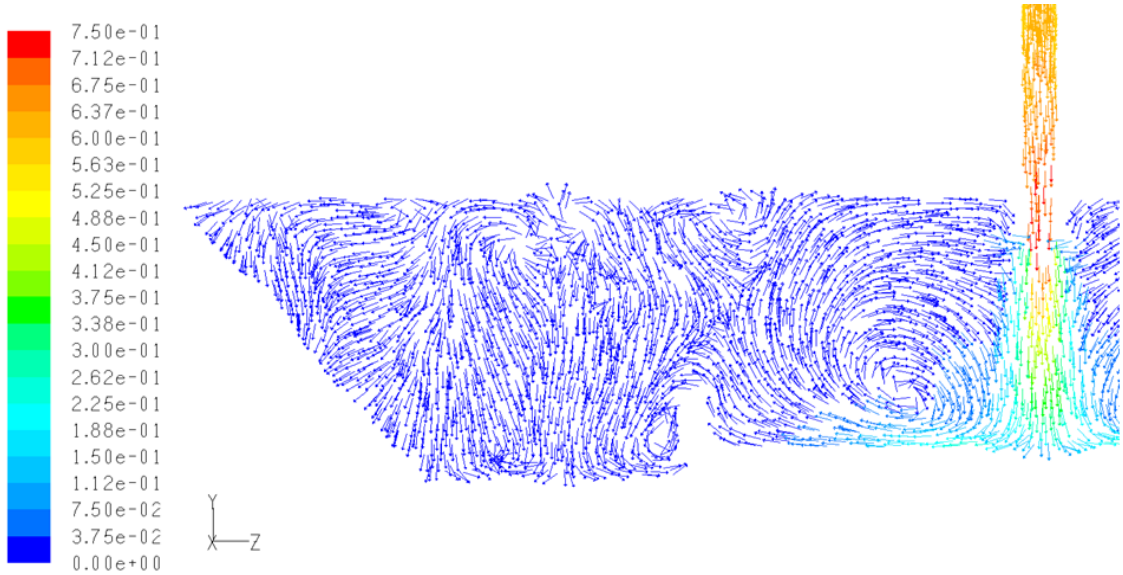

Figure 4.14b. Longitudinal plane along the axis shroud, showing the velocity fields for the LS-IP in m/s.

As the entry jet impacts the bottom of the tundish, recirculatory flows form within the volume of the impact pad for the LS-IP case. The motion of the fluid is constrained by the volume of the IP. There, the turbulence is decreased and as a consequence the fluid flow becomes more uniform throughout the volume of the tundish. The IP also directs the fluid towards the bath surface. The fluid is divided into two main parts, one large recirculatory flow going towards the inlet stream and the other directed outside the IP volume as smaller recirculations with less intense turbulence as observed in Figs. 4.14a and 4.14b. Therefore, eliminating the large recirculations observed in the previous cases formed after the fluid reached the back and delta-shaped walls. The ascending velocity near the delta-shaped wall is decreased as an effect of the IP.

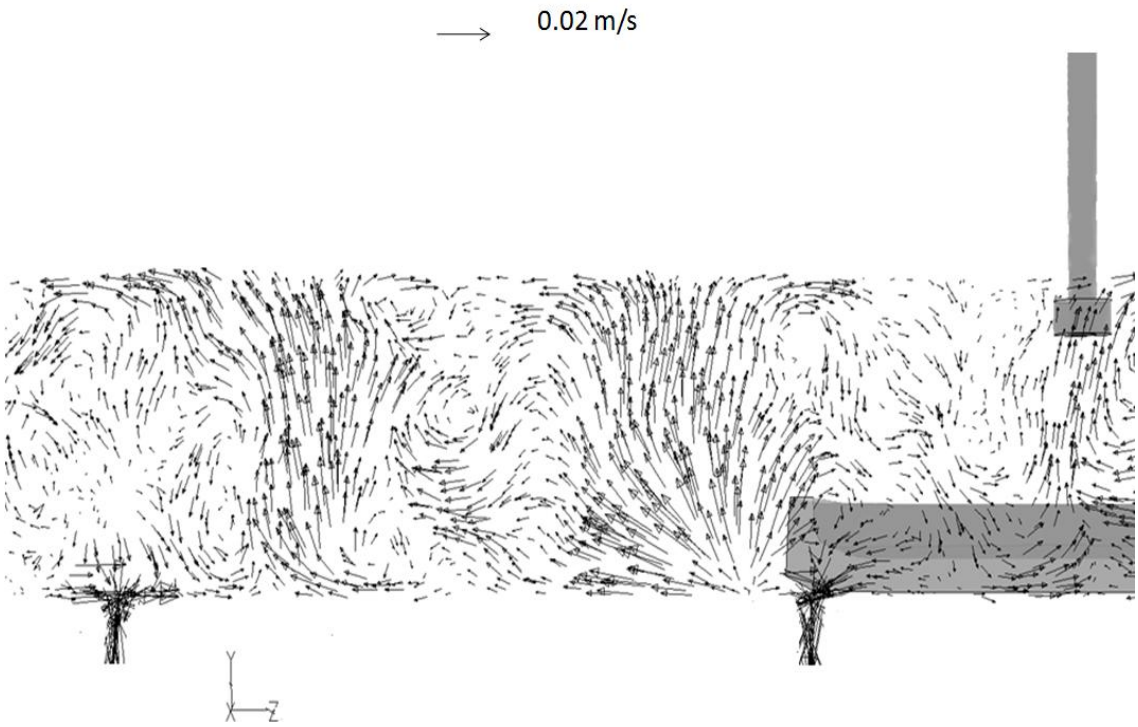

Figure 4.14c. Longitudinal plane over the outlets, showing the velocity fields for the LS-IP in m/s

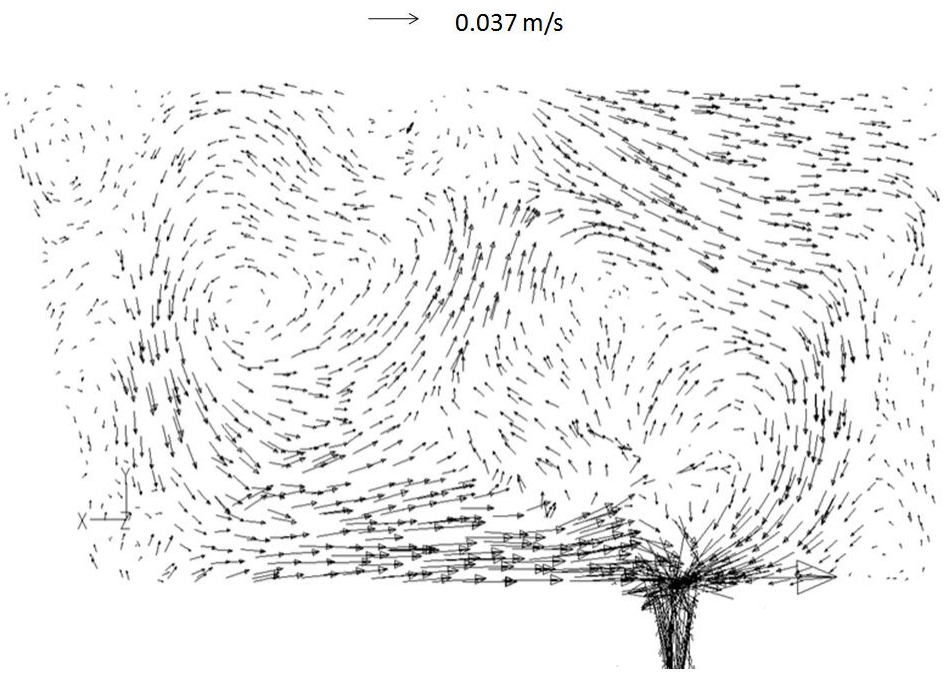

Figure 4.14d. Transverse plane along the inner strand, showing the velocity fields for the LS-IP, m/s

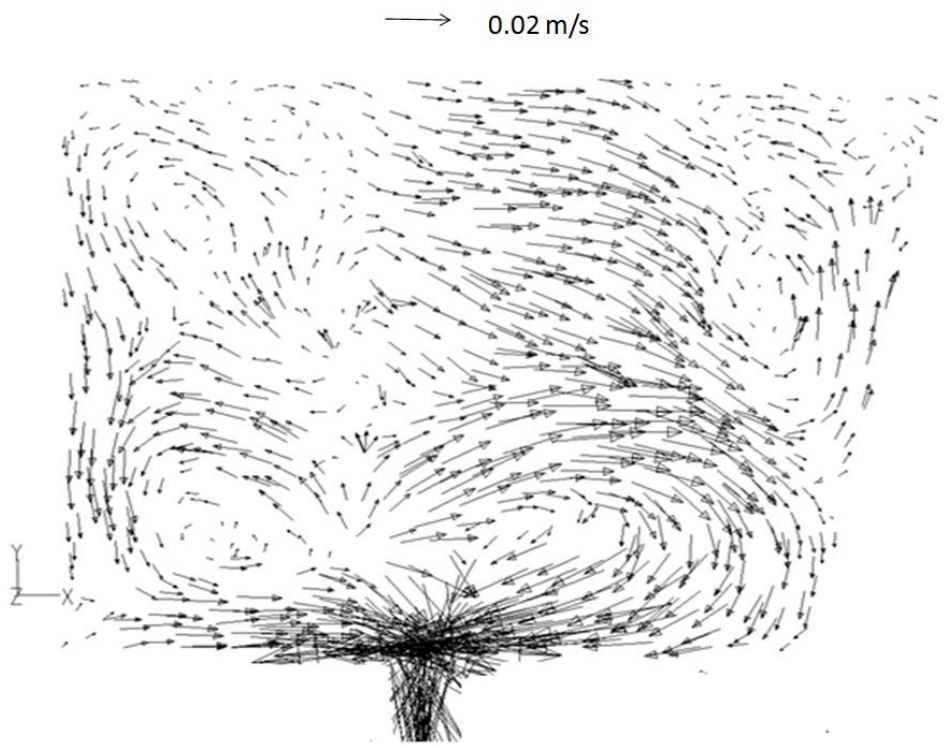

Figure 4.14e. Transverse plane along the outer strand, showing the velocity fields for the LS-IP, m/s

The IP prevents the motion of the fluid towards the front walls of the tundish. As the IP enhances the upward fluid flow, the velocity vectors are pointing towards the bath surface as seen in Fig. 4.14c. This can help the flotation of macro-inclusions. The high velocity vectors found in the LS-bare and DLS-bare cases, pointing towards the inner strand on the floor of the tundish, are decreased in magnitude for the LS-IP case, as the recirculatory flows are damped. The ascending velocity vectors near the delta-shaped wall, predicted in the transverse plane for the inner strand in the LS-bare and DLS-bare are eliminated, as seen in the Figs. 4.12d, 4.13d and 4.14d. In the outer strand, the fluid first impacts the walls, and after that, leaves the tundish through the outlet as seen in Fig. 4.14e. These results match with the experiments where the second peak is eliminated and the short-circuiting flow is delayed.

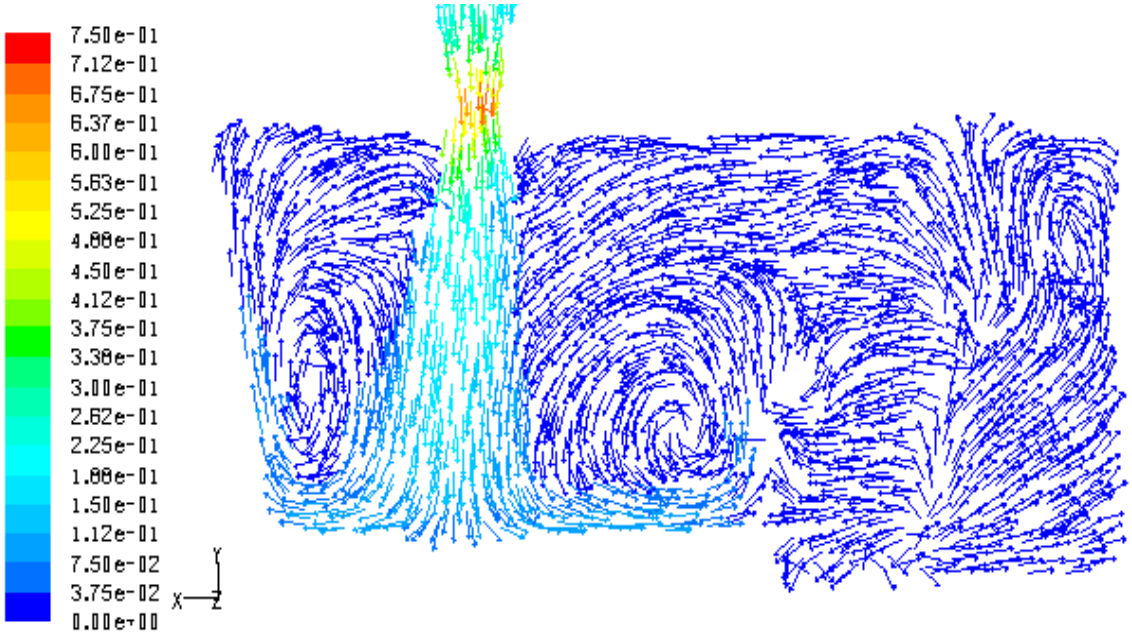

Figure 4.15a. Transverse plane along the vertical axis shroud, showing the velocity fields for the DLS-IP in m/s

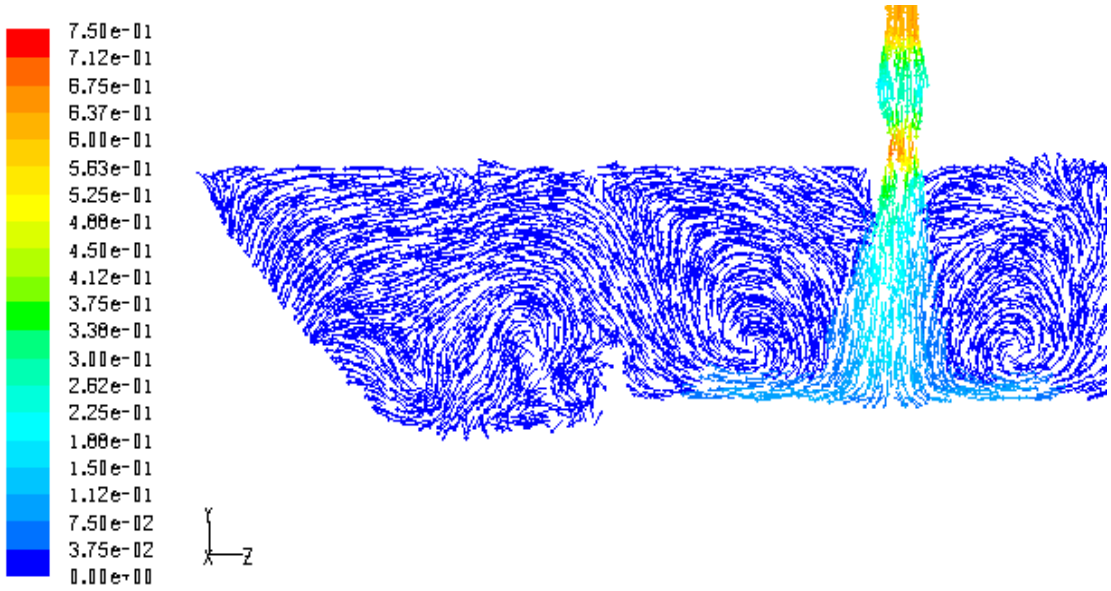

Figure 4.15b. Longitudinal plane along the axis shroud, showing the velocity fields for the DLS-IP in m/s

When the entry jet impacts the bottom of the tundish for the DLS-IP case, recirculatory flows are formed within the volume of the impact pad with less turbulence than the previous cases. The motion of the fluid, as in the LS-IP case, is directed towards the bath surface and divides into the two main portions mentioned before, forming one large recirculation going towards the inlet stream, and the other directed outside the IP volume as smaller recirculations with less turbulent motion than the previous cases. This is shown in Figs. 4.15a and 4.15b. The ascending velocity near the delta-shaped wall is less than the previous cases, caused by the effect of the DLS-IP arrangement.

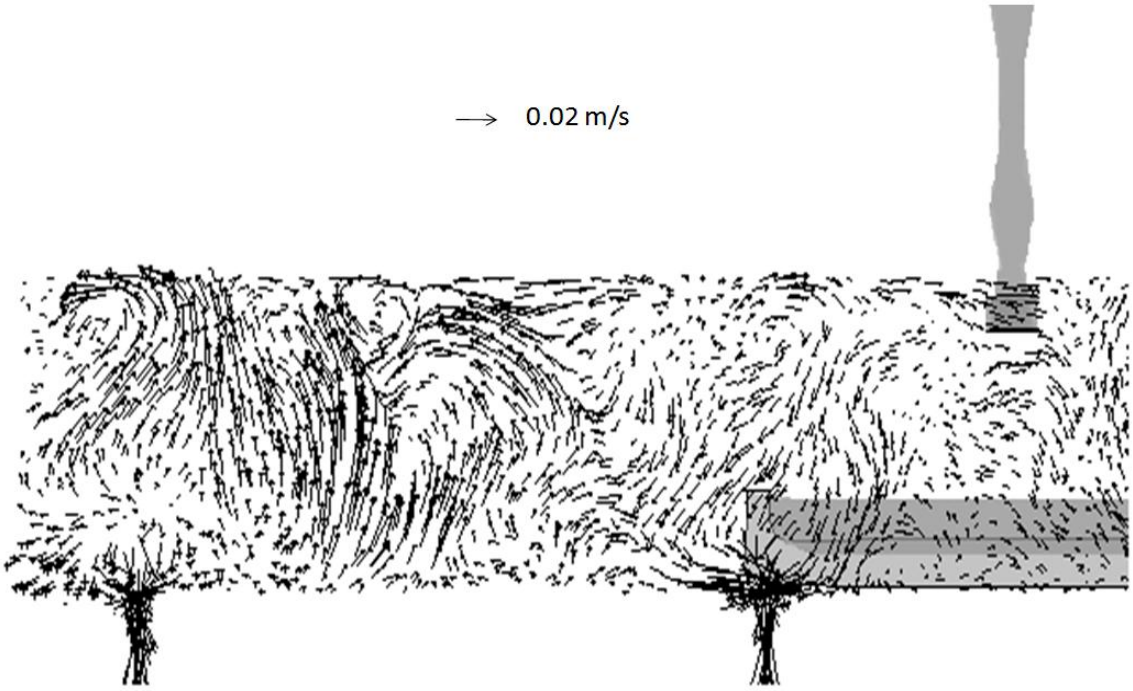

Figure 4.15c. Longitudinal plane over the outlets, showing the velocity fields for the LS-IP, m/s

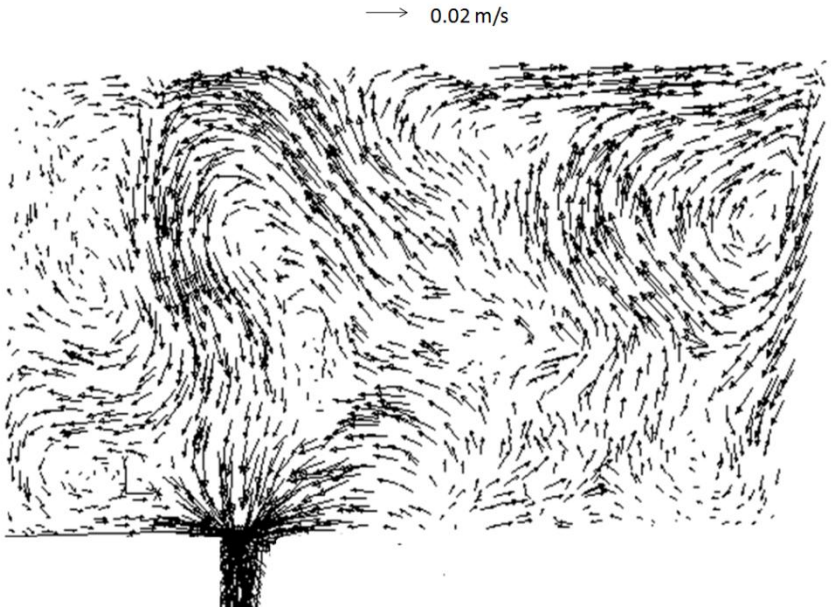

Figure 4.15d. Transverse vertical plane along the inner strand, showing the velocity fields for the DLS-IP, m/s

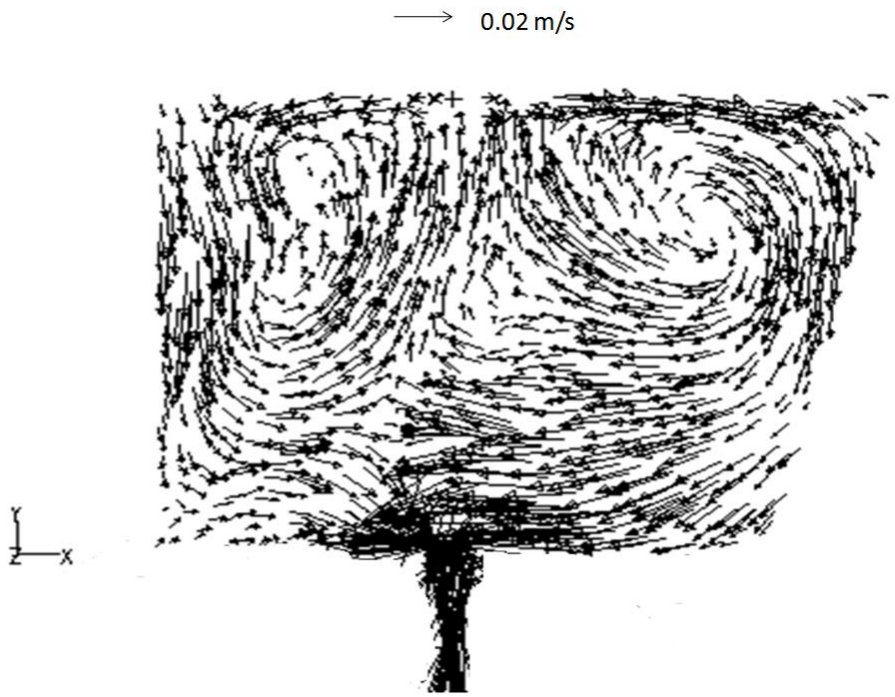

Figure 4.15e. Transverse vertical plane across the outer strand, showing the velocity fields for the DLS-IP, m/s

Similarly to the LS-IP, in the DLS-IP arrangement, velocity vectors are pointing towards the bath surface as seen in Fig 4.15c. The high velocity vectors found in the LS-bare, DLS-bare and LS-IP pointing towards the inner strand in the floor of the tundish, are eliminated in the DLS-IP case. The ascending velocity vectors near the delta-shaped walls, predicted in the transverse plane for the inner strand for the previous cases, are eliminated as well. This can be seen by comparing Figs. 4.12d, 4.13d, 4.14d and 4.15d. As the turbulence is decreased throughout the fluid volume of the tundish, and velocity magnitudes are reduced, as shown in the different planes. The fluid has more time to float out the inclusions. For the outer strand, the fluid is divided in two, the first part directed towards the bath surface and the second part towards the outlet (see fig. 4.15e). These results match with tracer experiments for which the DLS-IP had the largest and more even averaged residence times and the largest fractions of plug flow volume. The reason for this is the DLS, which distributes the liquid more evenly throughout the used volume of the tundish.

4.3 TRACER MIXING

As described in the previous section, the expansion of the jet caused by the DLS can be observed clearly when comparing tracer distributions in the bare tundish after a few seconds of the injection.Figures 4.16a, 4.16b, 4.16c, 4.16d, 4.16e and 4.16f.

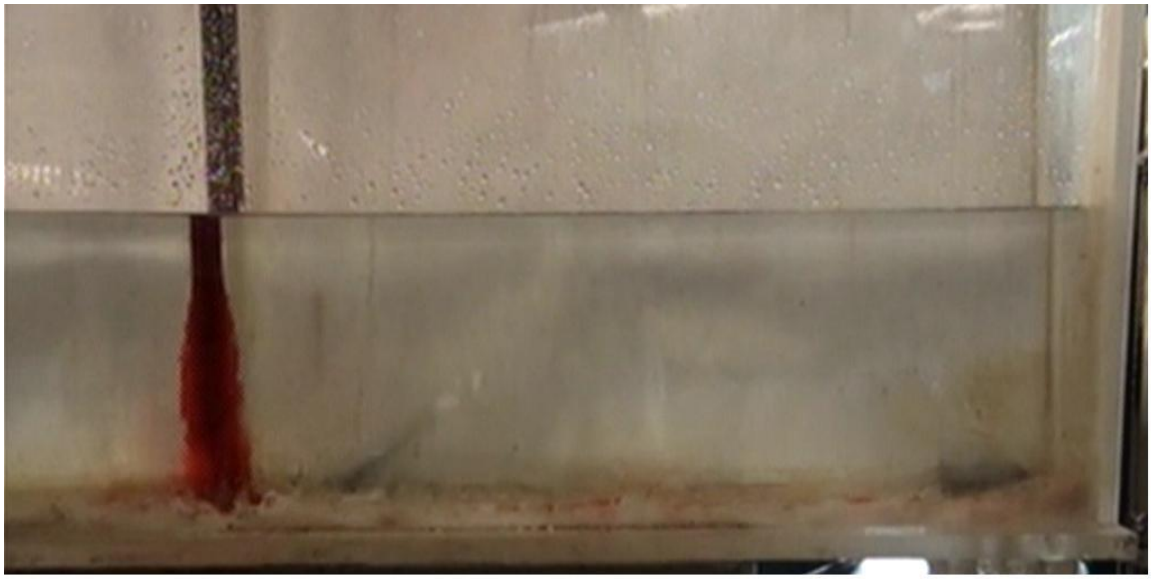

Figure 4.16a.Tracer distribution in the bare tundish arranged with the LS after 4s

Figure 4.16b.Tracer distribution in the bare tundish arranged with the DLS after 4s

Figure 4.16c. Tracer distribution in the bare tundish arranged with the LS after 5s

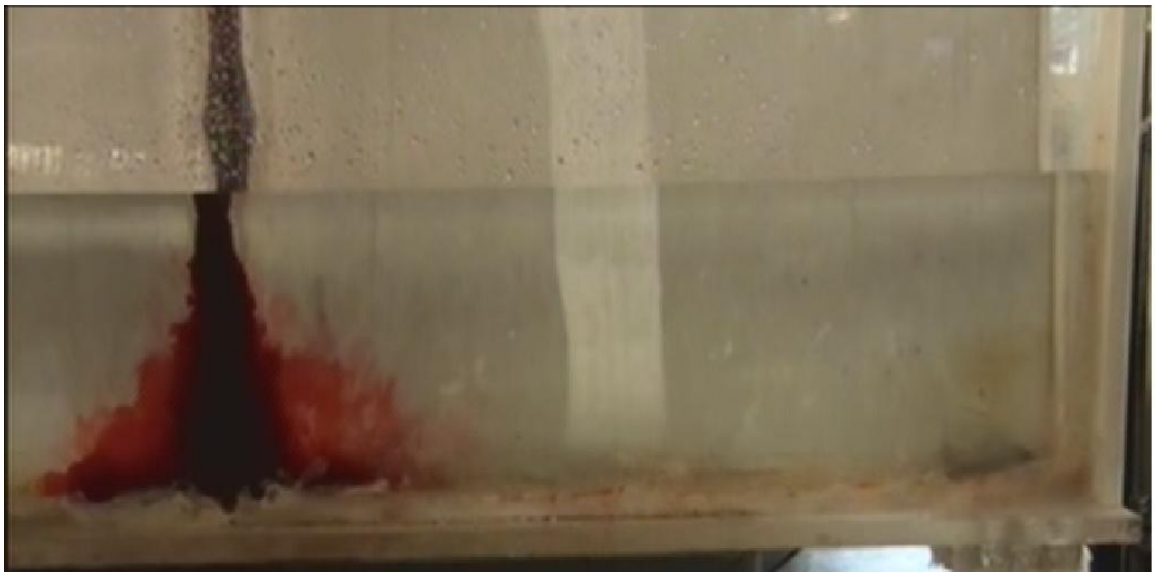

Figure 4.16d. Tracer distribution in the bare tundish arranged with the DLS after 5s

After the fluid impacts the bottom of the tundish, the tracer mixes quickly in the delta-shaped area along the transverse and longitudinal axes. The fluid exhibits high levels of turbulent motion.

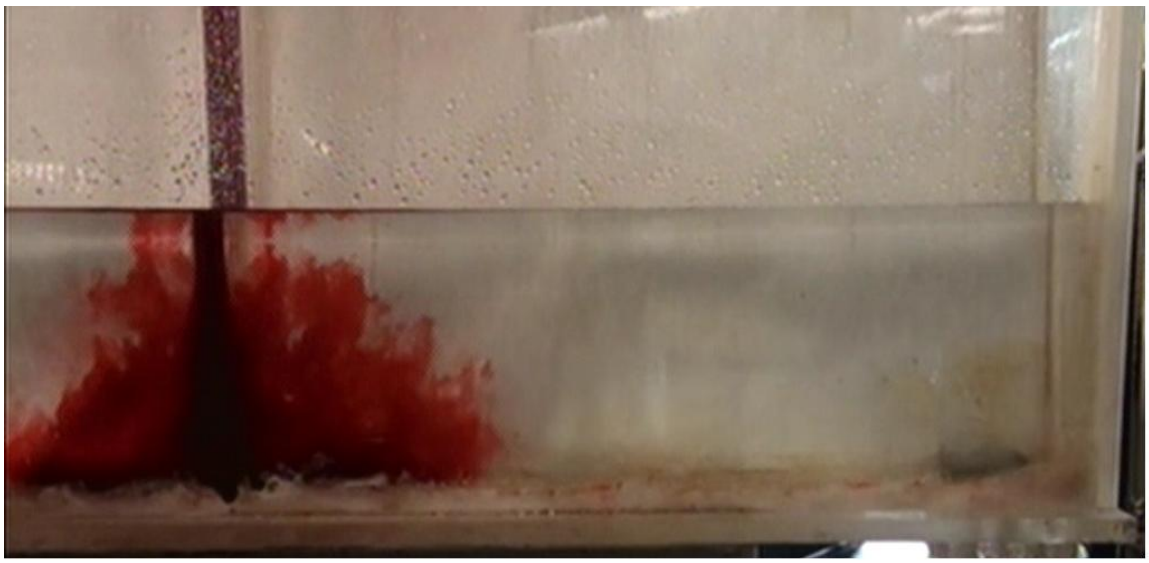

Figure 4.16e. Tracer distribution in the bare tundish arranged with the LS after 6s

Figure 4.16f. Tracer distribution in the bare tundish arranged with the DLS after 6s

For the LS-bare case, the tracer moves faster towards the back and delta-shaped walls than towards the front side direction. This explains the large difference in residence times between the inner and outer strands. After a further period of time, the dyed fluid adopts an irregular mixing front, with the C shape described by Shamik R. et al.[62]. The velocity is larger near the bath surface than in the bottom of the tundish. After the tundish impacts the lateral wall, it is directed towards the outer strand as seen in Figures 4.17a, 4.17b and 4.17c.

For the DLS-bare case, the fluid moves faster along the front side as compared to the LS-bare. As the tracer is more evenly distributed, it moves towards the outer strand with a more regular mixing front, similar to a fluid in plug flow conditions. The tracer reaches first the outer strand than the LS-bare case, which explains the more even averaged residence times in this case. Figures 4.18a, 4.18b, 4.18c.

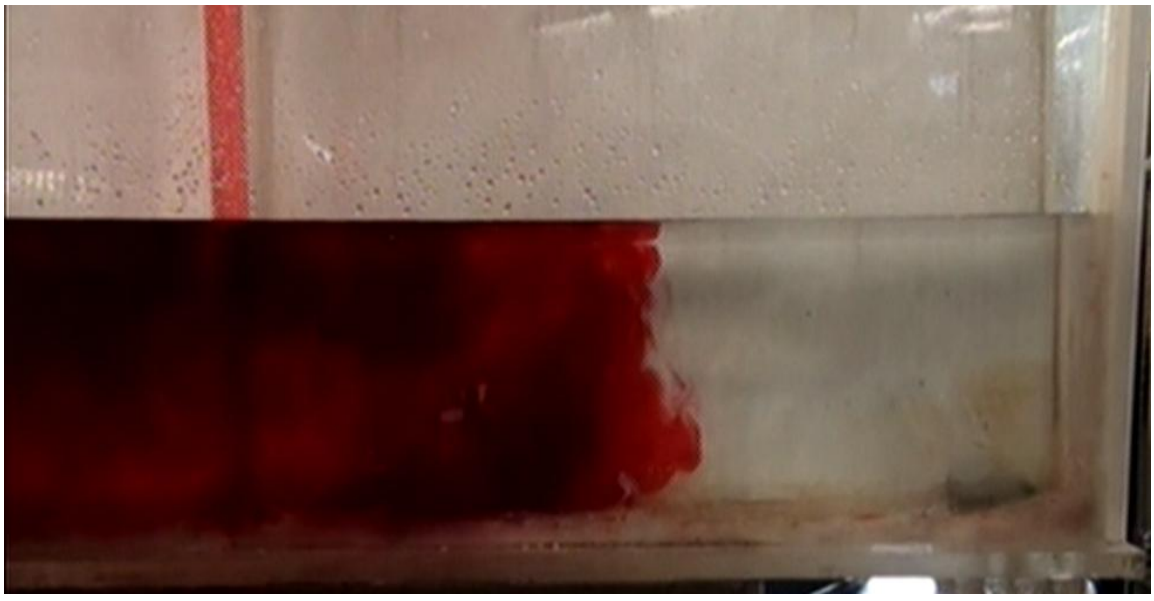

Figure 4.17a. Tracer distribution in the bare tundish arranged with the LS after 14s

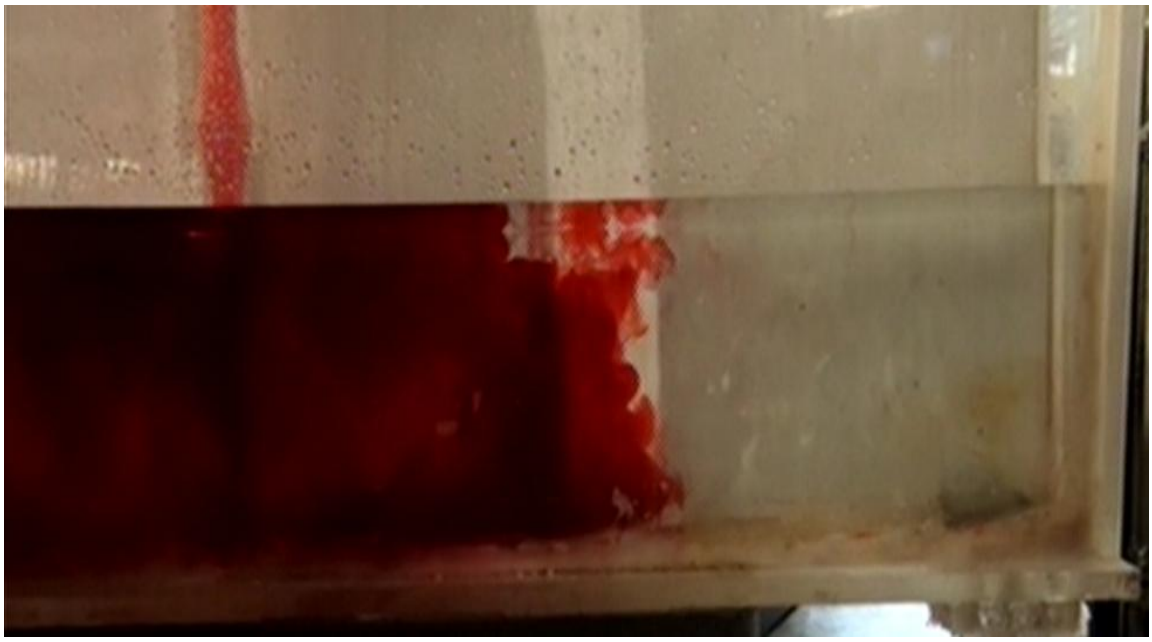

Figure 4.17b. Tracer distribution in the bare tundish arranged with the DLS after 14s

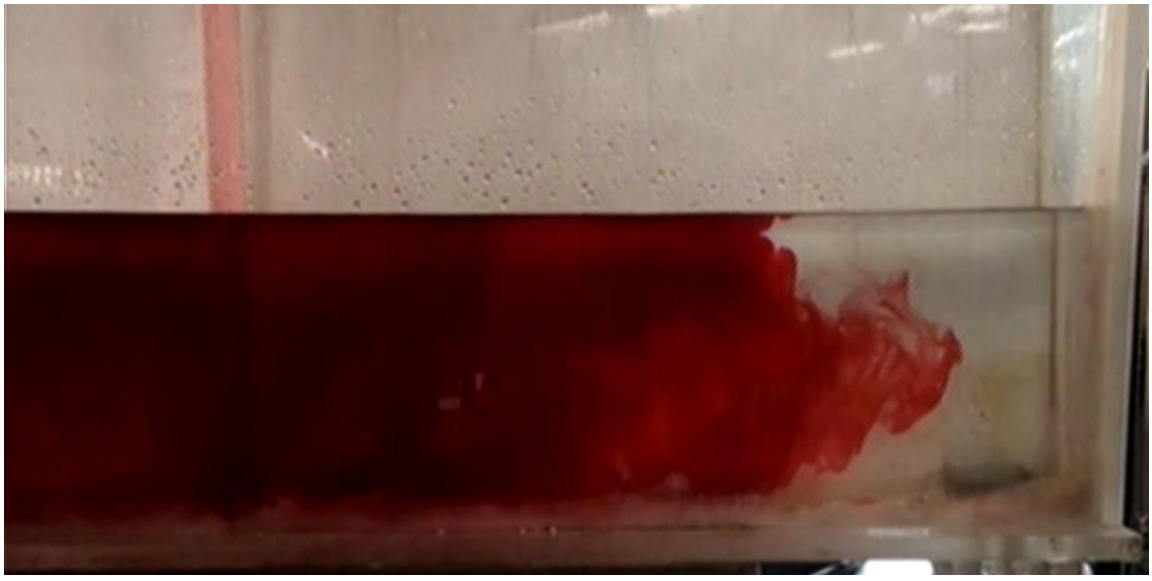

Figure 4.17c. Tracer distribution in the bare tundish arranged with the LS after 28s

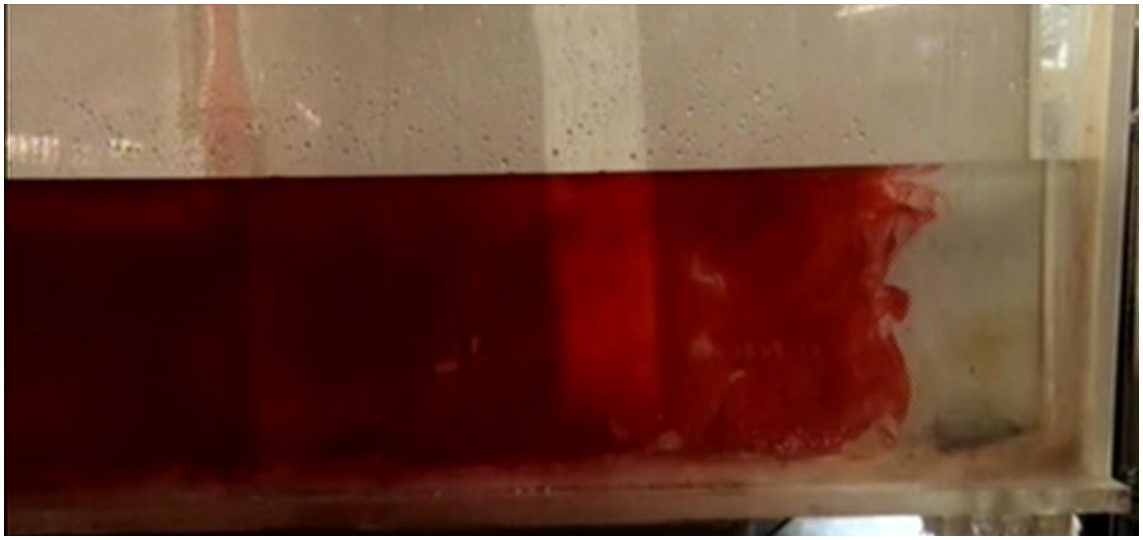

Figure 4.18a. Tracer distribution in the bare tundish arranged with the DLS after 28s

Figure 4.18b. Tracer distribution in the bare tundish arranged with the LS after 32s

Figure 4.18c. Tracer distribution in the bare tundish arranged with the DLS after 32s

There was a dead region observed in the upper corner of the tundish for both ladle shrouds, although it was less visible for the DLS-bare case(Figures 4.19a, 4.19b). The tundish is fully mixed at 120 s (Figures 4.19c, 4.19d).

Figure 4.19a. Tracer distribution in the bare tundish arranged with the LS after 60s

Figure 4.19b. Tracer distribution in the bare tundish arranged with the DLS after 60s

Figure 4.19c. Tracer distribution in the bare tundish arranged with the LS after 120s

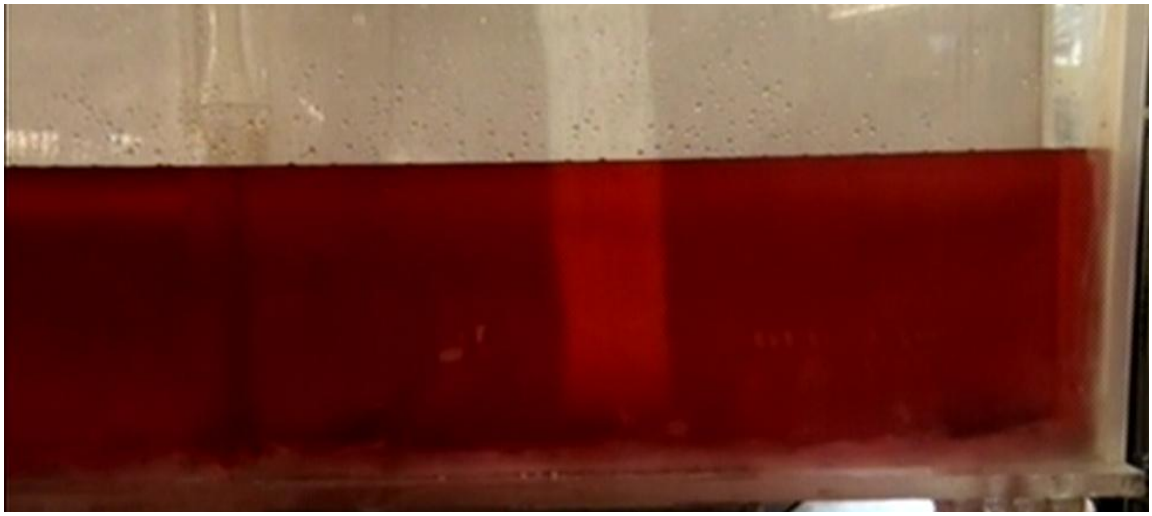

Figure 4.19d. Tracer distribution in the bare tundish arranged with the DLS, after 120s

The tracer distribution was also visualized for the LS-IP and DLS-IP cases. Similar patterns as in the bare tundish cases are found after few seconds of the injection as seen in figures 4.20a, 4.20b, 4.20c and 4.20d.

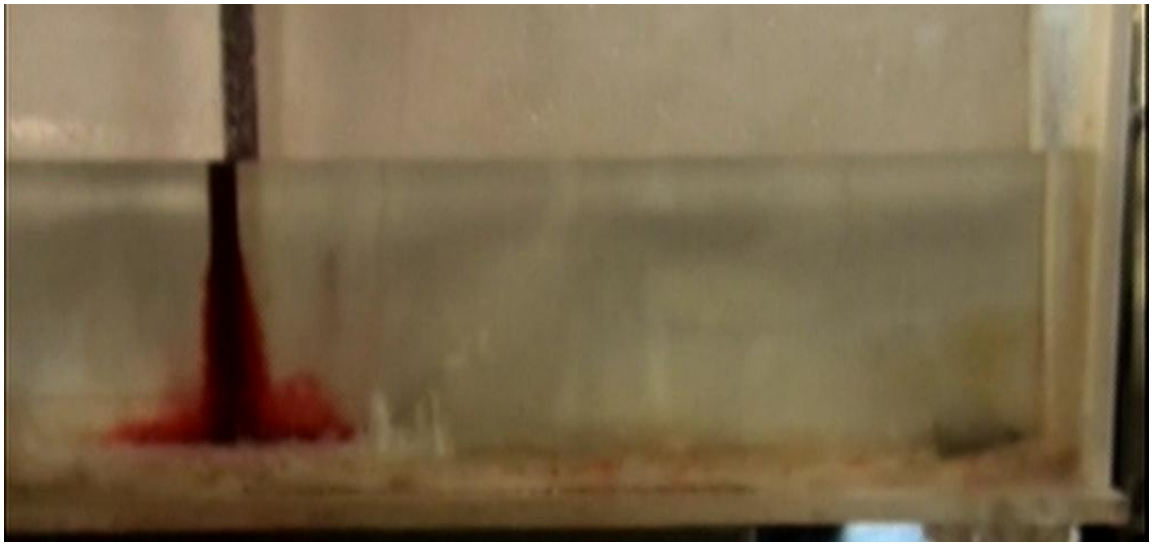

Figure 4.20a. Tracer distribution in tundish, arranged with the LS and IP, after 4s

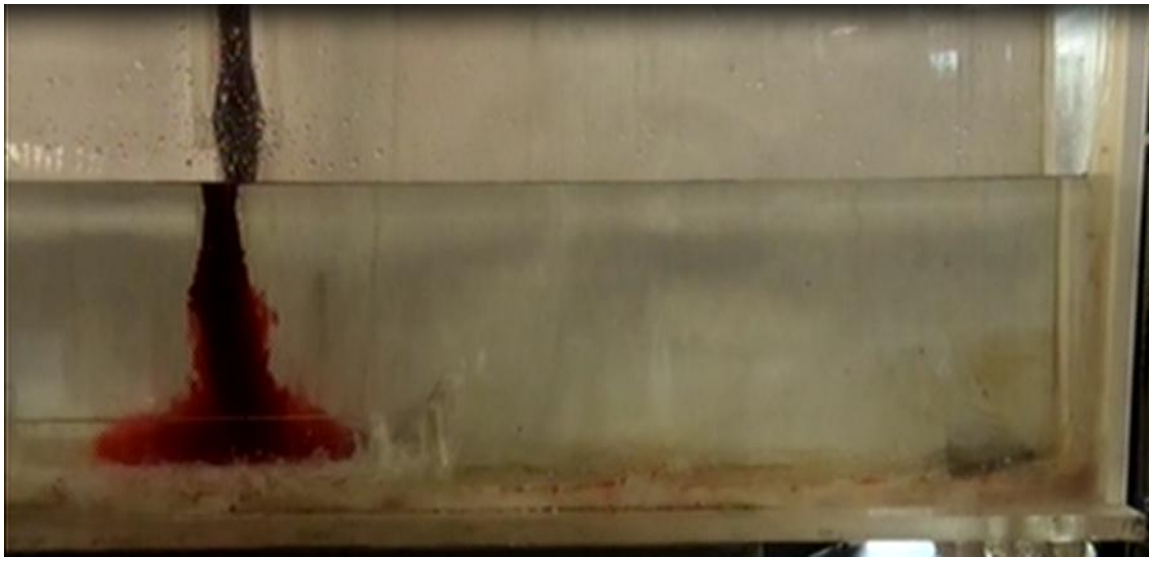

Figure 4.20b. Tracer distribution in tundish, arranged with the DLS and IP, after 4s

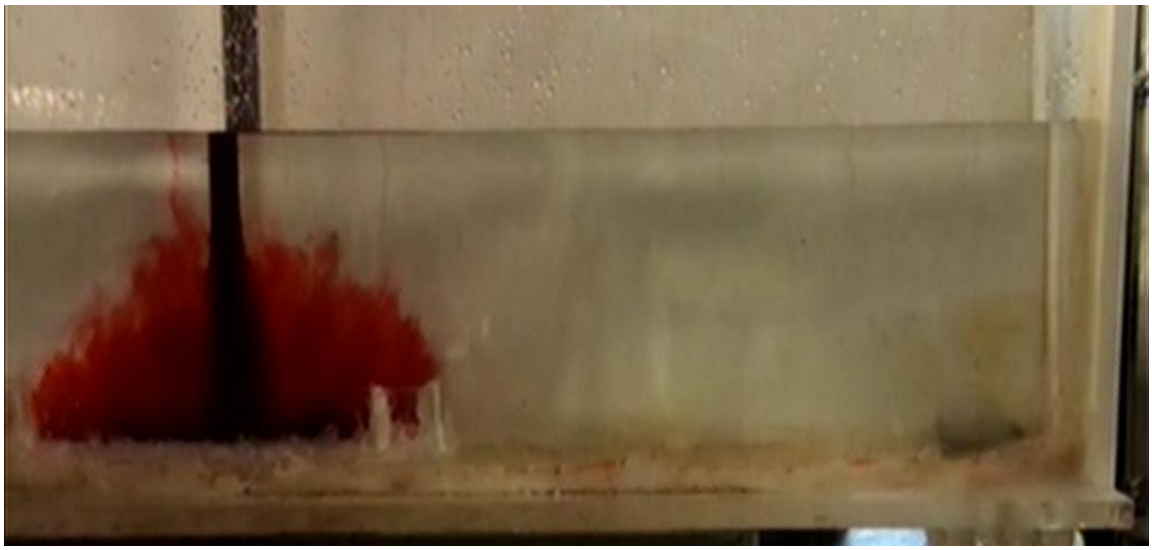

Figure 4.20c. Tracer distribution in tundish, arranged with the LS and IP, after 5s

Figure 4.20d. Tracer distribution in tundish, arranged with the DLS and IP, after 5s

In the LS-IP arrangement, it is observed that the fluid has an upward motion and mixes through its way, up and out of, the IP volume. The DLS-IP retains the fluid longer and mixes more inside the volume of the IP. It is observed that after 8s of dye injection, in the LS-IP case, the tracer reaches a higher height towards the bath surface than the DLS-IP(figures 4.21a and 4.21b).

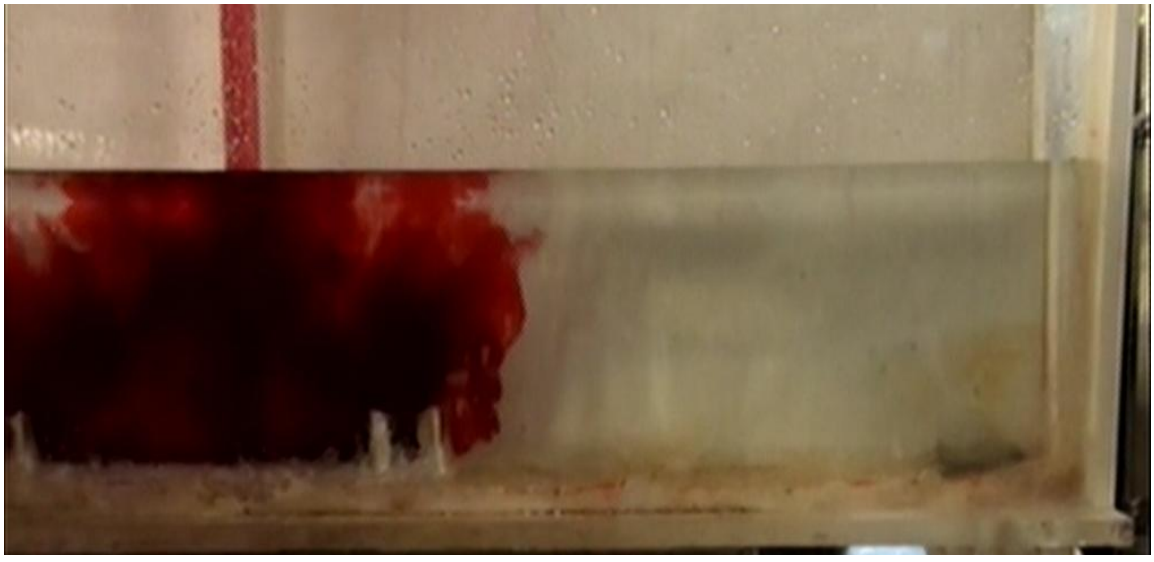

Figure 4.21a. Tracer distribution in tundish arranged with the LS and IP after 8s

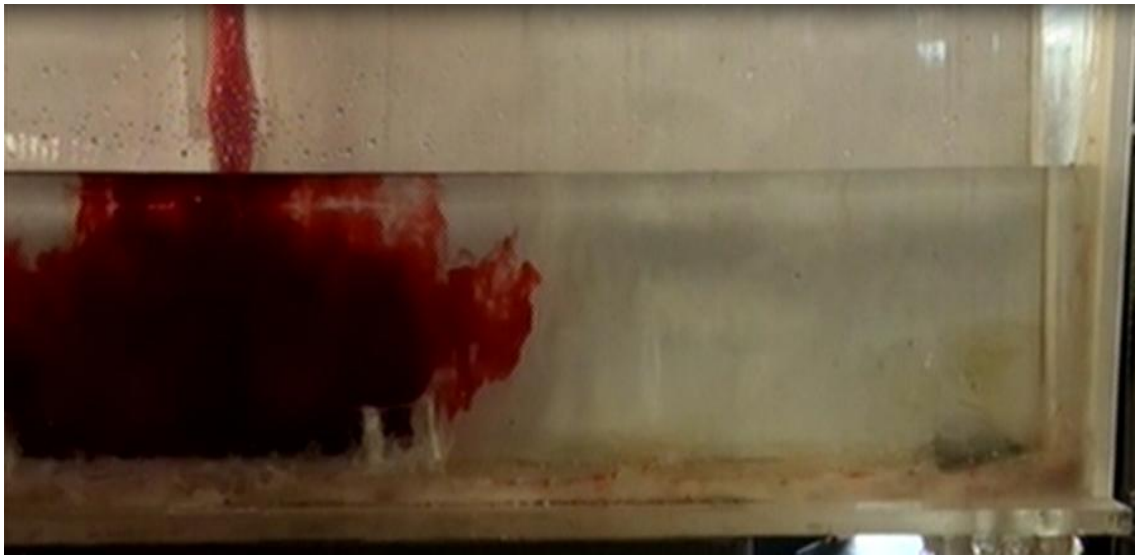

Figure 4.21b. Tracer distribution in tundish arranged with the DLS and IP after 8s

The IP damps the fluid motion along the transverse and longitudinal axes. In the LS-IP case, the tracer has a higher velocity near the bath surface than the DLS-IP. As the velocity distribution near the bath surface of the DLS-IP is less than that for the LS-IP, the fluid decays to the bottom of the tundish before reaching the outer strand while the LS-IP decays when the tracer is near the outer strand(figures 4.22a to 4.22f). Therefore, the tracer in the DLS-IP set-up, has even, and larger averaged residence times. The plug flow fractions are the largest for both strands.

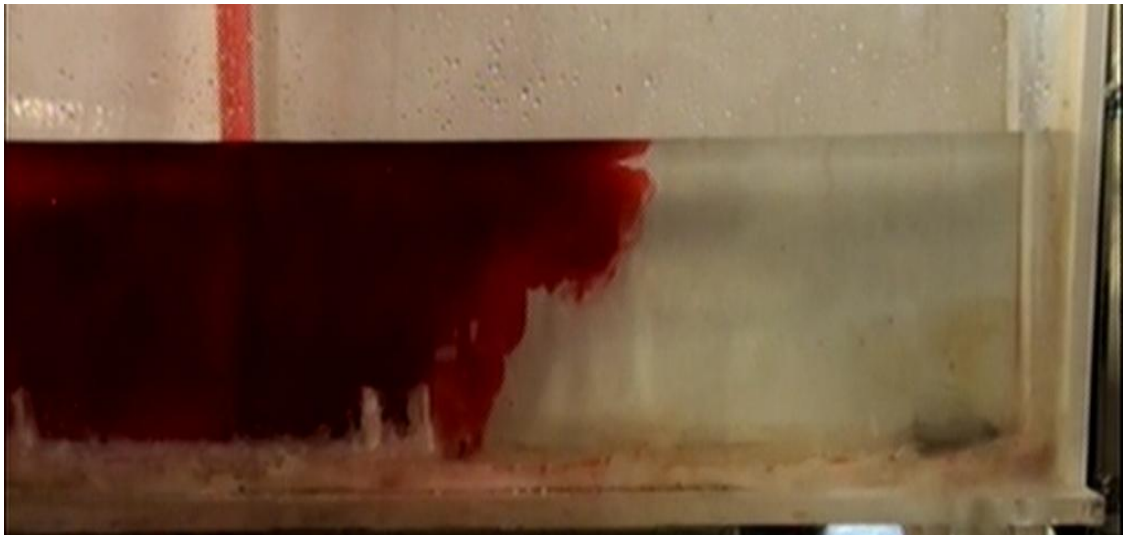

Figure 4.22a. Tracer distribution in tundish, fitted with the LS and IP, after 14s

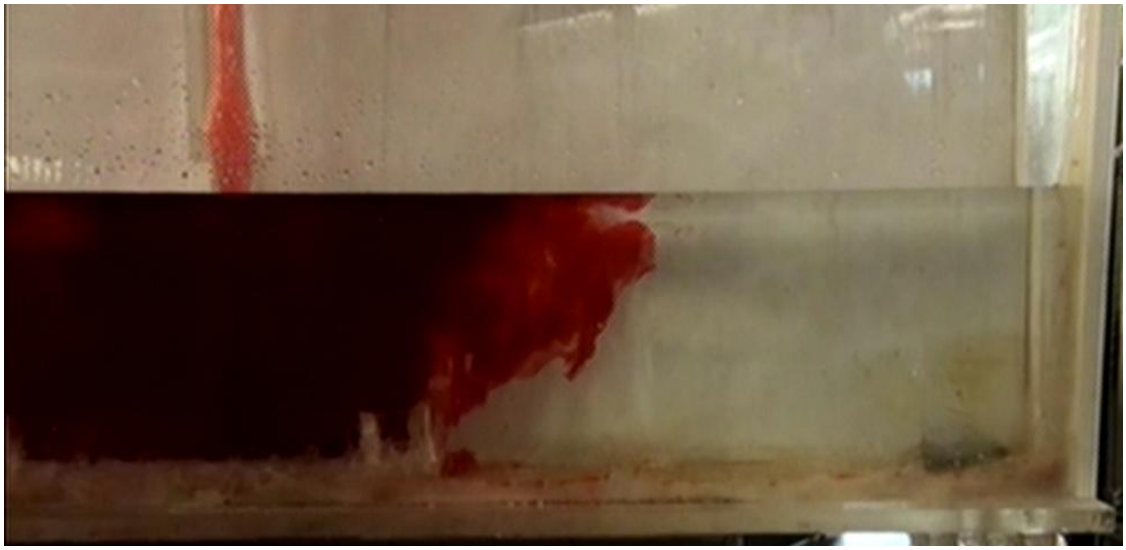

Figure 4.22b. Tracer distribution in tundish, fitted with the DLS and IP, after 14s

Figure 4.22c. Tracer distribution in tundish, fitted with the LS and IP, after 32s

Figure 4.22d. Tracer distribution in tundish arranged with the DLS and IP, after 32s

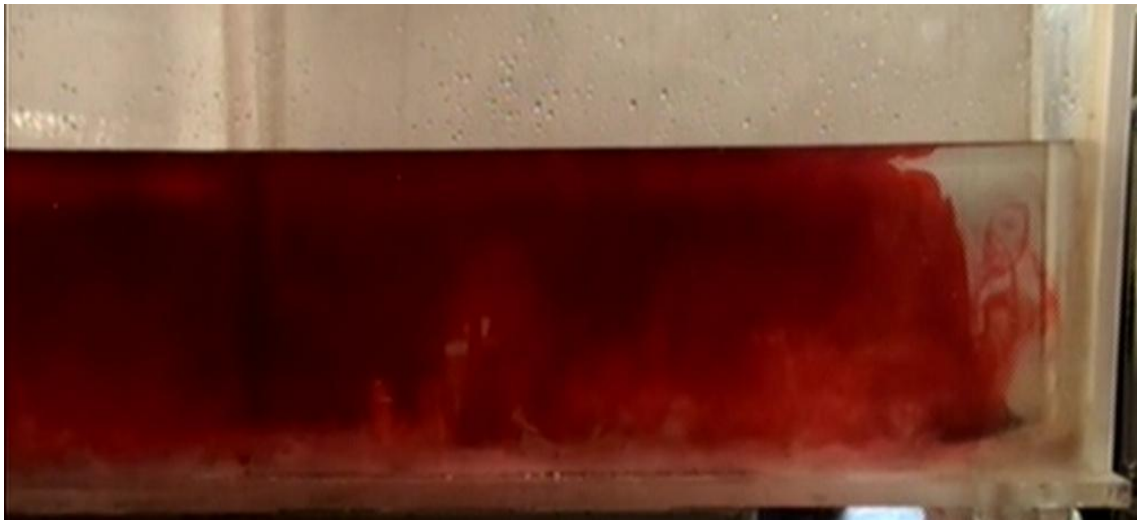

Figure 4.22e. Tracer distribution in tundish arranged with the LS and IP, after 40s

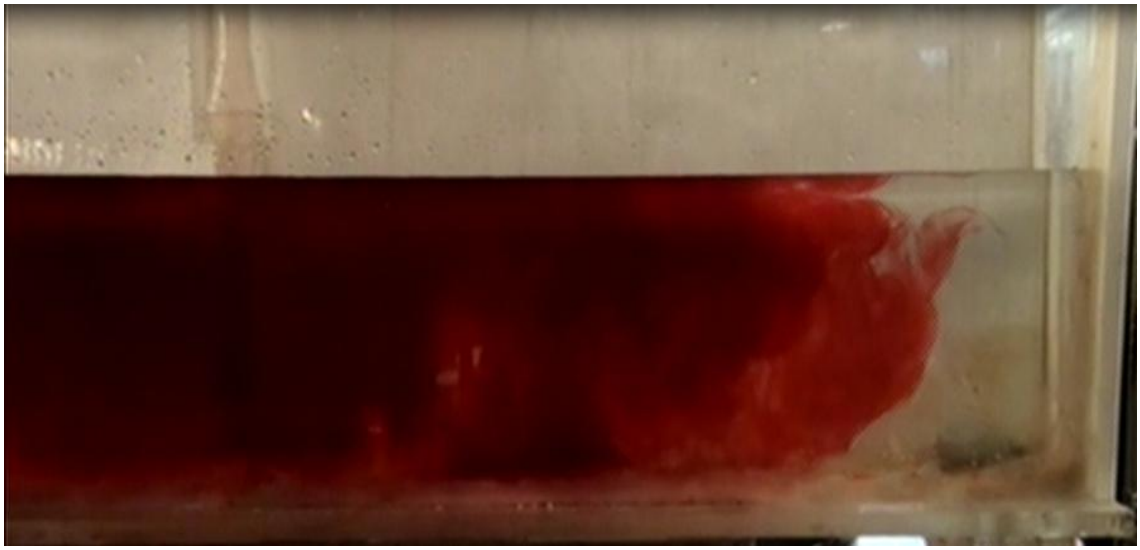

Figure 4.22f. Tracer distribution in tundish fitted with the DLS and IP, after 40s

A dead volume region is observed, as in the previous cases, at the upper area of the outer strand(figures 4.23a and 4.23b). The tundish liquid is completely mixed after 120 s, as seen in Figure 4.24a and 4.24b.

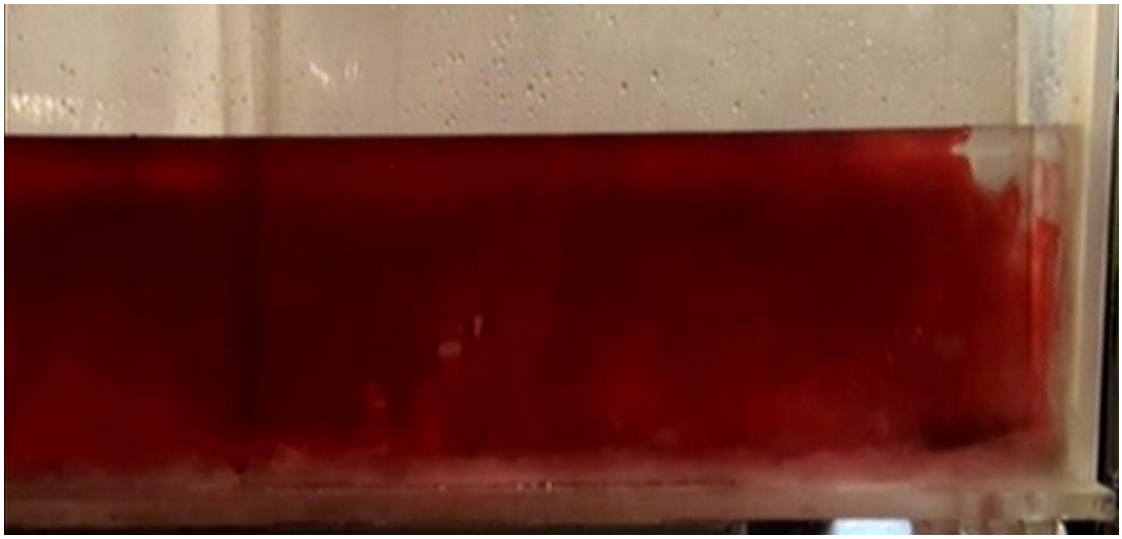

Figure 4.23a. Tracer distribution in tundish fitted with the LS and IP, after 60s

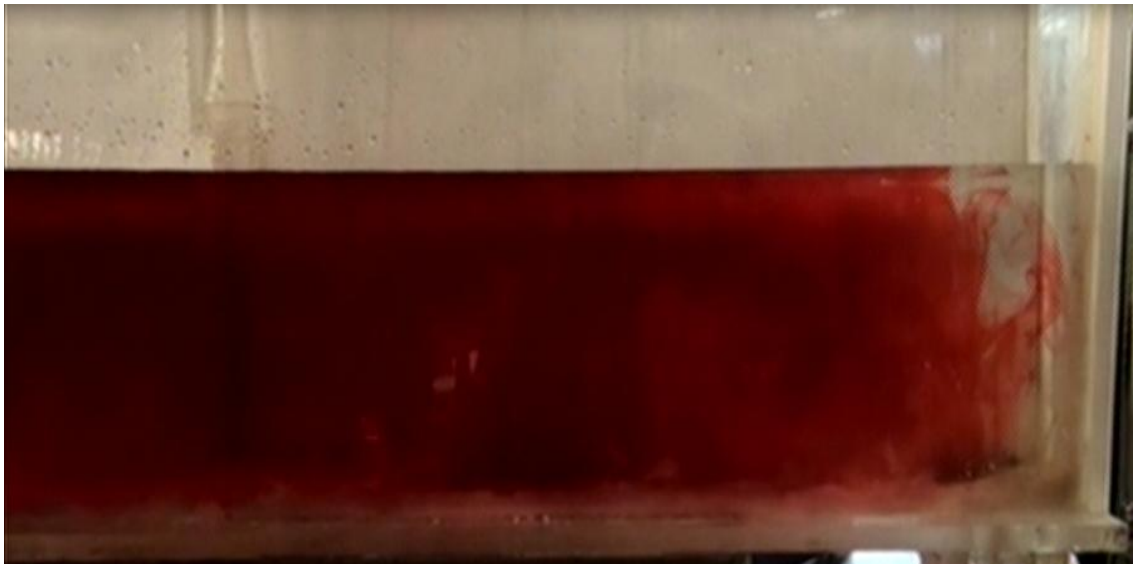

Figure 4.23b. Tracer distribution in tundish fitted with the DLS and IP after, 60s

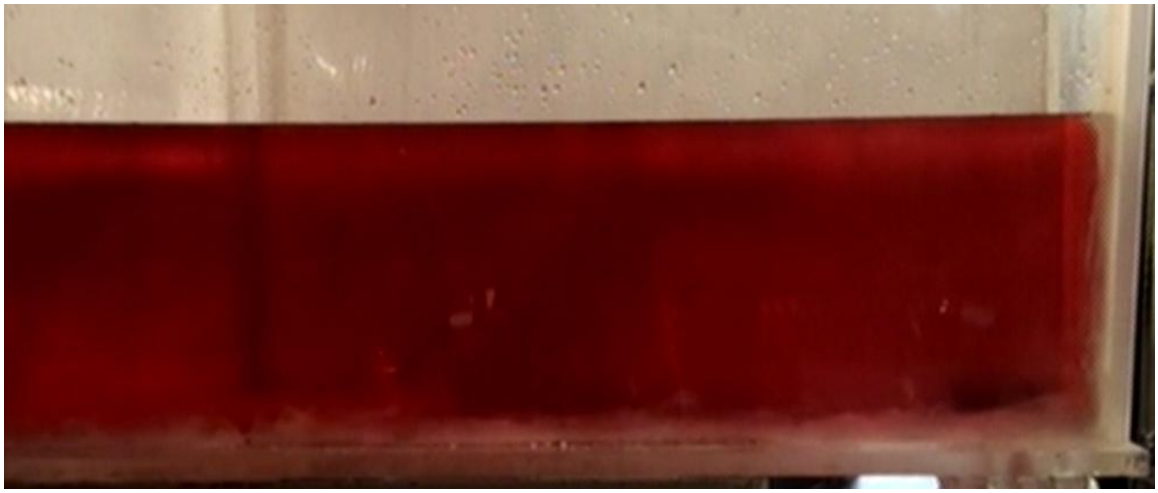

Figure 4.24a. Tracer distribution in tundish fitted with the LS and IP, after 120s

Figure 4.24b. Tracer distribution in tundish arranged with the DLS and IP, after 120s

4.4 PARTICLE IMAGE VELOCIMETRY(PIV) STUDIES

4.4.1 INTRODUCTION

In this section of the thesis, the experimental results using the Particle Image Velocimetry (PIV) Technique, are explained. Before, it is worth mentioning that these experiments were focused on the dynamic behavior of the entry jet, rather than on the fluid flow within the vessel itself, since it is actually the fluid dynamics of the jet that governs the rest of the flow within the tundish.

These experiments include water flow rates of 11 l/min, which is the equivalent steel throughput in the actual caster, plus two higher flow rates of 20 and 30 l/min, in order to observe the jet dynamics under extreme conditons. These conditions occur when the tundish is rapidly filled up, following a ladle change operation, or at the beginning of a casting sequence.

4.4.2 DISSIPATIVE LADLE SHROUD

Figures 4.25a-4.25d show the velocity fields of the entry jet at 11 l/min, corresponding to steady state tundish operations. They refer to different times, separated by $\Delta t = 0.25$ seconds. Figure 4.25a, considered to occur at an arbitrary time of 0 seconds, shows the jet core, with the largest downward velocities. The drag effects on the surrounding fluid are small due to the relatively low turbulence. In the next time step, Figure 4.25b, the jet has twisted to the right side and the surrounding fluid is slightly entrained by the shearing stresses along the jet boundary. After the second time step, Figure 4.25c, the jet has now twisted to the left side, with similar effects on the surrounding fluid. The last time step, in Figure 4.25d, shows a straightening effect on the jet coming back to a similar pattern to that shown in Figure 4.25a.

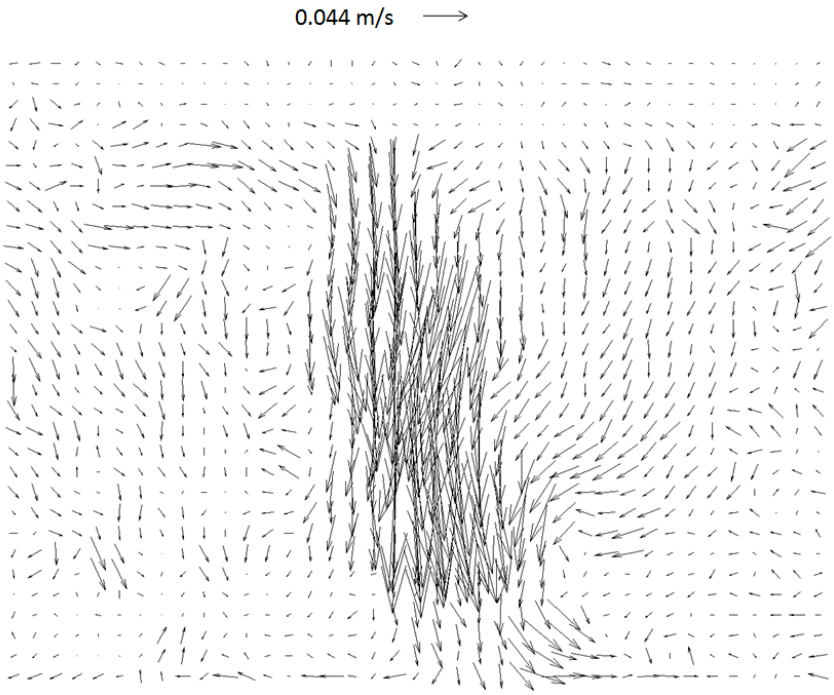

Figure 4.25a. PIV velocity fields on the shroud outlet axis from the DLS-bare. The velocity vectors have a downward direction using a flow rate of 11 L/min, Δt = 0 s

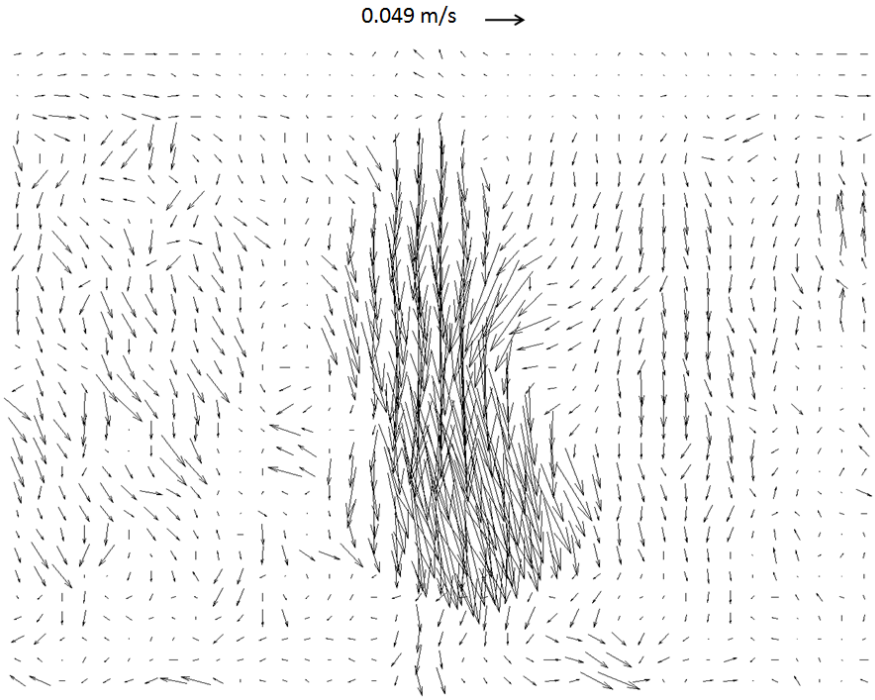

Figure 4.25b. PIV velocity fields on the shroud outlet axis from the DLS-bare. The entry jet is twisted to the right side using a flow rate of 11 L/min, Δt = 0.25 s

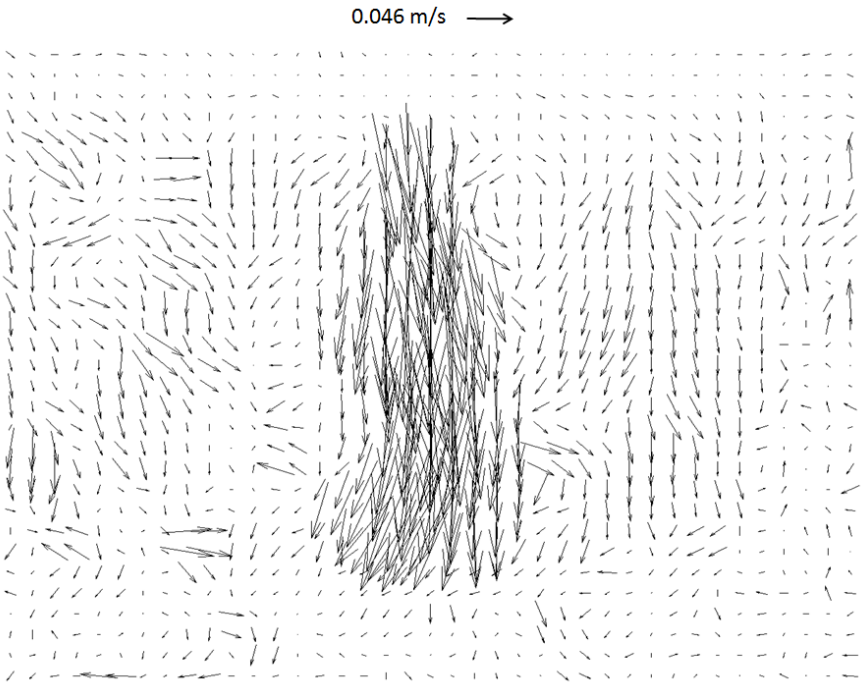

Figure 4.25c. PIV velocity fields on the shroud outlet axis from the DLS-bare. The entry jet is twisted to the left side using a flow rate of 11 L/min, Δt = 0.5 s

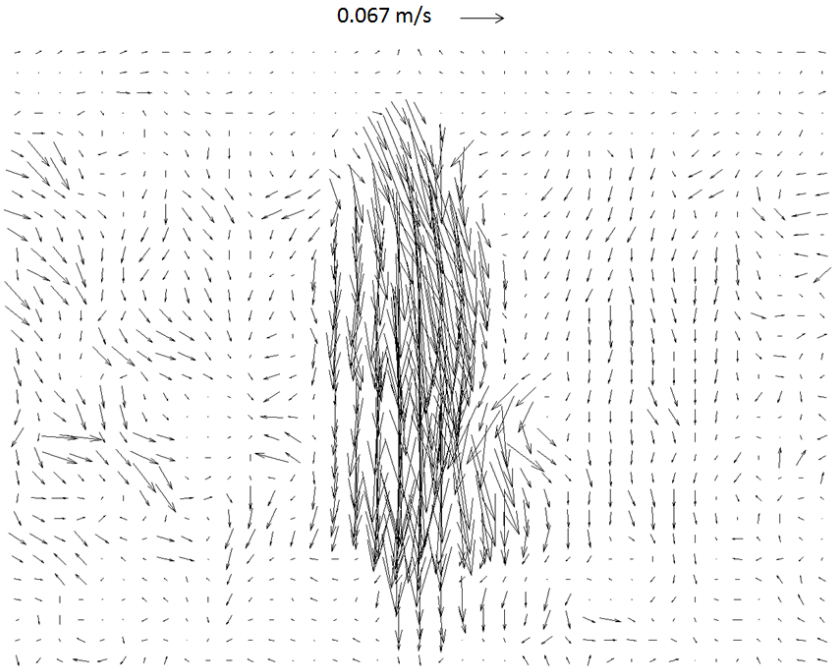

Figure 4.25d. PIV velocity fields on the shroud outlet axis from the DLS-bare. The entry jet is directed straightly using a flow rate of 11 L/min, Δt = 0.75 s

Figures 4.26a-4.26d show the corresponding velocity fields of the entry jet at 20 l/min, at Δt intervals of 0.25 seconds. Figure 4.26a, at time zero, shows an entry jet that has twisted three times along its length, with the highest velocities located close to the tip of the DLS. The stronger jet deformation in the exiting flow had a larger turbulence level, which interacts more rapidly with the surrounding fluid which is more efficiently entrained by the shearing stresses along the jet boundary. At the next time step, Figure 4.26b, the largest jet velocities are observed along its entire length, corresponding to the wide velocity profile close to the exit of the DLS tip, and thinner towards the tundish bottom. The results during the second time step, Figure 4.26c, shows a jet strongly tilted to the right side. As seen, the entrainment effects on the surrounding flow involve practically the full area of the velocity field. The last time interval, Figure 4.26d, shows a straightening effect on the jet coming back to a similar pattern of that shown in Figure 4.26a.

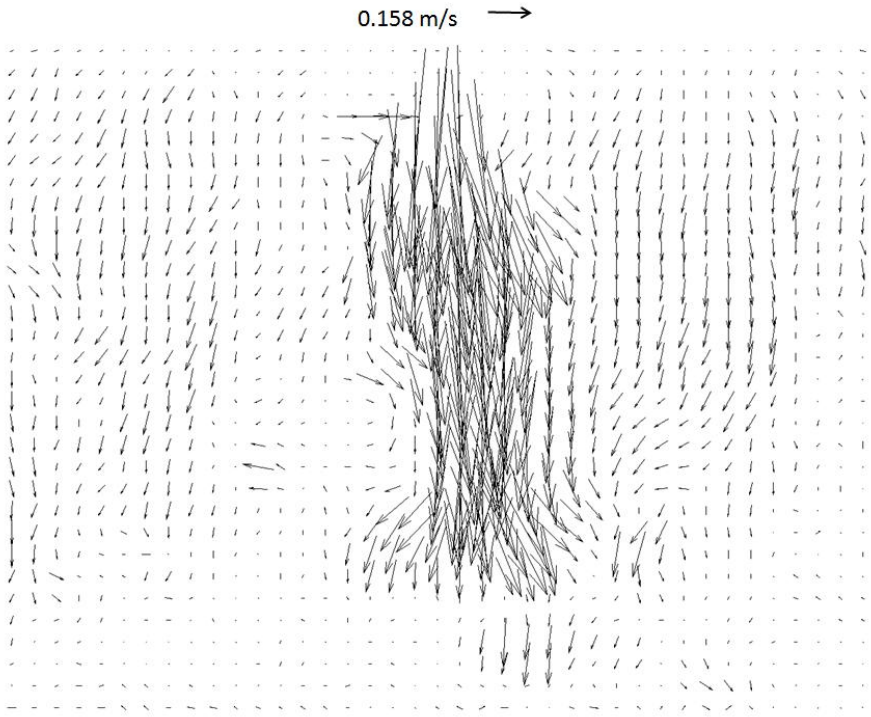

Figure 4.26a. PIV velocity fields on the shroud outlet axis from the DLS-bare. The entry jet is strongly deformed to the left. A flow rate of 20 L/min was used, Δt = 0

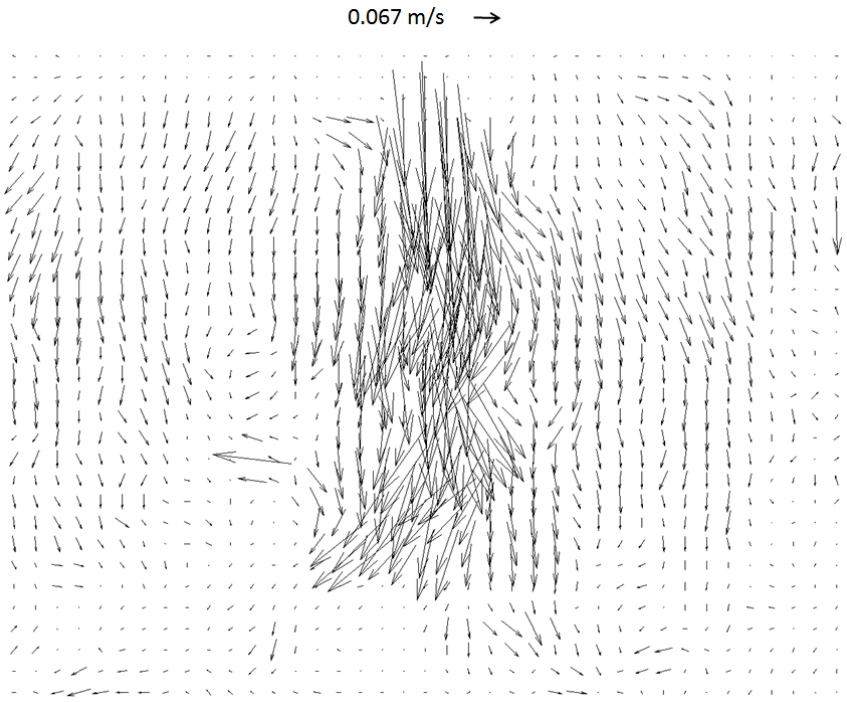

Figure 4.26b. PIV velocity fields on the shroud outlet axis from the DLS-bare. The entry jet is stretched as it descends. A flow rate of 20 L/min, Δt = 0.25s

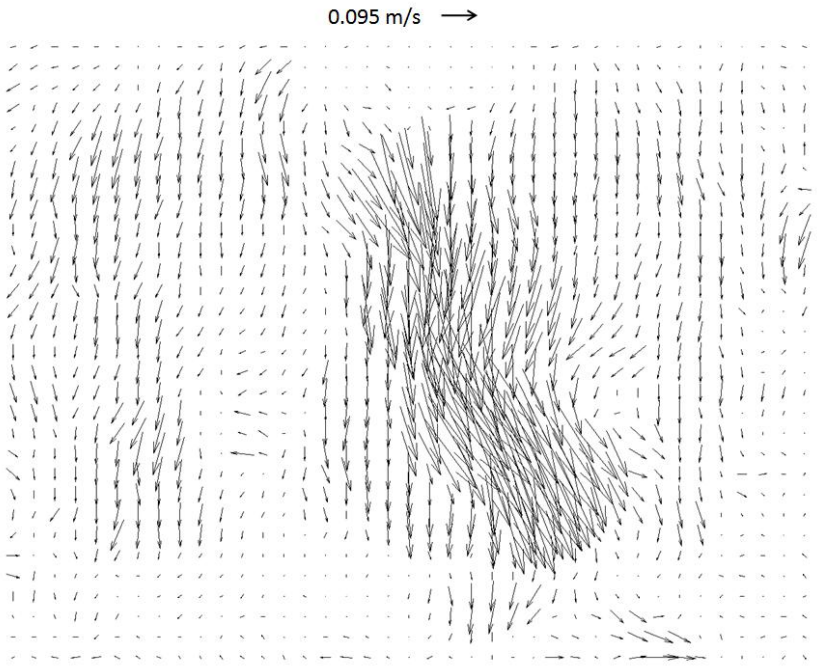

Figure 4.26c. PIV velocity fields on the shroud outlet axis from the DLS-bare. The entry jet is deformed to the right side. A flow rate of 20 L/min was used, Δt=0.5 s

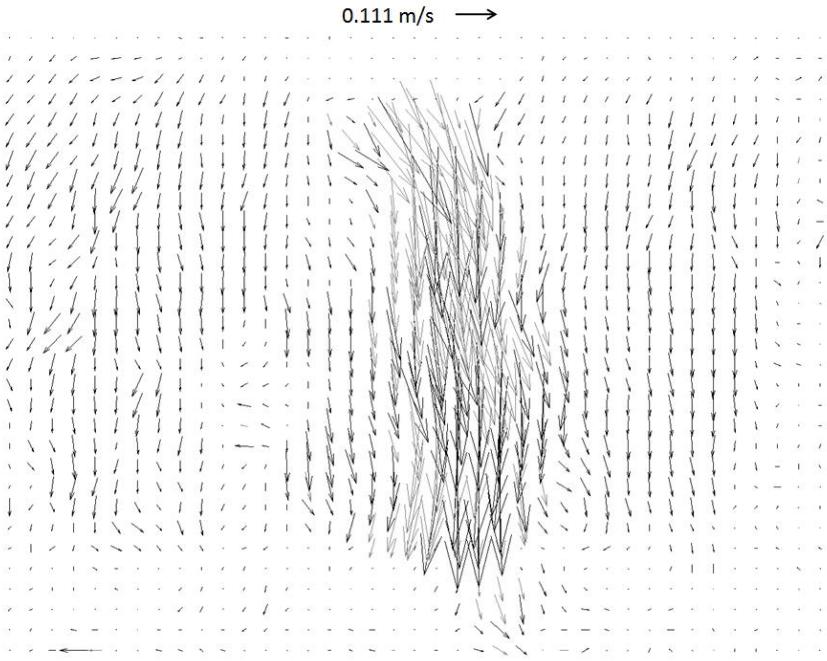

Figure 4.26d. PIV velocity fields on the shroud outlet axis from the DLS-bare. The entry jet is directed vertically. A flow rate of 20 L/min was used, Δt = 0.75 s

Figures 4.27a-4.27d show the corresponding velocity fields of the entry DLS jet at a flow rate of 30 l/min, separated 0.25 second intervals. Figure 4.27a shows that with this flow rate, the entrainment effects of the jet on the surrounding fluid involve the full flow field, generating a very complex, turbulent flow. Figure 4.27b shows only the lower part of the jet, due to the deformation effect which shadows the rest of the jet length located in a different plane, and the strong effects of the surrounding flow entrained by the jet entry operation. A doubly twisted jet is shown in Figure 4.27c during the next time step with the end of the jet pointing to the left side. Figure 4.27d shows a double twisted jet, to the right in the upper side and it is divided downstream into two mainstreams to the right and to the left in the lower part.

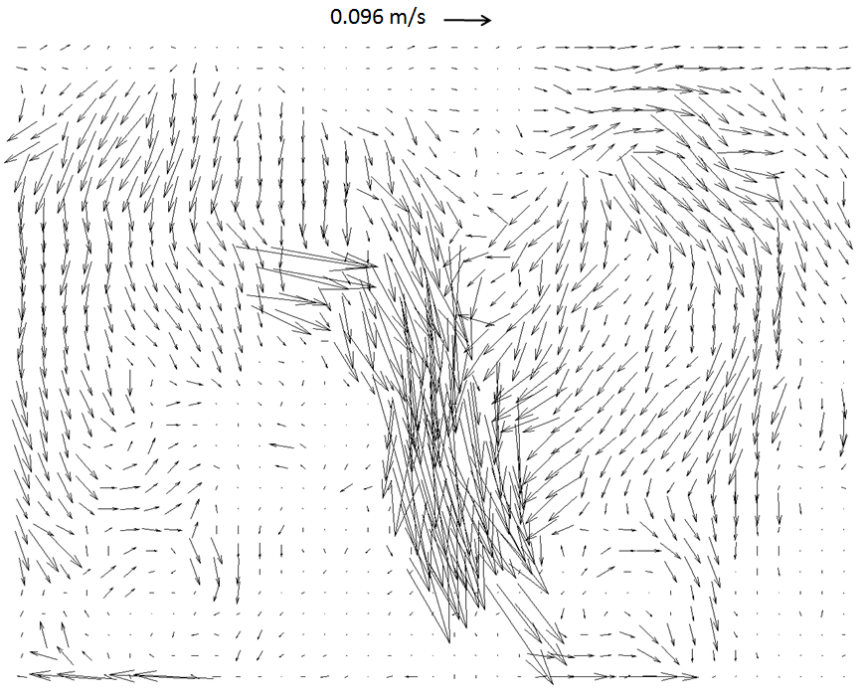

Figure 4.27a. PIV velocity fields on the shroud outlet axis from the DLS-bare. The entry jet is twisted to the right side using a flow rate of 30 L/min, Δt = 0 s

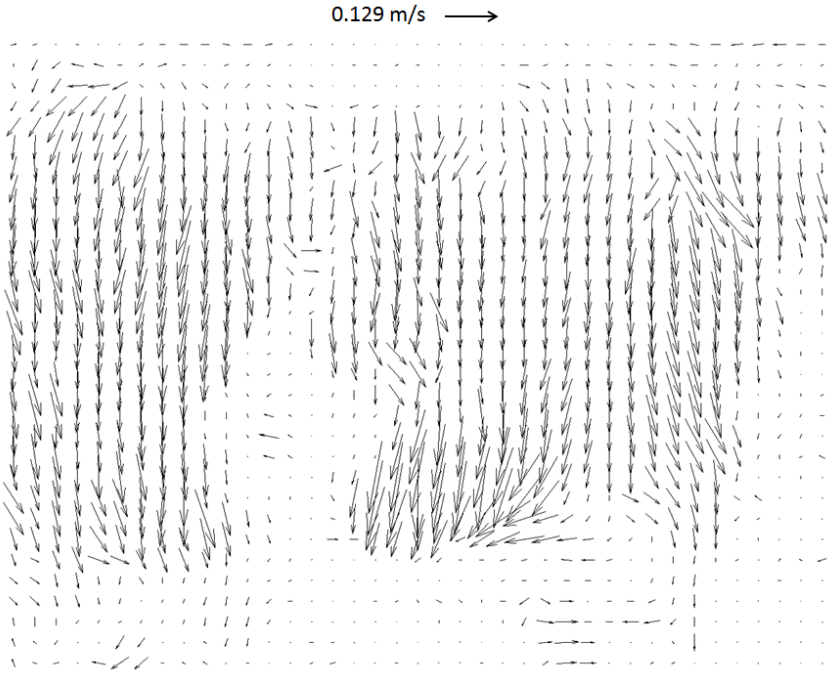

Figure 4.27b. PIV velocity fields on the shroud outlet axis from the DLS-bare. The entry jet is out of the plane using a flow rate of 30 L/min, Δt = 0.25 s

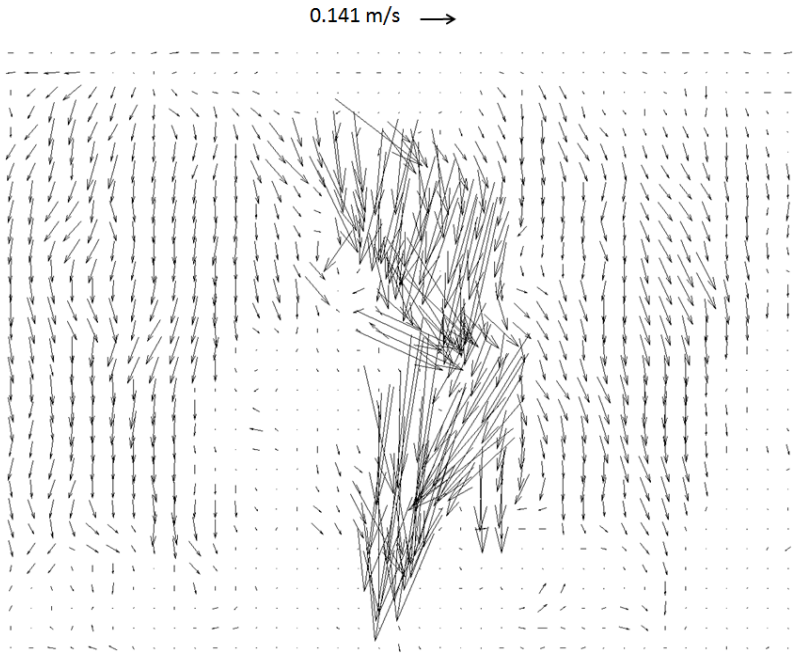

Figure 4.27c. PIV velocity fields on the shroud outlet axis from the DLS-bare. The entry jet is twisted to the left side using a flow rate of 30 L/min, Δt = 0.5 s

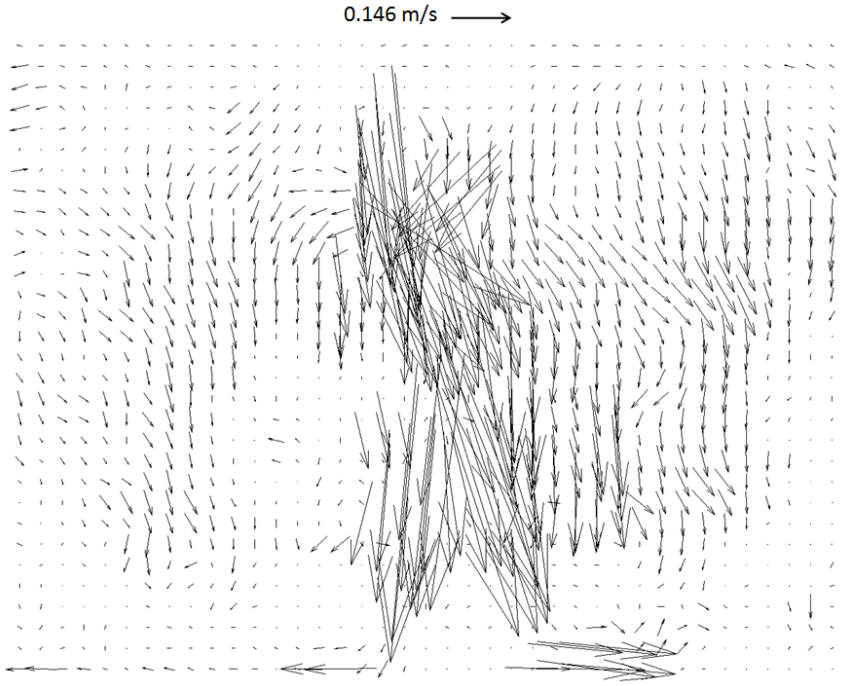

Figure 4.27d. PIV velocity fields on the shroud outlet axis from the DLS-bare. The entry jet is divided in two mainstreams using a flow rate of 30 L/min, Δt = 0.75 s

As is evident from Figures 4.25, 4.26 and 4.27, the entry jet through the DLS induces a deformation that increases at larger entry flow rates. It is expected that the deformation effect of the jet must be an important mechanism in dissipating the kinetic energy through shearing stresses and velocity gradients formed with the surrounding fluid, enhancing entrainment rates of liquid and jet-bulk liquid interactions.

4.4.3 CONVENTIONAL LADLE SHROUD

Flow fields generated by the LS yielded contrasting results as compared with the DLS. It can be seen that the entry jet maintains a straight trajectory, as can be seen in Figures 4.28a-4.28c, at different times, for a flow rate of 20 l/min. Indeed, as seen in these Figures, the entry jet remains straight at all times. Because of this condition, the entrainment effects on the surrounding fluid are significantly less.

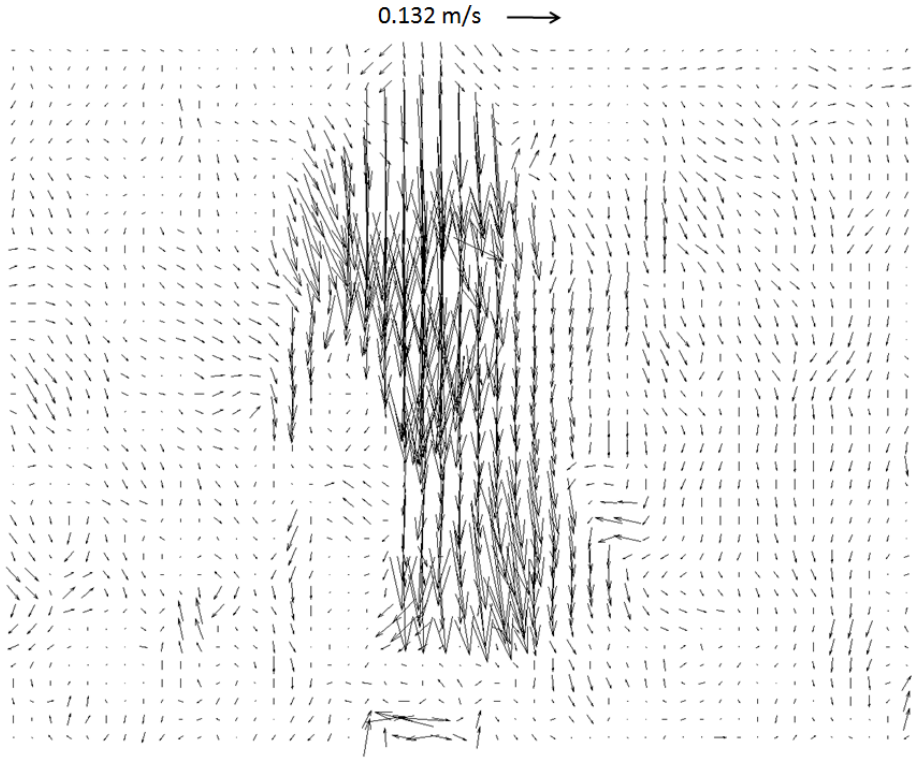

Figure 4.28a. PIV velocity fields on the shroud outlet axis with the LS-bare at the initial time of the sequence for a flow rate of 20 L/min, Δt = 0s

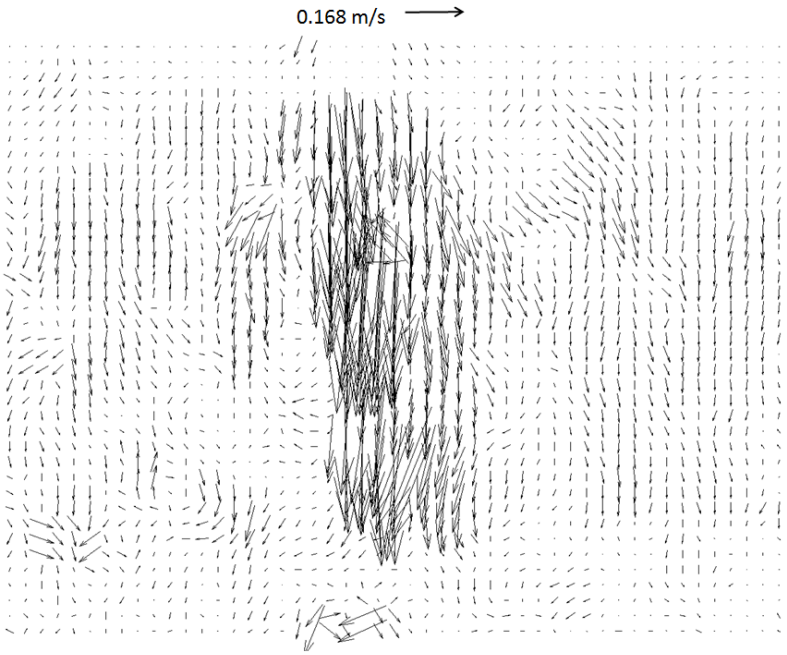

Figure 4.28b. PIV velocity fields on the shroud outlet axis with the LS-bare at the next time step of the sequence for a flow rate of 20 L/min, Δt = 0.25 s

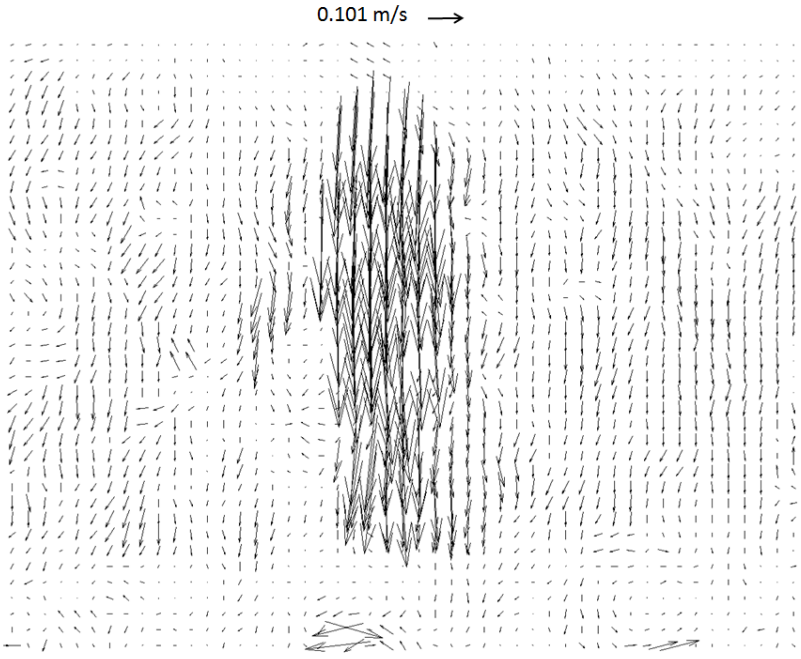

Figure 4.28c. PIV velocity fields on the shroud outlet axis with the LS-bare at the final time step of the sequence for a flow rate of 20 L/min, Δt = 0.5 s

4.4.4 VORTICITY FIELDS

It is a fundamental principle that turbulence produces vorticity flows whose magnitudes become larger as the kinetic energy of the entry jet increases. Indeed, Figures 4.29a, 4.29b and 4.29c show the vorticity fields corresponding to the most radical changes in the velocity fields for each of the flow rates studied here; 11, 20 and 30 l/min, respectively. Therefore, Figure 4.29a corresponds to the velocity field shown in Figure 4.25b, Figure 4.29b corresponds to the velocity field shown in Figure 4.26c and Figure 4.29c corresponds to Figure 4.27a.

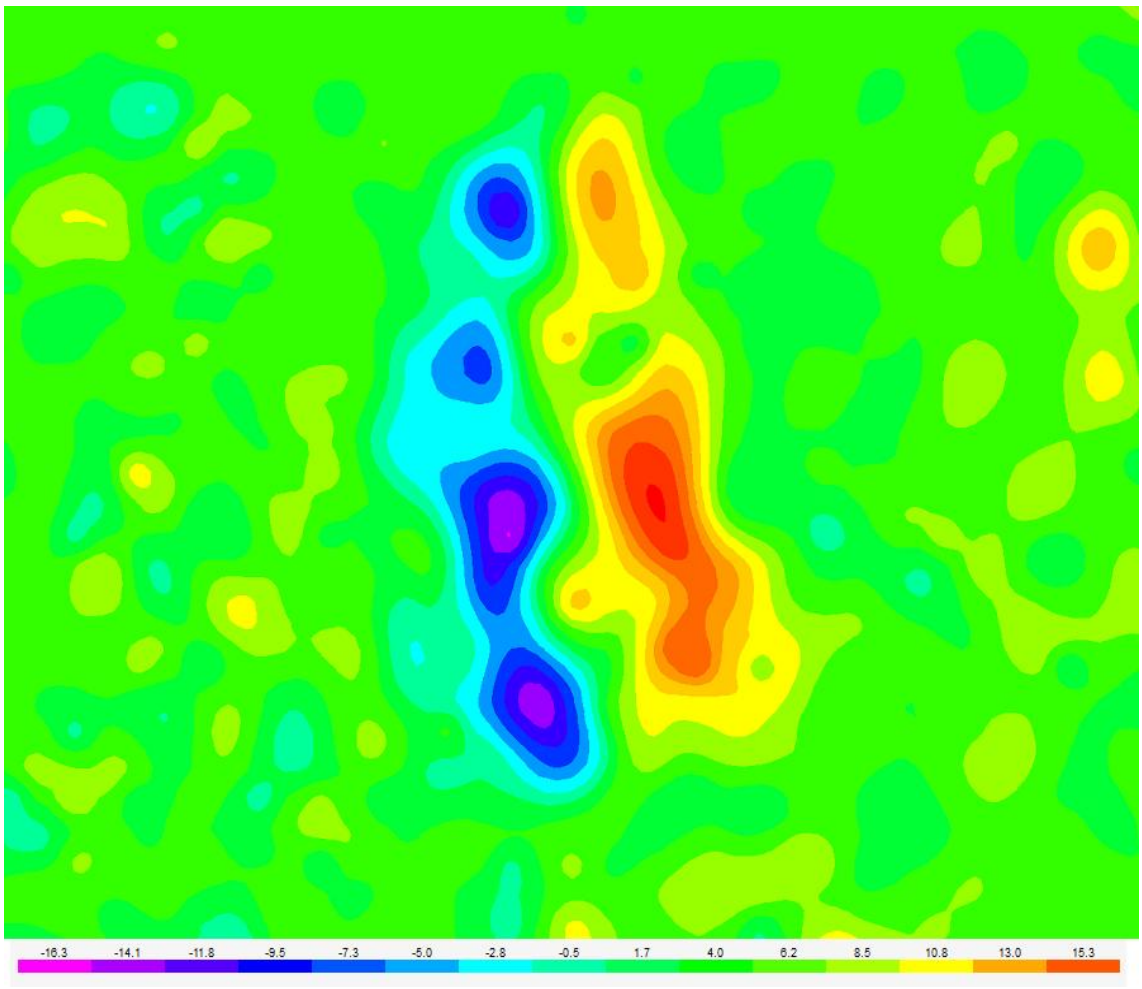

Figure 4.29a. Vorticity contours corresponding to the velocity fields at 11 L/min in Figure 4.25b, s^{-1}

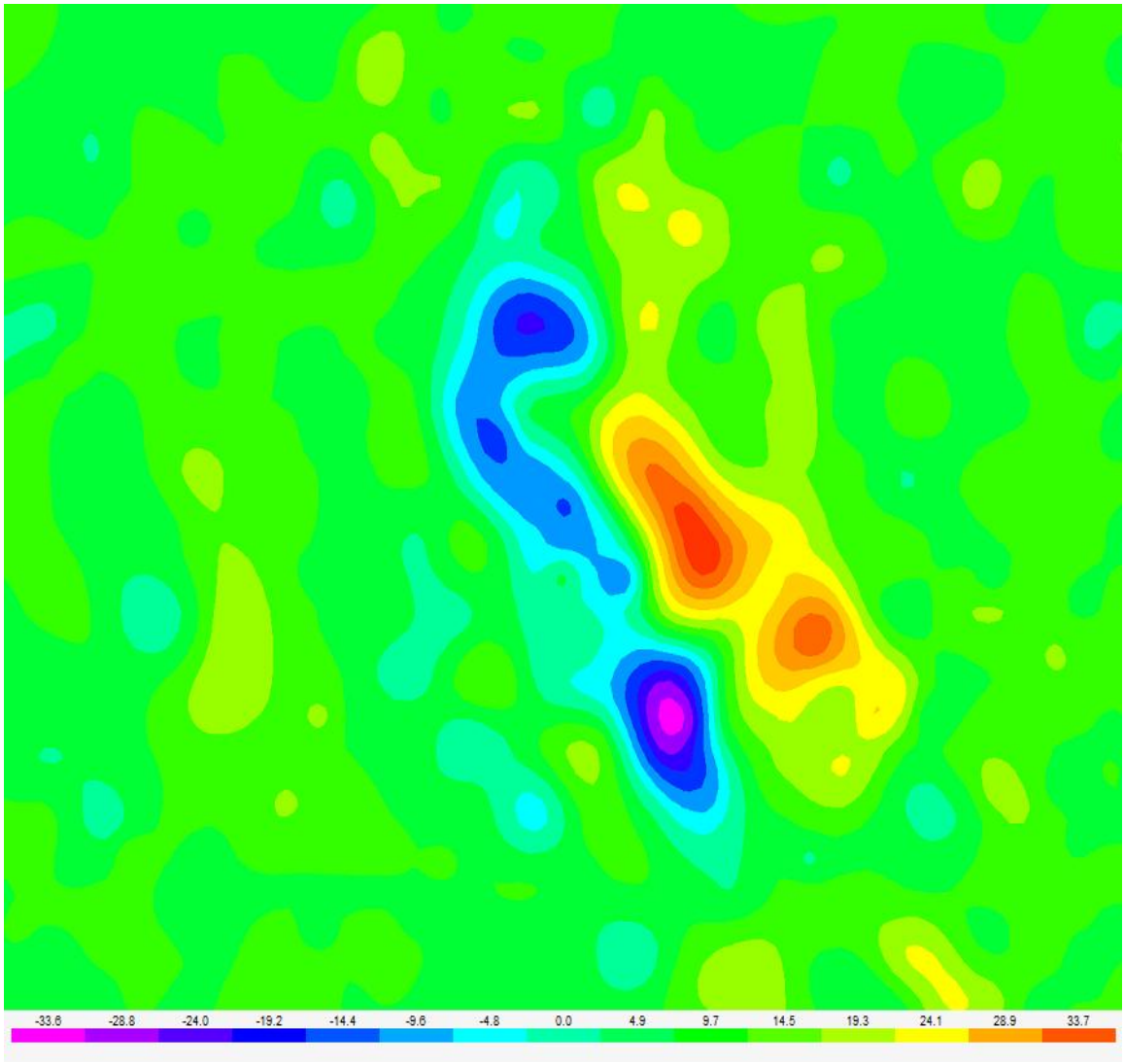

Figure 4.29b. Vorticity contours corresponding to the velocity fields at 20 L/min in Figure 4.26c, s^{-1}

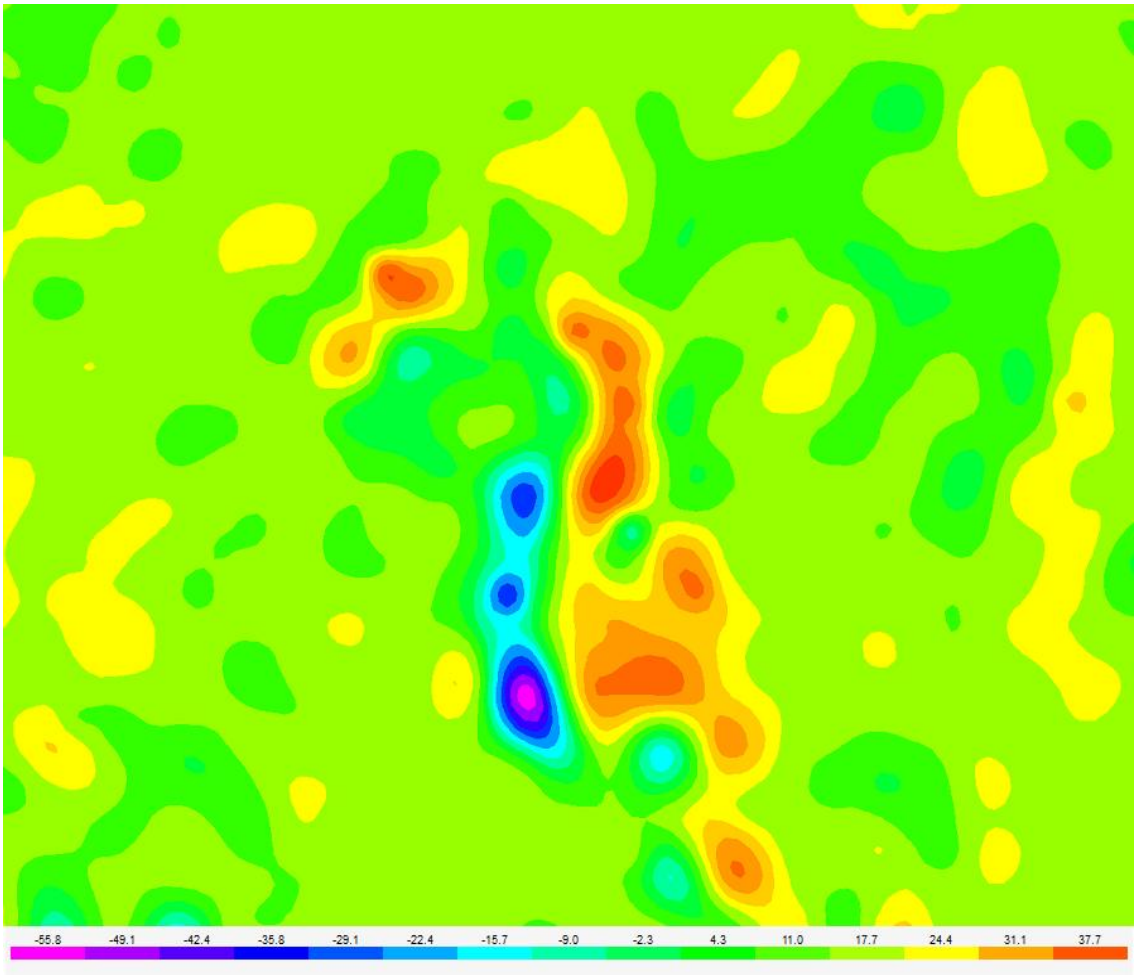

Figure 4.29c. Vorticity contours corresponding to the velocity fields at 30 L/min in Figure 4.27a, s^{-1}

The twisted jet to the right side in Figures 4.25b and 4.29a yields a well defined jet axis characterized by relatively small vorticity magnitudes. At both sides of the jet axis, negative (clockwise) and positive (anticlockwise) vorticity is generated. The islands of weak vorticity are formed in the rest of the flow field area. Since the magnitudes of the vorticity are generated throughout the field of observation, this indicates that the DLS efficiently dissipates the turbulent kinetic energy. The largest and smallest vorticity magnitudes in this case are -15 and +15 s^{-1}. With a flow rate of 20 l/min, Figure 4.29b, yields a highly distorted vorticity field, with magnitudes varying from -33 to +33 s^{-1}. Different to the previous case, the vorticity of the jet is now divided into upper and lower islands separated by a

distorted jet axis. At the highest flow rate, vorticity magnitudes vary in the range -56 and +37 s^{-1} , with an entry jet divided by positive and negative islands of vorticity. In the rest of the flow, mixtures of irrotational and highly rotational islands of fluid are generated by the input jet´s kinetic energy.

The magnitudes of the generated vorticity field when using the LS are very large, varying from -72 to +85 s^{-1}. The integrity of the jet remains identifiable and few islands of finite vorticity in the observation field are formed as seen in Figure 4.30.

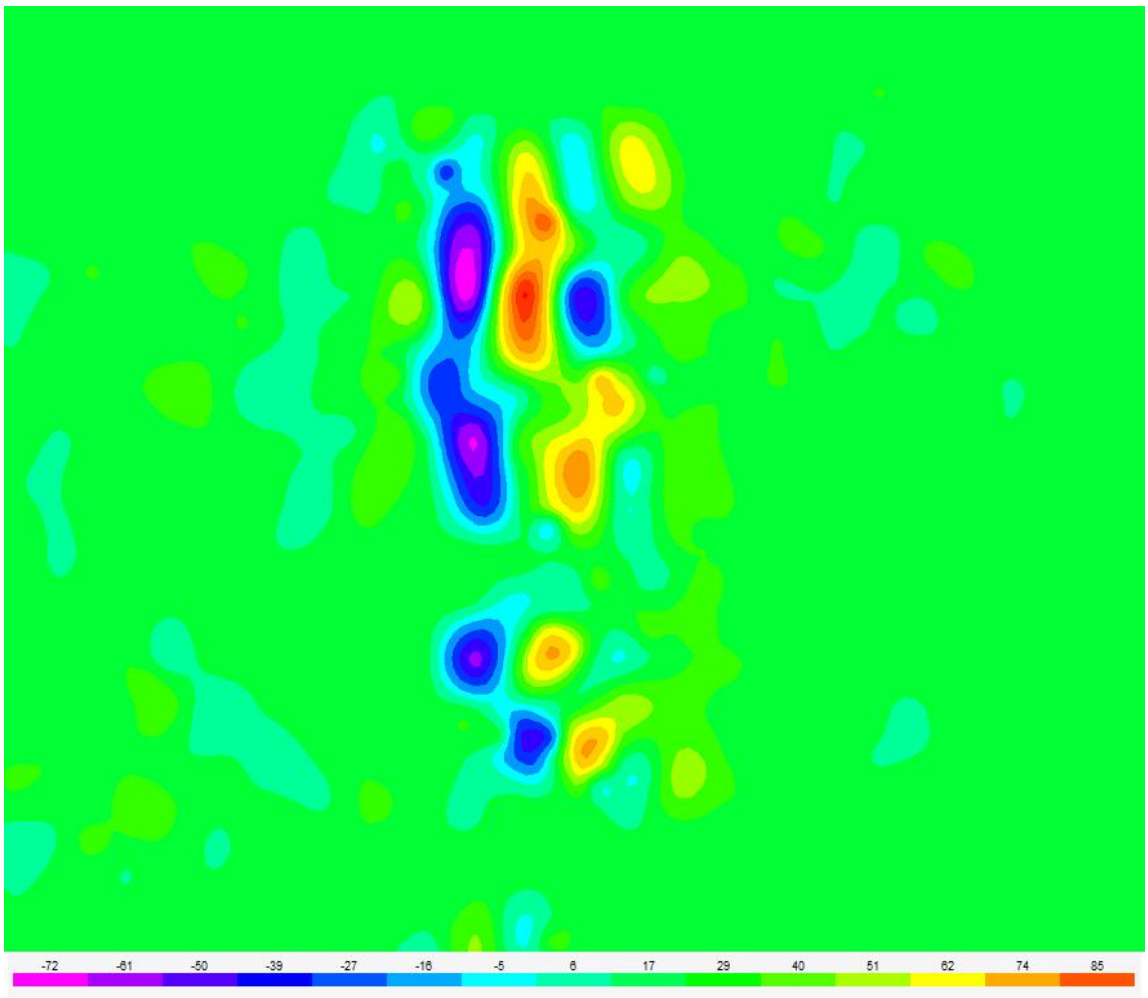

Figure 4.30.Vorticity contours corresponding to the LS at a flow rate of 20 L/min, s^{-1}

It is important to point out here, that the magnitudes of the vorticity at both sides of the entry LS jet axis are larger than those corresponding to the flow rate of 20 l/min using the DLS and even larger than those for the flow rate of 30 l/min using also the DLS.

4.5 MECHANISMS OF MOMENTUM TRANSFER

In a typical one-phase submerged jet flow, self-similarity exists even in metallurgical processes. For example, in jets discharging through submerged entry nozzles into slab continuous molds, as demonstrated by P. Lopez-Ramirez et al. [53]. Momentum transfer in the tundish is carried out mainly by the momentum of the entry jet into the vessel providing shearing stresses in the intermittent boundary layer developed between the jet and the surrounding flow. As seen in Figures 4.28a-4.29c, the efficiency of the entry jet, produced by the conventional LS, to transfer momentum to the surrounding flow to promote liquid entrainment is rather poor, owing to the essentially straight shape of the jet. Unfortunately, the cylindrical body of the ladle shroud reflected the laser light sheet very strongly, making it impossible to record the velocity field in its interior, in order to understand more details of the momentum transfer mechanisms. However, according to the results presented in Figures 4.25, 4.26 and 4.27, it is evident that the DLS provides the surrounding liquid with a strongly deformed entry jet. The deformed jet, transfers more momentum to the surrounding flow, which, as a consequence, leads to a larger dissipation rate of kinetic energy. The twisting effects make the intermittent boundary layers between the jet and the surrounding liquid were more transitory with the DLS, intensifying their interactions, and forming islands of negative and positive vorticity in the whole observation field. The vorticity maps shown in Figures 4.29a-4.29c correspond to the vector perpendicular to the page, ς_z. Vorticity can be made explicit in the Navier-Stokes equations through the total differentiation of the fluid acceleration, using turbulent averaged velocities (Reynolds decomposition is given by $u_i =$

$\bar{u}_i + u_i'$ where u_i is the instantaneous velocity, $\bar{u}_i$ is the averaged turbulent velocity and u_i' is the fluctuating velocity) according to;

$$a = \frac{d\bar{u}}{dt} = \frac{\partial \bar{u}}{\partial t} + (\bar{u} \cdot \nabla)\bar{u} \qquad (14)$$

The first term is the usual variation of fluid velocity with time while the second is known as the convection, or advection, of the fluid acceleration. Through vector calculus, it is possible to demonstrate that the term for advection of acceleration can be written as;

$$(\bar{u} \cdot \nabla)\bar{u} = \nabla\left(\frac{\bar{u}^2}{2}\right) + \bar{u} \times (\nabla \times \bar{u}) = \nabla\left(\frac{\bar{u}^2}{2}\right) + \bar{u} \times \varsigma \qquad (15)$$

The last term in Equation (15) arises from the definition of the vorticity, $\zeta = \nabla \times \mathrm{u}$. Therefore, by multiplying Equation (15) by the fluid density and introducing the result in the momentum transfer balance (in N m^{-3}), the Navier-Stokes equations for turbulent flows becomes,

$$\rho\left[\frac{\partial \bar{u}_i}{\partial t} + \nabla\left(\frac{{\bar{u}_i}^2}{2}\right) + \bar{u}_i \times \varsigma_i\right] = -\nabla\bar{P} + \rho\nabla(-gx_i) + \nabla \cdot \bar{\tau}_{ij}^{l} + \nabla \cdot \tau_{ij}^{t} \qquad (16)$$

The last two terms in the right hand side of Equation (16) are the laminar viscous stresses and Reynolds stresses, respectively. Rearranging Equation (16) into units of N*kg^{-1} becomes;

$$\frac{\partial \bar{u}_i}{\partial t} + \nabla\left(\frac{\bar{P}}{\rho} + \frac{\bar{u}_i^2}{2} + gx_i\right) = -\bar{u}_i \times \varsigma_i + \frac{1}{\rho}\left(\nabla \cdot \tau_{ij}^{l} + \nabla \cdot \bar{\tau}_{ij}^{t}\right) \qquad (17)$$

Therefore the vector product, $\bar{u}_i \times \varsigma_i$, is the vorticity force, which is one part of the momentum transfer by convection mechanisms. It interacts with the tensor of the Reynolds stresses. The sum of these two forces is equal to the gradient of the total mechanical energy plus the fluid acceleration, on the left side of equation 17. The gradient vector of a scalar, such as the total mechanical energy, always points in the direction of its maximum magnitude, as does the fluid acceleration. Both point downwards along the jet stream. The sum of these two vectors is

equal to the accelerations of the fluid provided by vorticity and Reynolds stresses. If the flow is irrotational, such as in those regions outside the direct influence of the entry jet, the vorticity term approaches zero, leaving only the contributions of viscous and Reynolds stresses. As such, any twisting effects are negligible. When the jet enters straight into the tundish, vorticity is generated on both sides of its axis. However, when the jet enters deformed, from the DLS tip, the viscous-Reynolds stresses interact with the asymmetric vorticity, and the fluid provides jet twisting effects, generating islands of vorticity that can be far away from the jet. Using the right hand rule, the 2D vorticity maps in Figures 4.29a-4.29c are vectors which are perpendicular to the page, forming a plane with the velocity vectors. The cross product of these two vectors gives the vorticity force, which has an angle of 90^0 with this plane. When the conventional LS is used, a "symmetric" field of vorticity is formed, giving rise to a "symmetric" force field with relatively constant magnitudes and with opposite sense, providing a straightening effect of the jet. This is shown schematically in Figure 4.31a in an isometric 3D view. Under these conditions, the main shearing stresses are those oriented downstream, and shearing occurs in the radial direction of the jet. On the other hand, when the jet exiting the shroud is strongly deformed out of the tip of the DLS, the plane formed by the vorticity and velocity fields is no longer parallel to the jet axis, and changes with time, making different angles with it. Consequently, the force vector of the fluid, which is always perpendicular to the velocity-vorticity plane, varies more in magnitude, forming an asymmetric 3D distribution around the entry jet (see scheme in Figure 4.31b). Figures 4.31c and 4.31d are schemes for the straight jet using the conventional LS and using the DLS respectively. These figures are 2D views. As can be seen, the velocity-vorticity fields in 2D views were obtained through PIV.

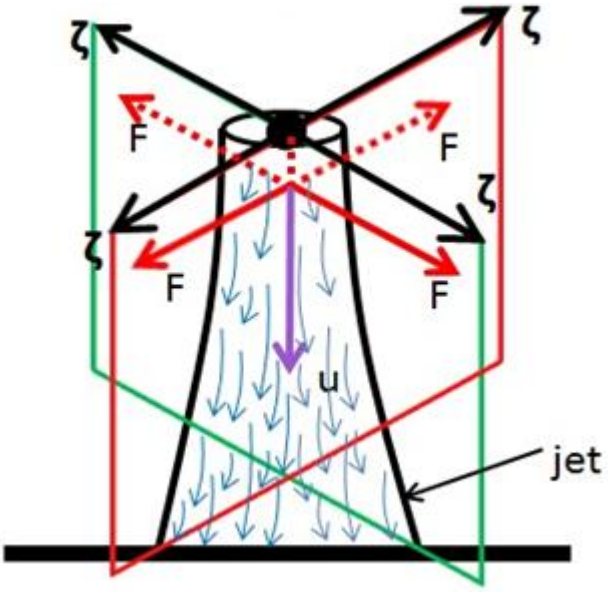

Figure 4.31a. Schematic representation of vorticity, velocity and force vectors in the downward entry jet with the Conventional LS in the three-dimensional domain

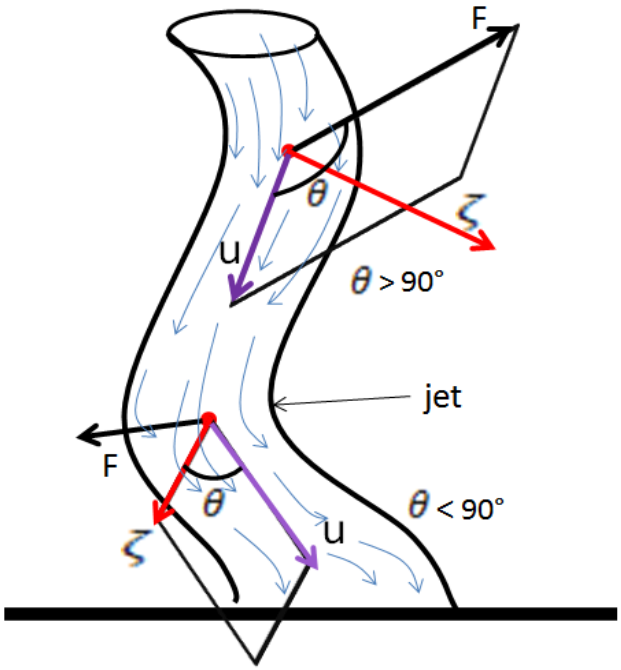

Figure 4.31b. Schematic representation of vorticity, velocity and force vectors in the downward entry jet with the DLS in the three-dimensional domain

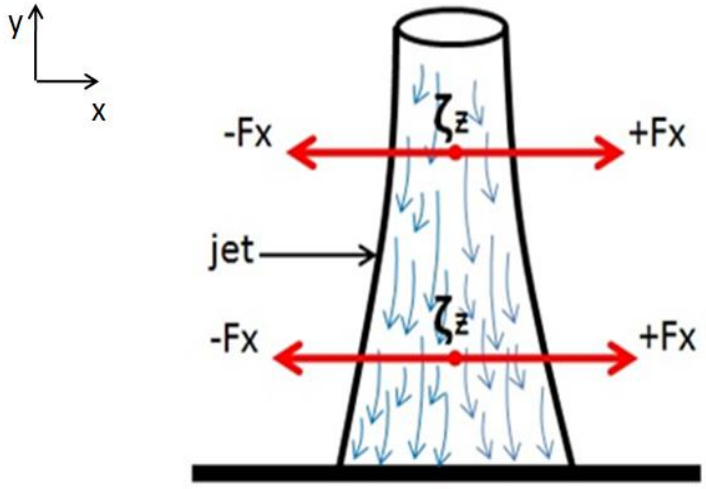

Figure 4.31c. Two-dimensional representation corresponding to the vorticity force in the x direction, the velocity in the y direction and the vorticity in the z direction for the LS jet

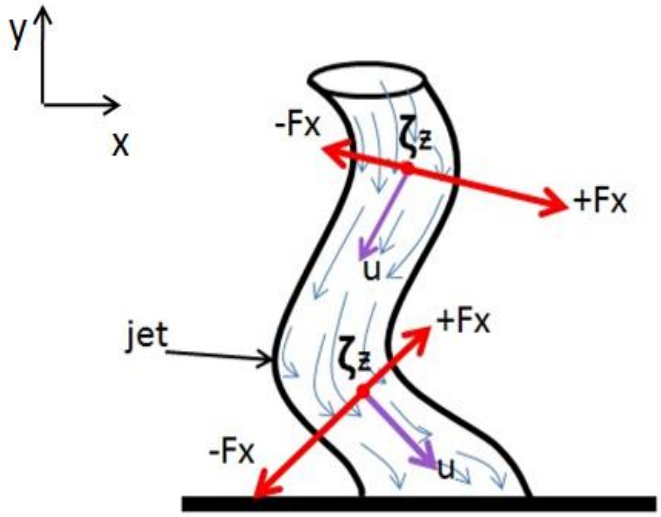

Figure 4.31d. Two-dimensional representation corresponding to the vorticity force in the x direction, the velocity in the y direction and the vorticity in the z direction for the DLS jet

CHAPTER 5

SUMMARY AND CONCLUSIONS

From the tracer injection experiments, it was found that the DLS distributes the entering fluid evenly throughout the volume of the tundish, when working without fluid flow modifiers. When the DLS is fitted with the Impact Pad, the mean residence times are larger and more equally distributed between the inner and outer strands. The DLS-IP had the largest plug flow fractions of the four cases studied. The bare tundish with the conventional LS yields a very strong bypass flow to the nearest strand. This effect was also observed in all other cases studied, but was less evident. The average residence times increases in the order; bare-LS, bare-DLS, LS-IP and DLS-IP.

With the aid of the mathematical simulations, the velocities through the ladle shrouds were described. It was possible to observe an expansion of the submerged jet, once the fluid is discharged into the tundish. From the different planes taken, the fluid flow was analyzed qualitatively and related to the RTD curves. The fluid flow patterns generated inside the tundish were able to explain the differences in the curves for each of the cases studied.

The visualization of the fluid flow using the tracer injection proved useful in understanding the patterns of the jets, as well as liquid flows throughout the volume of the tundish. The tracer showed a fluid flowing through the tundish with plug flow characteristics in the case of the DLS-bare. When the DLS was used in conjunction with the Impact Pad, it was observed that the tracer remained longer in the tundish, thereby attaining longer mean residence times for both the inner and outer strands.

By visualizing the velocity fields using the Particle Image Velocimetry (PIV) technique, it was possible to provide a more detailed description of fluid flow patterns. The entry jet into the tundish using the LS provides a characteristic one-phase submerged straight jet, having small interactions with the surrounding liquid, unless the input of kinetic energy is high. Using the DLS, a deformed jet is developed, whose frequency of oscillation increased with increases in kinetic energy input or (water/steel throughput). The entering jet´s kinetic energy and fluid velocities are radically decreased by the DLS, thanks to the high dissipation rate of kinetic energy spent in creating intermittent-turbulent boundary layers with the surrounding fluid, generated by the twisting jet motions.

As the mathematical simulations predicted, an expansion of the jet was observed, being distributed through the discharge space as oscillatory deformations. When using a higher flow rate, such as 30 L/min, the fluid also oscillates around the space of discharge. These results suggest that the DLS could be useful when a ladle change takes place and higher flow rates are used for recovering the steady state level. Finally, the feasibility of substituting flow control devices in current tundishes in the continuous casters using a DLS has been demonstrated technically.

FUTURE WORK

- To perform mathematical simulations of inclusion behavior and to compare these with the results obtained from the RTD experiments.
- To physically simulate the slag with overlying oil, and perform experiments at different flow rates in order to observe bath surface motions.
- Mathematical simulations with different turbulent models to analyze the penetrating entry jet in more detail.
- To design a fluid flow modifier inside the tundish to be fitted in conjuction with the DLS, in order to further improve fluid flow patterns and inclusion float out.

APPENDIX 1

The velocity and Reynolds stresses for the ladle shrouds were extracted from [17].

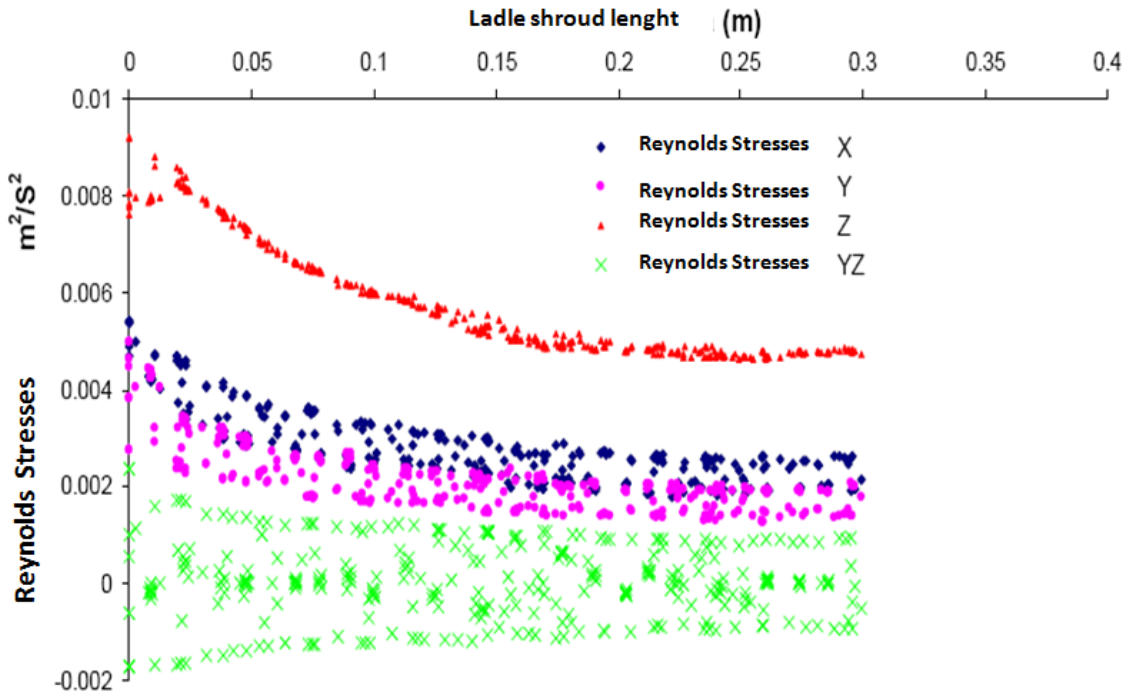

Figure 5.1 Reynolds stresses in an axial plane located at the center of the conventional ladle shroud (LS)

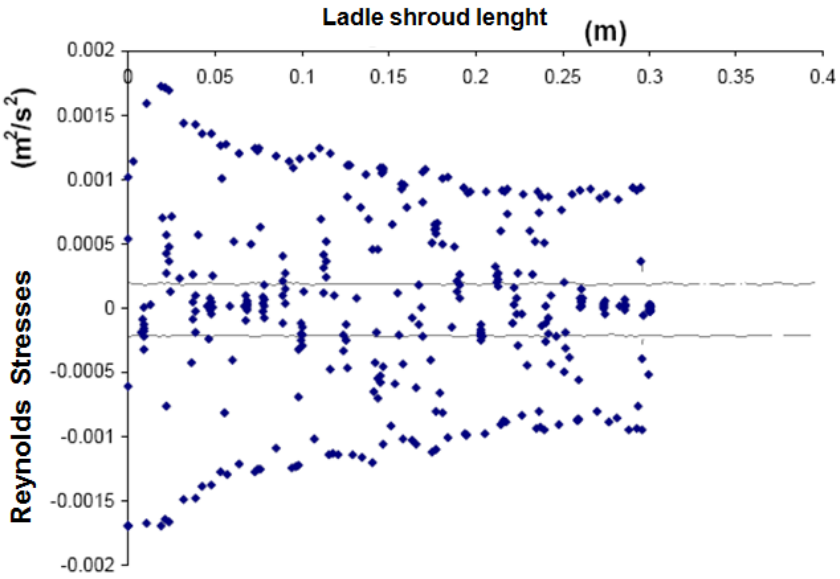

Figure 5.2 Reynolds stresses (τ_{yz} = - $\overline{v'_y v'_z}$) in the YZ axial plane located at the center of the conventional shroud (LS)

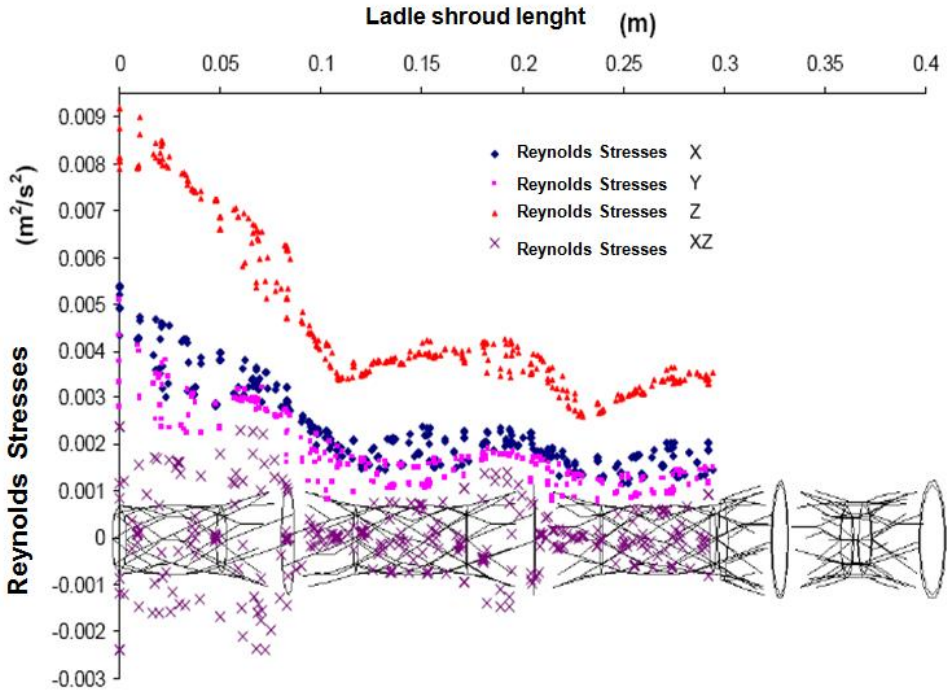

Figure 5.3 Reynolds stresses in an axial plane located at the center of the Dissipative ladle shroud (DLS)

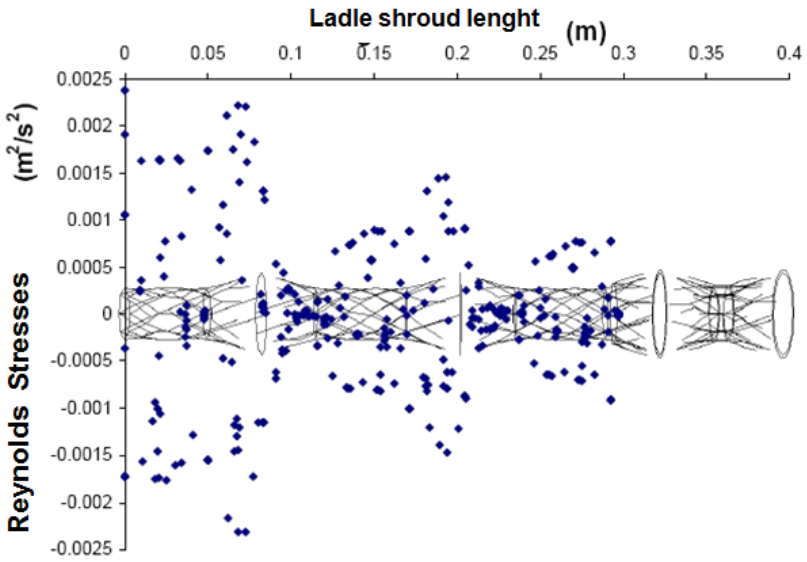

Figure 5.4 Reynolds stresses (τ_{yz} = - $\overline{v'_y v'_z}$) in the YZ axial plane located at the center of the Dissipative Ladle Shroud (DLS)

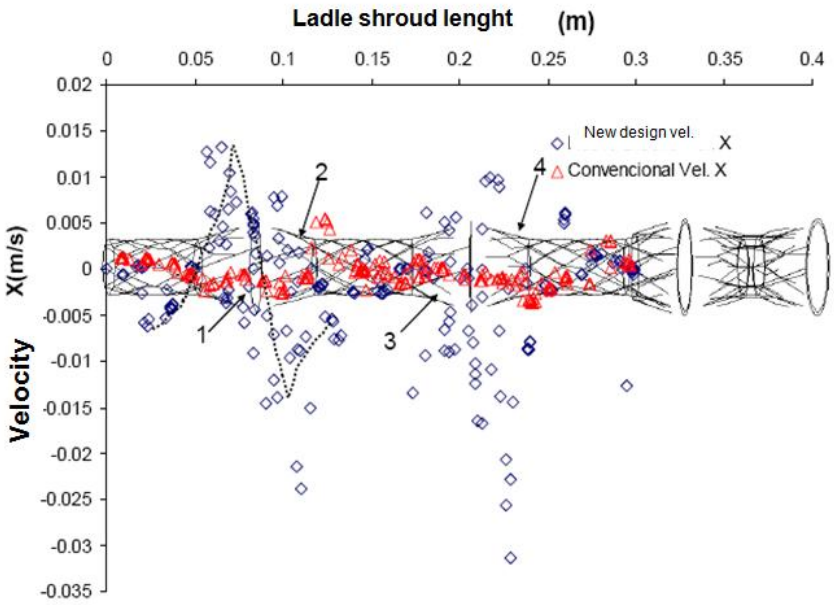

Figure 5.5 Component of the velocity magnitude in the X direction located at an axial plane in the center of the Dissipative Ladle Shroud (DLS)

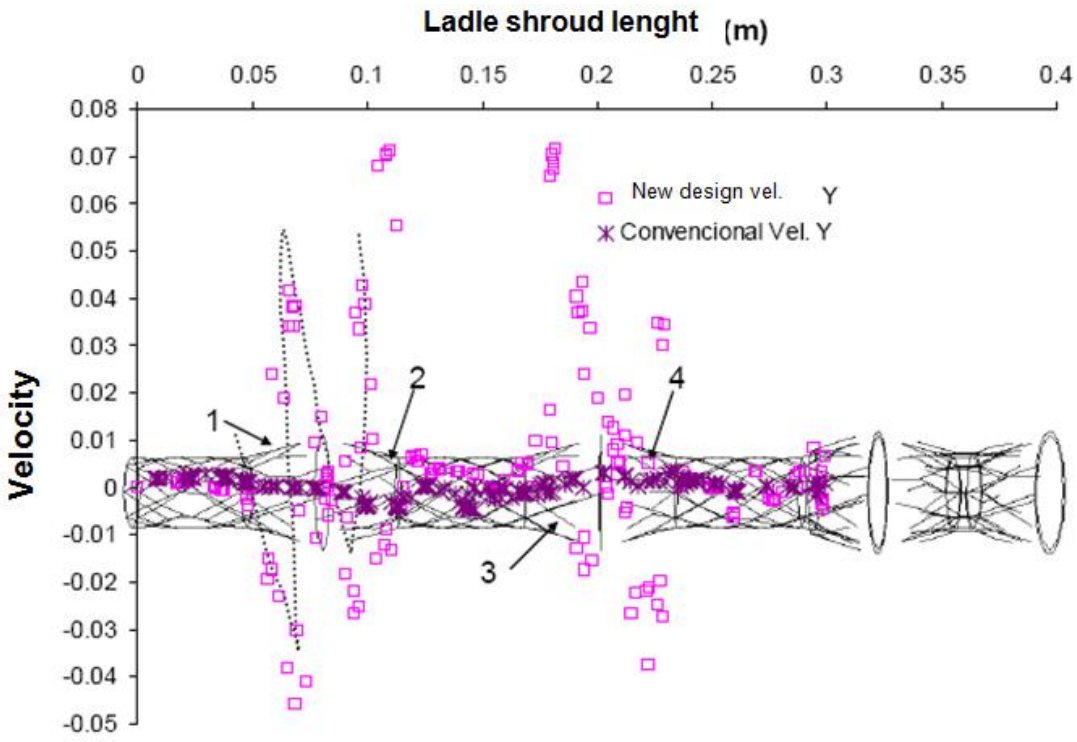

Figure 5.6 Component of the velocity magnitude in the Y direction located at an axial plane in the center of the Dissipative Ladle Shroud (DLS)

REFERENCES

1.Y.Sahai and T.Emi, Tundish Technology for Clean Steel Production, World Scientific Publication Co. Pte. Ltd. 2008.

2.HE Youduo and Y. Sahai, Influence in some factors on fluid flow in continuous casting tundishes, ACTA METALL SIN (CHINESE EDN), 1989 pp B272-B276.

3.Roderick. I. L. Guthrie, Fluid Flows in Metallurgy: Friend or Foe, Metallurgical and Materials Transactions B, Vol 35B, Jun 2004, 417.

4.Dipak Mazumdar and Roderick. I. L. Guthrie ISIJ International, Vol. 39, 1999, No-6, pp 524-547.

5.C.M. Fan, S.M. Pan, H.S. Wang, and W.S. Hwang, Design of single element flow control device in twin strand billet tundish for continuous casting of steel using flow simulation model, Iron and Steelmaking, vol. 29, 2002.

6. K.J. Craig, D.J. de Kock, K.W. Makgata and G.J. de Wet, Design Optimization of a single-strand continuous caster tundish using residence time distribution data, ISIJ International, Vol. 41(2001), 1194-1200.

7. C.M. Fan, R.J. Shie and W.S. Hwang, Studies by mathematical and physical modeling of fluid flow and inclusion removal phenomena in slab tundish for casting stainless steel using various flow control designs, Iron and Steelmaking, 2003, pp 341-347.

8. S. Joo, R.I.L. Guthrie (1993): “Inclusion Behavior and Heat Transfer Phenomena in Steelmaking Tundish Operations, Part I – Aqueous Modeling”, Vol. 24B, pp. 755-765. (Extraction and Processing Technology Award, 1997)

9. S. Joo, J.-W. Han, R.I.L. Guthrie (1993): "Inclusion Behavior and Heat Transfer Phenomena in Steelmaking Tundish Operations, Part II – Mathematical Model for Liquid Steel in Tundishes", *Metall. Trans.*, Vol. 24B, pp. 767-777. (Extraction and Processing Technology Award, 1997)

10. S. Joo, J.-W. Han, R.I.L. Guthrie (1993): "Inclusion Behavior and Heat Transfer Phenomena in Steelmaking Tundish Operations, Part III – Applications Computational Approach to Tundish Design", *Metall. Trans.*, Vol. 24B, pp. 779-788. (Extraction and Processing Technology Award, 1997)

11. Shamik Ray, Mihaiela Isac, Roderick Guthrie, "Modelling the performance of a 4 strand, 12 tonne, delta-shaped continuous casting tundish, fitted with different flow modifying arrangements for better steel quality" Accepted for publication in Metallurgical Transactions B, 2010

12. A. Ramos-Banderas, R.D. Morales, L. García-Demedices and M. Díaz-Cruz. Mathematical Simulation and Modeling of Steel Flow with Gas Bubbling in Trough Type Tundishes, ISIJ International, Vol. 43(2003), pp.653-662.

13. A. VARGAS-ZAMORA, R.D. MORALES, M. DÍAZ-CRUZ, J. PALAFOX-RAMOS, and J. DE J. BARRETO-SANDOVAL, Inertial and Buoyancy Driven Water Flows under Gas Bubbling and Thermal Stratification Conditions in a Tundish Model, METALLURGICAL AND MATERIALS TRANSACTIONS B VOLUME 35B, APRIL 2004—247.

14. R. D. Morales, J de J Barreto, S Lopez-Ramirez, J Palafox-Ramos and M Diaz-Cruz, Mathematical simulation of the influence of buoyancy forces on the molten steel flow in a continuous casting tundish, Modelling Simul. Mater. Sci. Eng. (2000) 781–801.

15. R. D. MORALES, S. LOPEZ-RAMIREZ, J. PALAFOX-RAMOS and D. ZACHARIAS, Numerical of Liquid and Steel Modeling Analysis in a Tundish with of Fluid Flow and Heat Transfer Difterent Flow Control Devices, ISIJ International, Vol. 39 (1 999), No, 5, pp. 455-462.

16. A. Tripathi and S. K. Ajmani: Numerical Investigation of fluid flow phenomenon in curved shape tundish of billet caster, ISIJ Int., 45 (2005), No. 11, 1616.

17. Gildardo Solorio Diaz, Flow control of steel liquid in a continuous casting process through the feeding ladle shroud, Phd. Thesis, Instituto Politecnico Nacional, 2004.

18. Kinnor CHATTOPADHYAY, Mihaiela ISAC and Roderick I. L. GUTHRIE, Physical and Mathematical Modelling of Steelmaking Tundish Operations: A Review of the Last Decade (1999–2009), ISIJ International, Vol. 50 (2010), No. 3, pp. 331–348.

19. Kinnor Chattopadhyay, Mihaiela Isac and Roderick I.L. Guthrie, "Applications of Computational Fluid Dynamics (CFD) in Iron and Steel Making"- Part 1, Ironmaking & Steelmaking, Volume 37, No 8, November, 2010, pp. 554-561.

20. Kinnor Chattopadhyay, Mihaiela Isac and Roderick I.L. Guthrie "Applications of Computational Fluid Dynamics (CFD) in Iron and Steel Making"- Part 2, Kinnor Chattopadhyay, Mihaiela Isac and Roderick I.L. Guthrie, Ironmaking & Steelmaking, Volume 37, No 8, November, 2010 , pp. 562-569.

21. R.D. MORALES, J. de J. BARRETO, S. LO´ PEZ-RAMIREZ, J. PALAFOX-RAMOS, and D. ZACHARIAS, Melt Flow Control in a Multistrand Tundish Using a

Turbulence Inhibitor, METALLURGICAL AND MATERIALS TRANSACTIONS B, VOLUME 31B, DECEMBER 2000.

22. Kinnor Chattopadhyay, Mihaiela Isac, and Roderick I.L. Guthrie ; “Physical and Mathematical Modelling of Inert Gas Shrouding in a Tundish.” Accepted in ISIJ International. (Article in press).

23.H.B.Kim, M.Isac and R.I.L.Guthrie; “Physical modelling of transport phenomena in a delta-shaped, four strand tundish with flow modifiers” Steel Research International, vol 76, no 1, pp 53-58.

24. Jorge MADIAS, Diego MARTIN, Matias FERREYRA, Roberto VILLORIA and Arturo GARAMENDY, Design and Plant experience using and advance pouring box to receive and distribute the steel in a six strand tundish, ISIJ International, Vol. 39 (1 999), No. 8, pp. 787-794.

25. Anil KUMAR, Dipak MAZUMDAR and Satish C. KORIA, Modeling of Fluid Flow and Residence Time Distribution in a Four-strand Tundish for Enhancing Inclusion Removal, ISIJ International, Vol. 48 (2008), No. 1, pp. 38–47.

26. G. SOLORIO-DÍAZ, R. D. MORALES, J. PALAFAX-RAMOS, L. GARCÍA-DEMEDICES and A. RAMOS-BANDERAS, Analysis of Fluid Flow Turbulence in Tundishes Fed by a Swirling Ladle Shroud, ISIJ International, Vol. 44 (2004), No. 6, pp. 1024–1032.

27. G. SOLORIO-DÍAZ, R. D. MORALES, J. PALAFAX-RAMOS and A. RAMOS-BANDERAS, Modelling the effects of a swirling flow on temperature stratification of liquid steel and flotation of inclusions on a tundish, ISIJ International, Vol. 45 (2005), No. 8, pp. 1129–1137.

28. Qinfu HOU, Qiang YUE,Huanyang WANG, Zongshu ZOU and Aibing YU., Modelling of Inclusion Motion and Flow Patterns in Swirling Flow Tundishes with Symmetrical and Asymmetrical Structures, ISIJ International, Vol. 48 (2008), No. 6, pp. 787–792.

29. ANIL KUMAR, DIPAK MAZUMDAR, and SATISH C. KORIA, Experimental Validation of Flow and Tracer-Dispersion Models in a Four-Strand Billet-Casting Tundish, METALLURGICAL AND MATERIALS TRANSACTIONS B, VOLUME 36B, DECEMBER 2005—777.

30. Octave Levenspiel, Chemical Reaction Engineering, Third Edition, John Wiley & Sons.

31. Anil KUMAR, Satish C. KORIA and Dipak MAZUMDAR, An Assessment of Fluid Flow Modelling and Residence Time Distribution Phenomena in Steelmaking Tundish Systems, ISIJ International, Vol. 44 (2004), No. 8, pp. 1334–1341.

32. D. B. Spalding: Int. J. Num. Math. Eng., 1972, Vol. 4.

33. B. E. Launder and D. B Spalding: Mathematical Models of Turbulence, Academic Prees, London, 1972.

34. S.B. Pope: Models of Turbulence, Cambridge University Press, New York, London 2000, 65.

35. A. V. Kuklev et al.: Metallurgist, 48 (2004), Nos. 3–4, 000.

36. P. K. Jha, S. K. Dash, and S. Kumar, Effect of outlet positions, height of advanced pouring box, and shroud immersion depth mixing in six strand billet caster tundish, Ironmaking and St 2002 Vol. 29 No. 1.

37. T. MERDER, J. PIEPRZYCA, M. WARZECHA, NUMERICAL MODELING OF STEEL FLOW IN THE SIX-STRAND TUNDISH WITH DIFFERENT FLOW CONTROL DEVICES, METALURGIJA 48 (2009) 3, 143-146.

38. Guanghua Wen et al., Modelling study on fluid flow and inclusion motion in 6-strand bloom caster tundishes, Journal of University of Science and Technology, Beijing, Vol 11, No. 4, Aug 2004, Pg 310.

39. A. Espino-Zarate, R. D. Morales, A. Nájera-Bastida, M. J. Macias-Hernandez and A. Sandoval-Ramos, FLUID FLOW AND MECHANISMS OF MOMENTUM TRANSFER IN A SIX STRAND TUNDISH, Metallurgical and Materials Transactions B, Volume 41, Issue 5, pp.962-975.

40. Yun WANG, Yunbo ZHONG, Baojun WANG, Zuosheng LEI, Weili REN and Zhongming REN, Numerical and Experimental Analysis of Flow Phenomenon in Centrifugal Flow Tundish, ISIJ International, Vol. 49 (2009), No. 10, pp. 1542–1550.

41. Q. F. HOU, H. Y. WANG, Q. YUE, Z.S. ZOU and A.B. YU, PHYSICAL AND MATHEMATICAL MODELLING OF SWIRLING FLOW TUNDISH, Fifth International Conference on CFD n the Process Industries CSIRO, Melbourne, Australia 13-15 December 2006.

42. Fang WANG, Baokuan LI and Fumitaka TSUKIHASHI, Large Eddy Simulation on Flow Structure in Centrifugal Flow Tundish, ISIJ International, Vol. 47 (2007), No. 4, pp. 568–573.

43.Q. F. HOU and Zongshu ZOU, Comparison between Standard and Renormalization Group K-E Models in Numerical Simulation of Swirling Flow Tundish, ISIJ International, Vol. 45(2005), No. 3, pp. 325–330.

44. Pradeep K. Jha, Rajeev Ranjan, Swasti S. Mondal and Sukanta K. Dash, Mixing in a tundish and a choice of turbulence model for its prediction, International Journal of Numerical Methods for Heat & Fluid Flow Vol. 13 No. 8, 2003.

45. Nouri Alkishriwi, Matthias Meinke, and Wolfgang Schroder, Large-Eddy Simulation of Tundish Flow, New Res. in Num. and Exp. Fluid Mech. VI, NNFM 96, pp. 397–404, 2007.

46. Carlos A. LLANOS, Saul GARCIA-HERNANDEZ, J. Angel RAMOS-BANDERAS, Jose de J. BARRETO and Gildardo SOLORIO-DIAZ, Multiphase Modeling of the Fluidynamics of Bottom Argon Bubbling during Ladle Operations, ISIJ International, Vol. 50 (2010), No. 3, pp. 396–402.

47. KINNOR CHATTOPADHYAY, MAINUL HASAN, MIHAIELA ISAC and RODERICK I.L. GUTHRIE, Physical and Mathematical Modeling of Inert Gas-Shrouded Ladle Nozzles and their Role on Slag Behavior and Fluid Flow Patterns in a Delta-Shaped, Four-Strand Tundish, METALLURGICAL AND MATERIALS TRANSACTIONS B, VOLUME 41B, FEBRUARY 2010.

48. Shamik Kumar Ray, Water Modeling Studies to Predict Steel Quality in a 4 Strand Delta-Shaped Tundish, Masters thesis, McGill University, 2006.

49. Hyoungbae Kim, Modeling of transport phenomena in a delta-shaped four strand tundish, McGill University, PhD thesis, McGill University, 2003.

50. H.B. Kim, R.I.L. Guthrie and M. Isac, The Effect of Flow Modifiers on the Hydrodynamic Performance of a Delta-shaped four strand tundish, ISS Tech 2003 Conference Proceedings.

51. B.G. Thomas, “Continuous Casting: Modeling,” *The Encyclopedia of Advanced Materials*, (J. Dantzig, A. Greenwell, J. Michalczyk, eds.) Pergamon Elsevier Science Ltd., Oxford, UK, Vol. 2, 2001, 8p., (Revision 3, Oct. 12, 1999).

52. S. V. Patankar: Numerical Heat Transfer and Fluid Flow, McGraw Hill, New York, NY, (1980).

53. P. Ramirez-Lopez and R. D. Morales: “Self-similarity Phenomena of Discharge Jets in a Conventional Slab Mold”, Ironmaking and Steelmaking, Vol. 33, (2006), PAG. 157-168.

54. Zhang L, Taniguchi S, Cai K. Fluid Flow and Inclusion Removal in Continuous Casting Tundish [J]. Metall. and Mat. Trans, 2000, 31B(2): 253.

55. Nakajima K, Kawasaki M. Promotion of Inclusion Float-Out in Continuous Casting Tundish Bath by Gas Blowing CJ]. Tetsu to Hagane, 1987, 110.

56. Wang Laihua, Lee HaeGeon, Hayes Peter. New Approach to Molten Steel Refining Using Fine Gas Bubbles [J]. ISIJ International, 1996, 17.

57. A. Aguilar-Corona, R.D. Morales, M. Díaz-Cruz, J. Palafox-Ramos and L. García Demedices, Thermal stratification of steel flow in tundishes with off-centered ladle using different control designs, Canadian Metallurgical Quaterly, Vol. 42, No. 4 pp 455-464, 2003.

58. S. Lopez-Ramirez, R. D. Morales, J. A. Romero Serrano, NUMERICAL SIMULATION OF THE EFFECTS OF BUOYANCY FORCES AND FLOW CONTROL DEVICES ON FLUID FLOW AND HEAT TRANSFER PHENOMENA OF LIQUID STEEL IN A TUNDISH, Numerical Heat Transfer, Part A, 69- 86, 2000.

59. Pradeep K. JHA, P. Srinivasa RAO and Anupam DEWAN, Effect of Height and Position of Dams on Inclusion Removal in a Six Strand Tundish, ISIJ International, Vol. 48 (2008), No. 2, pp. 154–160.

60. Liangcai ZHONG, Baokuang LI, Yingxiong ZHU, Rengui WANG, Wenzhong WANG and Xiaojun ZHANG, Fluid Flow in A Four-strand Bloom Continuous Casting Tundish with Different Flow Modifiers, ISIJ International, Vol. 47 (2007), No. 1, pp. 88–94

61. WANG Jun, ZHU Miao-yong, ZHOU Hai-bing, WANG Ying, Fluid Flow and Interfacial Phenomenon of Slag and Metal in Continuous Casting Tundish With Argon Blowing, JOURNAL OF IRON AND STEEL RESEARCH, INTERNATIONAL. 2008, 26-31.

62. Shamik Kumar Ray, On the application of physical and mathematical modeling to predict tundish performance, Phd thesis, McGill University, 2009.